GEORGIA INSTITUTE OF TECHNOLOGY — OFFICE OF CONTRACT ADMINISTRATION

PROJECT ADMINISTRATION DATA SHEET

[x] ORIGINAL [ ] REVISION NO. ____

Project No. G-35-615 GTRI/~~GIT~~ DATE 5 / 23 / 84

Project Director: Dr. G. W. Grams School/~~COX~~ Geophysical Sciences

Sponsor: National Science Foundation

Type Agreement: Grant No. INT-8314539

Award Period: From 5/15/84 To 4/30/85 * (Performance) 7/31/85 (Reports)

Sponsor Amount:	This Change	Total to Date
Estimated: $		$ 16,800
Funded: $		$ 16,800

Cost Sharing Amount: $ n/a Cost Sharing No: n/a

Title: "Review of Work Related to Sensing of Stratospheric Aerosol and Gas Components" (U.S. - Japan Seminar)

ADMINISTRATIVE DATA OCA Contact Lynn Boyd x4820

1) Sponsor Technical Contact:

Charles W. Wallace
Central Processing Station
U. S. Japan Cooperative Science Program
National Science Foundation
Washington, DC 20550
(202) 357-9537

2) Sponsor Admin/Contractual Matters:

Joe Carrabino
Grants Official
National Science Foundation
Washington, DC 20550
(202) 357-9630

Defense Priority Rating: n/a Military Security Classification: n/a

(or) Company/Industrial Proprietary: n/a

RESTRICTIONS

See Attached NSF Supplemental Information Sheet for Additional Requirements.

Travel: Foreign travel must have prior approval – Contact OCA in each case. Domestic travel requires sponsor approval where total will exceed greater of $500 or 125% of approved proposal budget category.

Equipment: Title vests with GIT.

COMMENTS:

* no unfunded flexibility period is included in this award.

NOTE: Advance No. was authorized, but award was received prior to entering in computer.

Sponsor I.D. #02.107.000.83.055

COPIES TO:

Project Director
Research Administrative Network
Research Property Management
Accounting
Procurement/EES Supply Services
Research Security Services
Reports Coordinator (OCA)
Research Communications (2)
GTRI
Library
Project File
Other Newton

FORM OCA 4:383

ORGIA INSTITUTE OF TECHNOLOGY OFFICE OF CONTRACT ADMINISTRATION

SPONSORED PROJECT TERMINATION/CLOSEOUT SHEET

Date 3/16/88

oject No. G-35-615 School/~~XXX~~ Geo. Sci.

cludes Subproject No.(s) N/A

oject Director(s) G. W. Grams GTRC/~~XXX~~

onsor NSF

tle Review of Work Related to Sensing of Stratospheric Aerosol and Gas Components (U.S.-Japan Seminar)

fective Completion Date: 4/30/85 (Performance) 7/31/85 (Reports)

ant/Contract Closeout Actions Remaining:

- [X] None
- [ ] Final Invoice or Copy of Last Invoice Serving as Final
- [ ] Release and Assignment
- [ ] Final Report of Inventions and/or Subcontract:
  Patent and Subcontract Questionnaire sent to Project Director [ ]
- [ ] Govt. Property Inventory & Related Certificate
- [ ] Classified Material Certificate
- [ ] Other _____

ontinues Project No. _____ Continued by Project No. _____

OPIES TO:

roject Director
esearch Administrative Network
esearch Property Management
ccounting
rocurement/GTRI Supply Services
esearch Security Services
eports Coordinator (OCA)
rogram Administration Division
ontract Support Division
Facilities Management - ERB
Library
GTRC
Project File
Other _____

NATIONAL SCIENCE FOUNDATION
Washington, D.C. 20550

FINAL PROJECT REPORT
NSF FORM 98A

PLEASE READ INSTRUCTIONS ON REVERSE BEFORE COMPLETING

PART I–PROJECT IDENTIFICATION INFORMATION

1. Institution and Address	2. NSF Program	3. NSF Award Number
School of Geophysical Sciences Georgia Institute of Technology Atlanta, GA 30332	U.S.-Japan Cooperative Science	INT-8314539
	4. Award Period From 5/15/84 To 7/31/85	5. Cumulative Award Amount $16,800

6. Project Title
Review of Work Related to Sensing of Stratospheric Aerosol and Gas Components (U.S. - Japan Seminar)

PART II–SUMMARY OF COMPLETED PROJECT *(FOR PUBLIC USE)*

Various methods for observing stratospheric aerosols and gases provide a world-wide capability for quasi-routine observations. With additional coordinated efforts, data sets provided by those observations can be used to increase our knowledge of the spatial and temporal variability of the stratospheric constituents and to quantify their effects on the earth's climate and on other atmospheric physical and chemical processes. These techniques include optical sensing by satellite instruments. A series of stratospheric sensor launches began in the U.S. in 1979; two more sensors were to be launched independently by Japan and the U.S. in 1984 shortly after the seminar. Also, stratospheric measurement programs in both the U.S. and Japan use lidar, other ground-based remote sensing techniques and in-situ instruments carried on aircraft and balloons.

The seminar reviewed and compared results obtained by the different observation techniques. NSF provided seminar travel funds for the 6 American scientists described in Attachment C-1. Dr. Pepin was unable to attend the seminar and Dr. Patrick Hamill took his place; a copy of a letter to NSF describing Dr. Hamill's qualifications is included as Attachment C-2. All seminar participants are listed in Attachment C-3.

The meeting agenda is included as Attachment E-1. The seminar was viewed as highly successful by all participants. At the suggestion of the Japanese organizer, Dr. Hirono, all seminar papers which presented new scientific results were submitted for publication in the Journal of the Meteorological Society of Japan. Attachment B is a list of 10 published papers based on the seminar presentations; copies of those papers are included as Seminar Proceedings in Attachment E-2.

PART III–TECHNICAL INFORMATION *(FOR PROGRAM MANAGEMENT USES)*

ITEM *(Check appropriate blocks)*	NONE	ATTACHED	PREVIOUSLY FURNISHED	TO BE FURNISHED SEPARATELY TO PROGRAM	
				Check (√)	Approx. Date
a. Abstracts of Theses	X				
b. Publication Citations		X			
c. Data on Scientific Collaborators		X			
d. Information on Inventions	X				
e. Technical Description of Project and Results		X			
f. Other *(specify)*					

a. Principal Investigator/Project Director Name *(Typed)*	b. Principal Investigator/Project Director Signature	c. Date
Prof. Gerald W. Grams		1/27/88

NSF Form 98A (5-78) Supersedes All Previous Editions

Form Approved OMB No. 99R0013

TABLE OF CONTENTS

ATTACHMENT B

PUBLICATION CITATIONS

ATTACHMENT B: PUBLICATION CITATIONS

M.P. McCormick, P. Hamill and U.O. Farrukh, 1985: Characteristics of Polar Stratospheric Clouds as Observed by SAM II, SAGE, and Lidar. J. Meteor. Soc. Japan, 63, 267-276.

M. Takagi, Y. Morita, A. Iwata and Y. Kondo, 1985: On the Observation Techniques for Statospheric Aerosols. J. Meteor. Soc. Japan, 63, 277-282.

Y. Iwaska, 1985: Lidar Measurement of the Stratospheric Aerosol at Syowa Station, Antarctica. J. Meteor. Soc. Japan, 63, 283-287.

O. Uchino, 1985: On Dispersion Processes of the El Chichon Dust Particles in the Lower Stratosphere. J. Meteor. Soc. Japan, 63, 288-293.

M. Hirono, N. Fujiwara, M. Fujiwara and T. Shibata, 1985: Comparative Study of the Aerosol Properties Measured by Two-Wavelength Lidar and Detector on Balloon. J. Meteor. Soc. Japan, 63, 294-302.

M. Hirono, T. Shibata and M. Fujiwara, 1985: A Possible Relationship of Volcanic Aerosol Varations with El Nino Southern Oscillations - Lidar Observations of Volcanic Aerosols in the Atmosphere. J. Meteor. Soc. Japan, 63, 303-310.

R.M. Nagatani, M.P. McCormick and L.R. McMaster, 1985: A Comparison of SAGE I Data during the Stratospheric Warming of February-March, 1979. J. Meteor. Soc. Japan, 63, 311-319.

D.G. Murcray, F.H. Murcray and F.J. Murcray, 1985: Measurements of Atmospheric Emission at High Spectral Resolution. J. Meteor. Soc. Japan, 63, 320-324.

N. Iwagami, T. Ogawa and K. Shibasaki, 1985: Balloon Measurements of Stratospheric NO_2. J. Meteor. Soc. Japan, 63, 325-327.

A. Matsuzaki, T. Itoh and Y. Nakamura, 1985: On Observation of Middle Atmosphere with LAS (Limb-Atmospheric Infrared Spectrometer) on Board of Satellite "Ohzora" (EXOS-C). J. Meteor. Soc. Japan, 63, 328-333.

ATTACHMENT C-1

U.S. PARTICIPANTS LISTED IN PROPOSAL

PROPOSED U.S. PARTICIPANTS

1. Prof. Gerald W. Grams, School of Geophysical Sciences, Georgia Institute of Technology, Atlanta, GA 30332

   Prof. Grams is the Principal Investigator for this proposal. His observations of the stratospheric aerosol layer in the 1964-65 time period represent the first use of a lidar system for stratospheric research. He has subsequently developed and operated airborne instruments for observations of atmospheric aerosols, the most recent device being a laser polar nephelometer designed for operation at stratospheric altitudes on NASA's U2 aircraft for in-situ measurements of the angular distribution of light scattered from a parallel beam by aerosol particles. He has also served as member of the experiment teams organized by NASA to conduct scientific investigations using data obtained with the SAM II, SAGE, and SAGE II sensors for global observations of stratospheric aerosols and gases.

2. Prof. Theodore J. Pepin, Department of Physics and Astronomy, Univ. of Wyoming, Laramie, WY 82079

   The basic principle of operation of the satellite sensors used by NASA in their SAM, SAM II, SAGE, and SAGE II series was demonstrated during the mid-1960's by Dr. Pepin using instrumentation carried into the stratosphere on high-altitude balloons. Dr. Pepin has been a member of all of the experiment teams organized by NASA for their SAM, SAM II, SAGE, and SAGE II satellite sensors. He has also been Principal Investigator for the ONR-sponsored PAM (Preliminary Aerosol Measurement), PAM II, and POAM (Polar Ozone and Aerosol Experiment) sensors which operate on Air Force satellites. His in-depth involvement with the satellite programs and the balloon observation programs will be extremely valuable at the proposed seminar.

3. Dr. M. Patrick McCormick, Chief, Aerosol Research Branch (MS-275), NASA Langley Research Center, Hampton, VA 23665

   Dr. McCormick has been involved in stratospheric aerosol studies since he began using lidars for atmospheric research during the mid-60's. Under Dr. McCormick's direction, NASA Langley's "48-inch" lidar was developed in the early 1970's and their mobile airborne lidar was developed in the late 1970's. These lidar

systems are generally regarded as the state-of-the-art in lidar instrumentation in the United States, and the stratospheric observations obtained with these systems represent the most complete data set available on the spatial and temporal variability of the optical backscattering properties of stratospheric aerosol particles. Dr. McCormick was the NASA scientist who was responsible for transforming the sensor introduced by Pepin as a balloon-borne instrument into a very successful series of satellite sensors. In his role as NASA's Sensor Scientist for the SAM, SAM II, SAGE, and SAGE II experiments, he has background and experience in the design, fabrication and testing of hardware; in the development of the computer programs for processing the data; in the planning and execution of "ground truth" experiments using lidar, balloon and aircraft data for validating the satellite observations; and in the use of the satellite data for scientific investigations. With the forthcoming launch of the EXOS-C satellite, the breadth and depth of Dr. McCormick's experience in these areas will be of particular interest to our Japanese counterparts at the proposed joint seminar.

4. Prof. David G. Murcray, Department of Physics, Univ. of Denver, Denver, Colorado 80

Dr. Murcray is recognized as one of the most active and productive scientists in the area of research on trace gases in the lower stratosphere using aircraft or balloon-borne infrared spectroscopic instrumentation. Over the past 25 years, his research has included measurements of the distribution of water vapor and other minor constituents in the altitude region between 13 and 30 km, detection of nitric acid in the lower stratosphere, detection of nitrogen dioxide in the stratosphere, and numerous studies related to general problems of infrared radiative transfer involving in-situ observations with aircraft and balloon-borne instruments, ground-based observations, and laboratory experiments. Dr. Murcray has also been directly involved in satellite observations. He is a member of NASA's experiment team for the SAGE program and the forthcoming SAGE II program. He has also served as a member of the experiment team for NASA's CLAES (Cold Limb Atmosphere Etalon Spectrometer) satellite sensor. Dr. Murcray's extensive experience involving atmospheric observations from satellite, aircraft, balloon and ground-based platforms will also make significant contributions to our proposed seminar.

5. Prof. Benjamin J. Herman, Institute of Atmospheric Physics, Univ. of Arizona, Tucson, AS 85721

Prof. Herman's long-standing leadership role in applications of radiation transfer theory to atmospheric remote sensing make him an obvious choice for meeting our needs in discussing and evaluating the validity of the techniques currently in use or proposed to be used to process the data obtained by the satellite, airborne, or ground-based remote sensors. His research has directly addressed the effects of aerosol particles and gases on atmospheric radiation and includes many significant contributions in areas such as lidar and meteorological radar observations, ground-based sun photometer observations, and satellite observations. He has served on NASA experiment teams for the SAM II and SAGE sensors and, during the past two decades, has served on a wide variety of advisory committees making recommendations for research on atmospheric radiation transfer and remote sensing for organizations such as NSF's National Center for Atmospheric Research, NASA, and a number of DOD laboratories. Our seminar must consider the validity of any data analysis procedures that are being used (or are proposed to be used) for processing satellite and other remote sensing data, and Prof. Herman's presence will insure that these problems are handled properly.

6. Mr. Ronald Nagatani, NOAA National Meteorology Center, Climate Analysis Center, (W353, Rm. 201), Washington, D.C. 20333

During NASA's SAM II, SAGE, and SAGE II programs, it was established that the meteorological data was required for an adequate and proper analysis of the data. The Climate Analysis Center assumed the responsibility of providing this data to the various experiment teams, and the Center has developed operational procedures for providing the required data in a useable form. Mr. Nagatani is responsible for implementing this activity and his experience in this type of analysis will make a unique contribution to our seminar in the area of incorporating meteorological information into the data analysis procedures. Dr. Hirono and Mr. Nagatani have already established contact with regard to his potential contribution to Japan's EXOS-C activities, and we anticipate that this opportunity for him to meet with the satellite scientists in Japan will serve to strengthen the possibility of future joint studies between the U.S. and Japanese scientists.

ATTACHMENT C-2

LETTER ON DR. HAMILL'S BACKGROUND AND EXPERIENCE

Georgia Institute of Technology
A UNIT OF THE UNIVERSITY SYSTEM OF GEORGIA
ATLANTA, GEORGIA 30332
SCHOOL OF GEOPHYSICAL SCIENCES
404/894-3893

7 June 1984

Dr. Charles W. Wallace, Program Manager
U.S.-Japan Cooperative Science Program
Division of International Programs
National Science Foundation
Washington, DC 20550

Dear Dr. Wallace:

As we discussed during our telephone conversation earlier this week, an emergency for one of our participants caused him to cancel his plans to attend our seminar in Fukuoka next week. Prof. Pepin had been scheduled to deliver a paper entitled "Interpretation of satellite-based solar extinction measurements" at the seminar.

I was fortunate to be able to find a replacement for Dr. Pepin and his topic in the person of Prof. Patrick Hamill of San Jose State University. He has been actively involved in the interpretation of satellite solar extinction data for a number of years. He has published a good number of papers on the use of SAM II and SAGE data on the detection of polar stratospheric clouds and on the microphysics and formation mechanisms for such clouds. I believe that his background and experience will prove to be extremely valuable at the seminar and that he will fill the void that would otherwise exist because of Prof. Pepin's absence.

I am leaving for Japan tomorrow. I will be happy to supply you with more details on Dr. Hamill upon my return if you do need more information.

With Best Wishes.

Gerald W. Grams
Professor

ATTACHMENT C-3

LIST OF PARTICIPANTS AND OBSERVERS AT SEMINAR

JAPANESE - U.S. COOPERATIVE SCIENCE PROGRAM SEMINAR
REVIEW OF WORK RELATED TO SENSING OF STRATOSPHERIC AEROSOL AND GAS COMPONENTS

12 - 14 JUNE, 1984
Fukuoka, Japan

Participants and Observers

U.S.A.

G.W. Grams	Georgia Inst. Technology
D.M. Cunnold	Georgia Inst. Technology
P. Hamill	San Jose State University
B.J. Herman	Univ. of Arizona
C. Jensen	Ball Aerospace Systems Division
M.P. McCormick	NASA, Langley Research Center
L.R. McMaster	NASA, Langley Research Center
D.G. Murcray	Univ. of Denver
R. Nagatani	NOAA National Meteorol. Center

JAPAN

M. Hirono	Kyushu University
T. Aruga	Radio Research Laboratory
M. Fujiwara	Kyushu University
Y. Iwasaka	Nagoya Univ.
T. Kitamura	Kyushu Univ.
A. Matsuzaki	Space Science Inst. (Representing T. Itoh)
T. Nakashima	Tohoku Univ. (Representing M. Tanaka)
T. Ogawa	Tokyo Univ.
A. Ono	Nagoya Univ.
M. Takagi	Nagoya Univ.
O. Uchino	Meteorol. Research Inst.
M. Uryu	Kyushu Univ.
S. Hayashida	Nagoya Univ.
N. Iwagami	Tokyo Univ.
M. Maeda	Kyushu Univ.
O. Morita	Kyushu Univ.
R. Sawada	Kyushu Univ.
T. Shibata	Kyushu Univ.

CANADA

C.W. Cho	Memorial Univ. of Newfoundland

ATTACHMENT E-1

SEMINAR AGENDA

AGENDA

REVIEW OF WORK RELATED TO SENSING OF STRATOSPHERIC AEROSOL AND GAS COMPONENTS

SEMINAR
UNDER THE JAPAN-US COOPERATIVE SCIENCE PROGRAM

FUKUOKA INTERNATIONAL HALL
1-4-1 TENJIN, CHUO-KU, FUKUOKA, JAPAN

12-14 JUNE 1984

Tuesday, 12 June 1984
10:00 AM - 5:00 PM

Morning (10:00-12:00)

Overview of Sattelite Programs

Joint Session with the SAGE II Science Team Meeting

Chairman Dr. M. P. McCormick

Opening Address M. Hirono

Introduction G. W. Grams
M. Hirono

1. Description of Relevant On-going Sattelite Programs
SAGE II Science Team

LUNCH

Afternoon (13:00-17:00)

In-situ Observations of Stratospheric Aerosol and Gases

Chairman Dr. T. J. Pepin
Dr. M. Takagi

2. In-situ Observations of Aerosol Optical Properties for Validation of Sattelite-Based Aerosol Measurements
G. W. Grams

3. Optical Properties of Tropospheric and Stratospheric Aerosols as Estimated from light Scattering Measurements
M. Tanaka

COFFEE

4. In-situ Measurements of Molecular Forms of Stratospheric Aerosol Particles
A. ONO

5. Balloon Measurements of Stratospheric NO_2
T. Ogawa

6. (invited)
M. Uryu

Evening (17:30-19:30)

RECEPTION

Wednesday, 13 June 1984

9:30 AM - 5:00 PM

Morning (9:30-11:45)

Lidar Observations of Stratospheric Aerosol

Chairman Dr. G. W. Grams

7. Lidar Observations of Volcanic Aerosols in the Stratosphere over Fukuoka

M. Hirono

8. Comparisons between Observational Results of El Chichon Dust Layers by Ruby Lidar at Tsukuba (36.1 N) and Those by UV Lidar at Fukuoka (33.6 N)

O. Uchino

9. Lidar Observations of Stratopsheric Aerosols in the Antarctic and the Middle Latitude

Y. Iwasaka

10 Comment

LUNCH

Afternoon (13:30-17:00)

Lidar and Sattelite Observations of Stratospheric Aerosols

Chairman Dr. D. G. Murcray
Dr. M. Tanaka

11. Stratospheric Aerosol Measurements by Spacecraft Sensors and Lidar

M. P. McCormick

12. Observations of Stratospheric Aerosols Lidar, Balloon and Sattelite

M. Takagi

13. Application of Inversion Techniques to Stratospheric Extinction Data

B. J. Herman

COFFEE

14. Use of Meteorological Data in the Interpretation of Sattelite Observations of Stratospheric Constituents

R. Nagatani

15. Interpretation of Sattelite-Based Solar Extinction Measurements

T. J. Pepin

16. Some results of the SAGE I Data Analysis

M. Fujiwara

Thursday, 14 June 1984

9:30 AM - 5:00 PM

Morning (9:30-11:45)

Sattelite Observations of Stratospheric Constituents

Chairman Dr. B. J. Herman

17. Preliminary Results from Ohzora

T. Ogawa

18. Limb Atmospheric Infrared Spectrum Observed on the Sattelite Ohzora

A. Matsuzaki

19. Infrared Techniques for Measurements of Stratospheric Constituents

D. G. Murcray

20. Comment T. Aruga

LUNCH

Afternoon (13:30-17:00)

Possibility of Joint Studies

Joint Session with the SAGE II Science Team Meeting

Chairman Dr. M. P. McCormick

21. Comment D. M. Cunnold

Free Discussions All Members

Closing Address G. W. Grams

ATTACHMENT E-2

SEMINAR PROCEEDINGS

(Papers published in Journal of the Meteorological Society of Japan)

Characteristics of Polar Stratospheric Clouds as Observed by SAM II, SAGE, and Lidar[1]

By M. P. McCormick

Atmospheric Sciences Division, NASA Langley Research Center, Hampton, Virginia 23665

Patrick Hamill

Systems and Applied Sciences Corporation, Palo Alto, California 94306

and

U. O. Farrukh

Institute for Atmospheric Optics and Remote Sensing, Hampton, Virginia 23666

(Manuscript received 10 December 1984, in revised form 4 March 1985)

Abstract

The discovery of polar stratospheric clouds (PSC's) in the Arctic and Antarctic stratosphere during winter is described, and the directly observed and implied properties of these clouds are discussed. It is proposed that the more familiar "mother-of-pearl" or "nacreous" clouds are a special subset of PSC's. The size, location, prevalence and temperature dependence of the clouds as measured by the SAM II and SAGE satellite systems are outlined. Airborne lidar measurements have recently demonstrated that the PSC phenomenon is most probably associated with an extended stratospheric cloud bank existing within the cold polar vortex region during the winter period with the PSC's bounded by a 188 K temperature isotherm. The PSC's probably exist at a 50 percent frequency within the 193 K isotherm. Using the observed information on the cloud extinction and change in location with time we consider possible formation mechanisms, the size of the cloud particles, and show the descending motion of the cloud during wintertime.

1. Introduction

Polar stratospheric clouds (PSC's) were discovered several years ago during the analysis of the SAM II satellite data. Subsequently, continued remote sensing of the stratosphere by the SAM II and SAGE satellite systems and by a NASA airborne lidar system has yielded a great deal of information on the macroscopic and microphysical characteristics of the clouds. In this paper, we describe in some detail the properties of the PSC's as obtained from the satellite and lidar data sets. In addition to evaluating directly measurable characteristics of the clouds such as their extinction, backscatter coefficient, altitude, temperature, geographic location, and so on, we also infer certain unobservable properties of the clouds, such as the composition and formation mechanism for the cloud particles. Finally,

[1] This paper was presented at the Japan-U.S. Seminar on "Review of work related to sensing of stratospheric aerosol and gas components", Fukuoka, 12–14 June 1984.

we present evidence that the PSC's form an extensive cloud bank over the winter pole, estimate the cloud's particle size, and discuss alternative mechanisms for the apparent downward motion of the clouds.

2. Remote sensing of the stratosphere by the SAM II and SAGE satellite systems and by airborne lidar

In this section we review the three principal ways (SAM II, SAGE and lidar) in which information on polar stratospheric clouds has been obtained. The SAM II instrument consists of a single channel sun photometer which measures solar irradiance at 1 μm wavelength. The instrument is mounted on the Nimbus 7 satellite and is enabled each time the satellite enters into or emerges from the shadow of the earth. Thus, data are taken during each sunrise and sunset encountered by the satellite as indicated schematically in Fig. 1. The irradiances obtained during each scan are a measure of the transmission of solar light which has passed through different levels of the atmosphere. The technique, to invert the transmission versus altitude data and obtain profiles of extinction, is described in Chu and McCormick (1979). Nimbus 7 is in a high noon sun-synchronous orbit with a highly inclined (nearly polar) orbit and a period of 104 minutes. Consequently, 15 sunsets and 15 sunrises are encountered each day in the high latitude bands of about 64°N to 81°N and 64°S to 81°S, and are separated by about 26° in longitude.

The SAGE instrument is similar to SAM II except that it performs measurements at three additional wavelengths: 0.60 μm, 0.45 μm, and 0.385 μm, and extends measurements over a maximum latitude range of about 80°S to 80°N with variations in coverage depending on season. SAGE is mounted on a dedicated AEM-2 satellite with orbital period 96 minutes and inclination 55°. The SAGE system was operational from February 1979 until November 1981. A new instrument to measure stratospheric aerosols and gases has recently been launched from the Space Shuttle. This instrument (called SAGE II) has a latitudinal coverage similar to SAGE but has three more spectral channels. No data from SAGE II, however, will be presented in this paper. A detailed description of the SAM II and SAGE systems is given by McCormick *et al.* (1979).

The SAM II and SAGE results are generally expressed in terms of profiles of atmospheric extinction. During each year of operation, SAM II generates about 10,000 profiles and SAGE generates roughly four times as many (because it has four channels and there is one profile generated for each channel). In Fig. 2 we present an average extinction

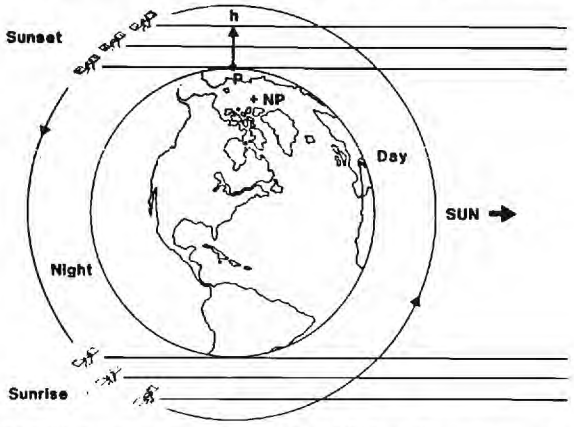

Fig. 1 Schematic representation of the SAM II or SAGE satellite measurement technique.

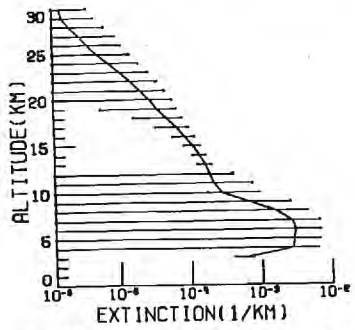

Fig. 2 SAM II average extinction profile for the month of January 1979 in the northern hemisphere. The horizontal bars indicate one standard deviation from the mean (McCormick *et al.*, 1982b).

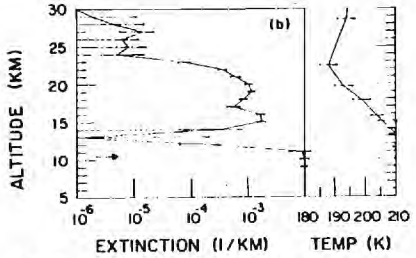

Fig. 3 A polar stratospheric cloud extinction profile obtained from SAM II data for January 23, 1979, at 68.7°N latitude and 27°N longitude (McCormick *et al.*, 1982b). The right panel shows the corresponding temperature profile. The horizontal bars on each curve are the one sigma errors in the measurements.

profile obtained using all of the SAM II northern hemisphere polar data for the month of January 1979. This figure is compiled from over 400 measurements. The horizontal bars represent one standard deviation from the mean. The large variation in extinction is below the 12 km average tropopause.

The airborne lidar system is the other remote sensing technique used to obtain information on polar stratospheric clouds. The airborne lidar system was developed to underfly and validate the SAM II and SAGE measurements. In addition, it has been used to study the spatial distribution of polar stratospheric clouds as well as the stratospheric volcanic veil from El Chichon and other eruptions (McCormick *et al.*, 1984).

3. The discovery of polar stratospheric clouds

The SAM II data for January 1979 showed several very unusual profiles in which the extinction at some heights was much greater than the average monthly extinction (McCormick *et al.*, 1982b). An example of such a profile is presented in Fig. 3. Thirteen of these "anomalous" profiles were observed at SAM II measurement locations in the northern hemisphere during the winter of 1978-79 and all were observed in very cold regions of the stratosphere. For the period July-September 1979 (southern hemisphere winter), however, several hundred similar profiles were observed at southern latitudes. Again, they correlated well with cold temperatures. The profiles showed very large values of extinction (up to values of 10^{-3}/km) at altitudes between about 17 and 24 km in the Arctic and between about 11 and 22 km in the Antarctic. They appeared to be limited in time and space, fairly randomly located geographically, and appeared in regions of very cold temperature. These facts suggested that the profiles might be due to the presence of localized clouds in the stratosphere. It is well known that mother-of-pearl clouds are occasionally observed in the stratosphere; however, according to the literature, these clouds are observed very infrequently. Stanford and Davis (1974) in a literature compilation found recorded evidence for only 148 clouds in a period of about 100 years. Mother-of-pearl or nacreous clouds have been reported to occur at altitudes of 22-26 km and preferrentially downwind of mountain ranges. This led Hesstvedt (1969) to propose an orographic lee wave model to describe mother-of-pearl cloud formation. Due to these significant differences between the SAM II observed phenomenon and the literature descriptions of mother-of-pearl clouds, and especially since it was not clear whether or not the features exhibited by the satellite data would be visible, it was felt that the satellite observations of

high extinction events could not be positively identified as mother-of-pearl clouds. Consequently, the term "polar stratospheric clouds" or PSC's was coined. It is not yet clear that the two phenomena are the same, but we shall show that it is reasonable to assume that the mother-of-pearl clouds are a special subset of the more prevalent PSC's.

4. Large-scale characteristics of polar stratospheric clouds

In this section we shall briefly review the retrieved information obtained on PSC's by the remote sensing techniques described above. We shall consider the extinction due to the clouds, the size of the clouds, their duration, the prevalence and location of the clouds both geographically and in altitude, and finally we shall consider the relation between low temperatures and cloud observations.

(a) *Extinction Measurements*

The SAM II extinction profiles of PSC's give the extinction as a function of height (in 1-km steps) thus yielding information on the vertical thickness of the cloud as well as the value of their extinction. It should be noted that the operational technique used to invert the transmission data rejects profiles with extinctions greater than 10^{-3}/km. Consequently, we only obtain a record of clouds with extinction less than this value. Visual inspection of the retrieved transmission profiles indicates that this results in the loss of a few cloud events from the record, but since so many clouds are observed, the loss is not significant. The extinction due to the clouds is quite variable. For example, during 1979 the northern hemisphere clouds had maximum extinction values ranging from 4.5×10^{-4}/km to 6×10^{-4}/km. Compared to measurements of extinction at the same altitude on days when no clouds were observed, these data correspond to increases in extinction by factors ranging from about 10 to over 200. It is found that in some cases the cloud is relatively thin (<1 km), but in the majority of the observed cases, and especially in the southern hemisphere, the clouds are several kilometers thick. Later in this paper we shall present lidar data which show Arctic PSC's with multiple thin layers sometimes even less than 1 km. Often in the southern hemisphere, PSC's appear to extend down to the tropopause.

(b) *Spatial Extent of the Clouds*

Fifteen extinction profiles are obtained by SAM II in each hemisphere per day. One can interpolate between these profiles to generate isopleth plots of extinction as a function of

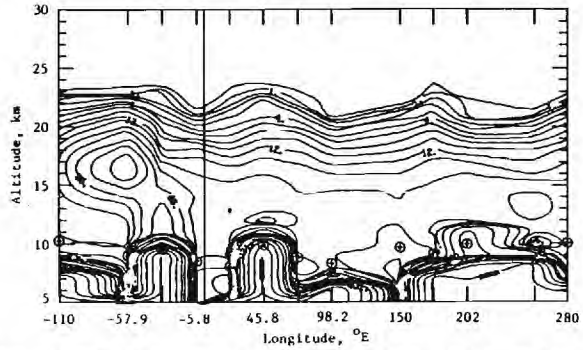

Fig. 4 Isopleth of extinction as a function of altitude and longitude for measurements obtained on June 28, 1979 at 65°S latitude. The tic marks on the upper horizontal border represent the longitudes at which measurements were made. The plot was generated by interpolating extinction values between these measured extinction profiles.

altitude and longitude. An example of such a plot where a PSC is observed in one measurement is presented in Fig. 4. Polar stratospheric clouds show up clearly on this type of plot, as can be appreciated by noting the high extinction region at 17 km altitude and −57.9° longitude. Actually, only one SAM II measurement (at 57.9°W longitude) on that day observed a PSC. A large number of examples of these plots are presented in McCormick *et al.* (1982a).

It is found that in the northern hemisphere, cloud observations tend to appear in only one or two profiles each day, whereas in the southern hemisphere, especially late in the winter, they tend to appear in nearly every profile. Thus, the northern hemisphere SAM II data tend to indicate small localized clouds whereas the southern hemisphere data suggest a large cloud bank. If one envisages the PSC's as forming an extensive cloud bank covering the pole, then it is possible that the northern hemisphere SAM II observations skirt the edge of the cloud bank and thus only sight an occasional cloud, whereas in the colder southern hemisphere stratosphere, the cloud bank possibly extends to lower latitudes so the SAM II observations would sight a cloud on each measurement.

The size of the clouds (or extent of the cloud bank) cannot be determined on the basis of the SAM II data alone since its measurement location is at a fixed latitude on a given day. To help answer this question, an airborne lidar mission was conducted during the period January 19-28, 1984 to the North Pole. A flight was performed on January 24, 1984, from Thule Air Base, Greenland (76.5°N, 68.7°W) to the North Pole along the 60°W meridian. During this flight, PSC's were observed continuously over the entire latitude range with the strongest backscatter occurring from 85° to 90°N. The altitude of the clouds ranged from about 19 km to 23 km. Ambient temperatures were less than 188 K (−85°C) in the region where the strongest clouds were observed. Figure 5 gives a composite picture of the lidar observations of PSC's on this flight. Strong lidar backscatter is indicated by the dark bands. Multiple layers are shown at most locations. Also note the general trend towards lower altitudes as one approaches the pole. Figure 6 gives an individual ruby lidar backscatter profile (at cross polarization and a wavelength of 0.6943 μm) at about 86°N in which the PSC at 19.5 km has a scattering ratio of 83.3. The volcanic loading at this time due to past eruptions produced a scattering ratio of about 3 centered near 15 km and

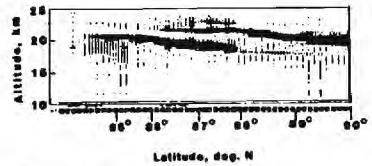

Fig. 5 Airborne lidar data from 83°N to 90°N at 60°W longitude on January 24, 1984. The darkness of the display is proportional to the backscattered lidar return signal. The return from 85.5°N to 87.8°N is for the cross polarized component which, in general, is an indicator of nonspherical particles.

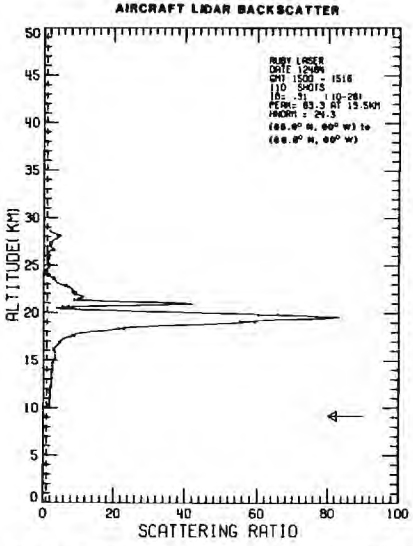

Fig. 6 Backscatter profile at 0.6943 μm for cross polarization obtained by airborne lidar on January 24, 1984 at 86°N, 60°W. The arrow indicates the height of the local tropopause.

would not, therefore, confuse the identification of PSC's.

A second mission was conducted on January 25 from Thule to 86°N, and PSC's were again detected within the region of temperatures less than 188 K from 81°N to 86°N. A third flight was conducted on January 27 to 87°N with no indication of PSC's. On this day, the low temperature region within the polar vortex had moved over the North Pole towards Siberia. Thus, we conclude from the lidar data that the PSC's are actually an extensive cloud bank composed of one or more layers which cover the polar region and are bounded at a minimum by a temperature isotherm of about 188 K. Further, we feel that PSC's occur at about a 50 percent frequency within the 193 K isotherm.

(c) *Duration, Prevalence and Location of PSC's*

From the satellite and lidar data, one can obtain a relatively good picture of the duration, prevalence, and location of the polar stratospheric clouds. The lidar data, indicating that the PSC's form a continuous cloud bank covering the Arctic area within a specific cold temperature contour are supported by the SAM II data indicating that a similar cloud bank exists over the Antarctic. The clouds are sighted in the northern hemisphere primarily during December, January and February, and the southern hemisphere clouds are sighted primarily during July, August, and September.

The histogram in Fig. 7 shows that the cloud sightings in the Antarctic for June-September 1981 were distributed fairly uniformly in longitude with a slight preference for longitudes between 20°E and 40°E. Other years show a slight bias nearer to Greenwich. All years had a lesser number of clouds at 180° longitude. This corresponds to a general trend for temperatures to be somewhat colder at these longitudes. For example, the data compilation by Taljaard *et al.* (1969) shows that during July and October at 70°S, the average temperature at 200 mb is 5 K colder at 0° longitude than at 180° longitude. At 100 mb the October temperature difference is 8 K colder. Thus, it is not surprising that the clouds are more prevalent near the Greenwich meridian.

The altitude distribution of the clouds is indicated in the histogram of Fig. 8 which shows clearly that the southern hemisphere clouds are found at lower altitudes than the northern hemisphere clouds. This also agrees with cold temperatures being lower in the Antarctic lower stratosphere than in the Arctic stratosphere. In Fig. 9, we have plotted the average weekly altitude of PSC's sighted by SAM II in the Antarctic during a 13-week period from June 28, 1981, to September 26, 1981. Although there is a large scatter in the data (note the large standard deviations), one can note a distinct trend towards lower altitudes as the winter progresses. A linear regression analysis of these data yield a line of

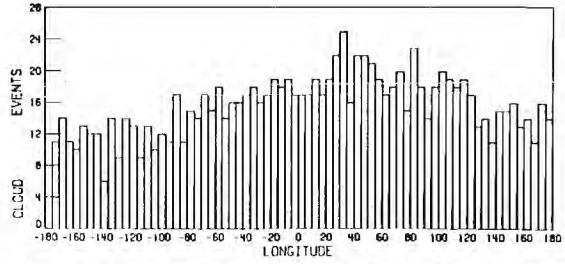

Fig. 7 Histogram illustrating the longitudinal distribution of PSC's for the Antarctic winter of 1981. Note that the clouds are nearly uniformly distributed but slightly more prevalent in 20°-40°E longitude and slightly less prevalent around 180° longitude.

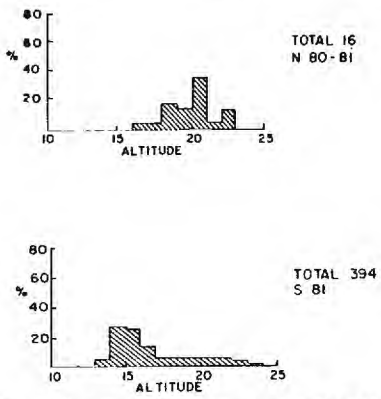

Fig. 8 Histogram of the frequency of PSC altitude in the two hemispheres during 1980-81. Top figure is for northern hemisphere winter and bottom figure is for southern hemisphere winter. The total number of PSC's observed is also indicated.

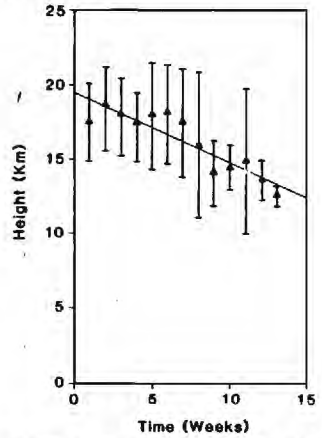

Fig. 9 Plot of average weekly altitude of clouds slighted during the southern hemisphere winter of 1980, as function of time (in weeks).

slope −0.465 km/week. Thus, the average altitude of the clouds appear to descend at a rate of 0.77 mm/sec (in agreement with the downward flux of air in the Arctic polar vortex determined in Kent *et al.*, 1985). This apparent downward trend of PSC's and temperature was also observed in McCormick

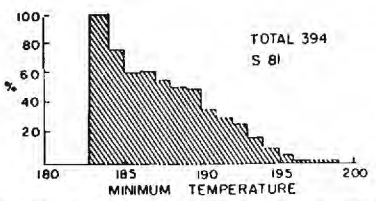

Fig. 10 Histogram of the frequency of cloud observations as a function of temperature for the southern hemisphere winter of 1981.

et al. (1981). One must be careful in interpreting Fig. 9, however, because the SAM II measurements over this period of time change from about 64°S to 80°S. Thus, this downward altitude change could be due to geographical changes of the altitude of the cold temperature field.

(d) *Correlation Between Low Temperatures and Cloud Occurrences*

The SAM II data, in conjunction with the temperature profiles generated by NOAA at the time and location of the SAM II measurements, reveal that the occurrence of clouds is highly correlated with low temperatures. For example, Fig. 10 shows that for the southern hemisphere winter of 1981, the probability of formation of PSC's when the minimum temperature fell below 184 K was about one, and whenever the temperature was above 199 K, no cloud was ever observed. These temperature statistics are slightly different in the northern hemisphere, and slight differences are noted from year to year; nevertheless, the general trend of cloud formation with low temperature is quite clear. For a complete description of the SAM II observations of PSC's in 1979 and their temperature dependence, see McCormick *et al.* (1982b).

5. Inferred microscopic properties of the cloud particles

The SAM II, SAGE, and lidar data can be used to infer certain microphysical properties of the polar stratospheric clouds. This involves assumptions concerning the mechanism for their formation. As described by Steele *et al.* (1983), the most probable cloud forma-

tion mechanism is the condensation of water onto pre-existing stratospheric aerosol particles. The aerosol particles (which act as cloud condensation nuclei, CCN) are believed to be liquid concentrated sulfuric acid droplets of about 75% H_2SO_4 by weight (Rosen, 1971; Hamill *et al.*, 1977). The equilibrium concentration of sulfuric acid in such a droplet is a function of temperature and the environmental water vapor content. Assuming that the stratospheric water content remains constant, a change in temperature will cause water vapor to condense onto the aerosol particles. This will result in a more dilute acid droplet, but will have a very small effect on the particle radius. Eventually, however, the droplet becomes so dilute it is essentially pure water (or pure ice if it freezes). From then on, deliquescence becomes important and decreases in temperature will be accompanied by large changes in radius. If this model is correct, then it is relatively easy to calculate particle radius as a function of temperature for a given stratospheric water vapor mixing ratio. Once the radius has been determined, one can evaluate the extinction by Mie scattering methods. Thus it is possible to calculate the extinction as a function of temperature and compare the results with SAM II measurements. The best fit to the data was shown in Steele *et al.* (1983) to occur for number densities of about 6.3/cm³ (see Fig. 11). It should be mentioned that for these calculations, the cloud droplets were assumed to be spherical ice crystals. However, the temperatures at which PSC formation occurs are more conducive to the formation of needle-like ice crystals, and this may lead to uncertainties in the expected extinction. (Hamill and McMaster, 1984).

It is possible to obtain a rough estimate of the size of polar stratospheric cloud particles by assuming they grow by the condensation of water vapor onto pre-existing stratospheric aerosol particles. The stratospheric sulfuric acid aerosol particles (the CCN) are believed to obey a log normal size distribution (Pinnick *et al.*, 1976) such that the number of particles having radii between r and $r+dr$ is given by

$$dN/dr=(N_0/\sqrt{2\pi}\, r \ln\sigma)\exp\left[-\frac{\ln^2 r/r_g}{2\ln^2\sigma}\right]$$

We have used this size distribution in a Mie scattering routine and found that the calculated values of extinction at 1.00 μm and at 0.45 μm, as well as the ratio of these extinctions and the backscatter coefficient at 0.6943 μm, are all in agreement with the SAM II, SAGE,

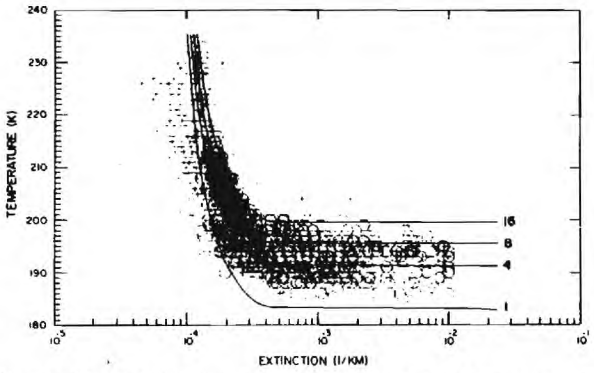

Fig. 11 Calculated extinction vs temperature curves at 20 km altitude for various values of stratospheric water vapor content assuming frozen spherical particles (in ppmv). Crosses represent northern hemisphere SAM II data and circles represent southern hemisphere SAM II data (Steele *et al.*, 1983).

and lidar observations of the background stratospheric aerosol if one uses in the log normal relation the values $N_0=6.3$ particles/cm³, $r_g=0.0725$ μm, $\sigma=1.86$.

If the growth of aerosol particles is modelled by simply assuming that the log normal distribution is shifted to a larger mode radius (not changing the total number of particles present or the width of the size distribution), we find general agreement between theory and the SAGE data (for the two PSC's observed by SAGE at the two wavelengths 0.45 and 1.0 μm) if the mode radius of the PSC droplets is between 0.1 and 0.3 μm. The SAM II data tend to indicate somewhat larger droplet sizes (up to 0.5 μm), and the lidar data are consistent with droplets of 0.2 to 0.3 μm.

The sedimentation rates for these particles can be evaluated by using Stoke's law with the Cunningham correction (List, 1951)

$$v(r)=\frac{2}{9}\frac{r^2\rho g}{\eta}\left(1+A\frac{l}{r}+Qe^{-br/l}\right)$$

where r is the particle radius, ρ is the particle density, η is the dynamic viscosity coefficient, and l is the mean free path of the atmosphere. A, b and Q are dimensionless empirical constants given by $A=0.864$, $Q=0.290$, and $b=1.25$. The U.S. Standard Atmosphere (1976) gives aeronomic parameters at 22 km. Using $\rho=1.0$ g/cm³ we find values of terminal velocity of the order of 10^{-2} mm/sec. This is a negligible velocity corresponding to fall distances of the order of 100 meters in 3 months.

Clearly, sedimentation does not explain the downward motion illustrated in Fig. 9 unless the PSC droplets are much larger in size than indicated by our calculations. The downward motion of the clouds could be due to descending air inside the polar vortex, however, as described by Kent *et al.* (1985) or if the particles are larger, a combination of sedimentation and downward mass flow. If we assume, for example, all of the available water substance is incorporated into the PSC particles, they can be as large as approximately 2 μm radius (Hamill and McMaster, 1984). Thus they would have an appreciable sedimentation rate.

In view of the fact that polar stratospheric clouds are generally found inside the vortex, it is safe to assume that they partake of this downward motion. It is possible that this downward motion of PSC's could represent a mechanism for moving water to at least the tropopause region. The amount of water substance removed from the stratosphere by this mechanism, however, would probably be a very small fraction of the total stratospheric water budget. This is fairly obvious if one considers the small cross-sectional area of the region of the earth where the PSC's occur. However, the water vapor distribution in the lower stratosphere could be affected.

Finally, preliminary calculations indicate that polar stratospheric clouds could have impact on the radiation balance of the polar region (Hamill and McMaster, 1984, and Pollack and McKay, 1985). Before definitive conclusions can be reached regarding the impact of PSC's on radiation and gaseous budgets and their general role in atmospheric processes, however, more data are needed on their microphysical and optical properties.

Acknowledgement

One of us (PH) was supported by NASA Grant number NASW-3762 and another (UOF) was supported by NASA Grant NAS-17032.

References

Chu, W. P. and M. P. McCormick, 1979: Inversion of stratospheric aerosol and gaseous constituents from spacecraft solar extinction data in the 0.38-1.0 μm region. *Appl. Opt.*, 18, 1404-1413.

Hamill, Patrick and L. McMaster, eds., 1984: *Polar Stratospheric Clouds, Their Role in Atmospheric Processes.* NASA Conference Publication 2318, 72 pp. Available from NTIS, Springfield, Virginia.

——, A. B. Toon, C. S. Kiang, 1977: Microphysical process affecting stratospheric aerosol particles. *J. Atmos. Sci.* **34**, 1104-19.

Hesstvedt, E., 1969: The physics of nacreous and noctilucent clouds. *Stratospheric Circulation*, W. L. Webb, Ed. Academic Press, 209-217.

Kent, G. S., C. R. Trepte, U. O. Farrukh and M. P. McCormick, 1985: Variation in the stratospheric aerosol associated with the north cyclonic polar vortex as measured by the SAM II satellite sensor. *J. Atmos. Sci.*, in press.

List, R. J., 1951: *Smithsonian Meteorological Tables*, 6th Ed., Smithsonian Institute Press, Washington, D.C., 527 pp.

McCormick, M.P., Patrick Hamill, T.J., Pepin, W.P. Chu, T.J. Swissler and L.R. McMaster, 1979: Satellite studies of the stratospheric aerosol. *Bull. Amer. Meteor. Soc.*, **60**, 1038-1046.

———, W P. Chu, G.W. Grams, Patrick Hamill, B.M. Herman, L.R. McMaster, T.J. Pepin, P.B. Russell, H.M. Steele and T.J. Swissler, 1981: High-latitude stratospheric aerosols measured by the SAM II satellite system in 1978 and 1979. *Science*, **214**, 328-331.

———, H.M. Steele and Patrick Hamill, 1982a: SAM II Measurements of the Polar Stratospheric Aerosol, Vol. II-April 1979 to October 1979. NASA Reference Publication 1088, Available from NTIS, Springfield, Virginia. March 1982, 78 pp.

———, H.M. Steele, Patrick Hamill, W.P. Chu and T.J. Swissler, 1982b: Polar stratospheric cloud sightings by SAM II *J. Atmos. Sci.*, **39**, 1387-1397.

———, T.J. Swisser, W.H. Fuller, W.H. Hunt and M.T. Osborn, 1984: Airborne and ground-based lidar measurements of the El Chichon stratospheric aerosol from 90°N to 56°S, *Geofisica Internacional*, **23-2**, pp. 187-221.

Pinnick, R.G., J.M. Rosen and D.J. Hoffman, 1976: Stratospheric aerosol measurements III: Optical model calculations. *J. Atmos. Sci.*, **33**, 304-314.

Pollack, J.B. and C.P. McKay, 1985: The impact of polar stratospheric clouds on the heating rates of the winter polar stratosphere. *J. Atmos. Sci.* in press.

Rosen, J.M., 1971: The boiling point of stratospheric aerosols. *J. Appl. Meteor.*, **10**, 1044-1045.

Stanford, J.L. and J.S. Davis, 1974: A century of stratospheric cloud reports: 1870-1972. *Bull. Amer. Meteor. Soc.*, **55**, 213-219.

Steele, H.M., Patrick Hamill, M.P. McCormick and T.J. Swissler, 1983: The formation of polar stratospheric clouds. *J. Atmos. Sci.*, **40**, 2055-2067.

Taljaard, J.J., H. van Loon, H.L. Crutcher and R.L. Jenne, 1969: *Climate of the Upper Air, Part 1—Southern Hemisphere, Vol. 1—Temperatures, Dew Points and Heights at Selected Pressure Levels.* NAVAIR 50-1C-55. Available from Naval Weather Service, Washington, D.C. 20390. (6 pp. text, 133 figures.)

U.S. Standard Atmosphere. U.S. Government Printing Office, Washington, D.C., 1976, 277 pp.

SAM II, SAGE およびライダーにより観測された極域成層圏雲の特性

M.P. McCormick

Atmospheric Sciences Division, NASA Langley Research Center, Hampton Virginia 23665

Patrick Hamill

Systems and Applied Sciences Corporation, Palo Alto, California 94306

and

U.O. Farrukh

Institute for Atmospheric Optics and Remote Sensing, Hampton Virginia 23666

北極および南極の冬期成層圏に見出された極域成層雲 (polar stratospheric clouds: PSC) のについて述べると共に，それらの雲の性質についての議論を行なう。よく知られた"真珠母雲"は PSC 特殊例と考えられる。SAM II と SAGE により観測された PSC の大きさ，位置，卓越性，温度依存性の概要をまず述べるが，航空機搭載のライダーによる観測は，PSC 現象が冬期に極域寒冷渦内に存在する extended stratospheric cloud bank とおそらく関連して起っていることを示している。PSC は頻度 50% で 193 K の等温線内に存在していると考えられる。雲の extinction および位置の時間変化についての観測事実にもとずき，考えられる形成機構，雲粒子の大きさを考察し，さらに，冬期の雲の下降を示す。

NOTES AND CORRESPONDENCE

On the Observation Techniques for Stratospheric Aerosols[1)]

By Masumi Takagi, Yasuhiro Morita, Akira Iwata and Yutaka Kondo

Research Institute of Atmospherics, Nagoya University, Toyokawa 442

(Manuscript received 7 November, 1984, in revised form 23 January 1985)

1. Introduction

It has been recognized that the existence of stratospheric aerosols is important not only climatologically but also on the environmental stand point, and the observation of temporal and spatial behaviors of aerosols is requested. We have adopted a few different kinds of techniques to measure the distribution of aerosols in the lower stratosphere. Here described is an outline of these techniques which we have actually used recent years. Some examples of observed results are also shown.

2. In situ measurement by using balloons

In order to obtain accurate, though local, information on aerosols, it is most essential to carry out in situ measurement by directly sampling the air into an apparatus. The apparatus of our balloon use is based on the principle of counting individual aerosol particles one by one through detecting their scattering light pulses. The number of detected light pulses in a unit time interval shows the aerosol density and the pulse height indicates the particle size. The size of detectable aerosols is limited to those usually larger than 0.3 μm because the visible light is used as the light source. Fig. 1 shows the optical system of our aerosol counter. The rays from the light source is focussed on the scattering chamber, where the sampled air flows with an appropriate rate (0.3-1 *l*/min) perpendicularly to the ray path. The particle in sampled air scatters the light, which is detected in the scatter angle of 60° by a photomultiplier tube. A part of air flow, after passing through a filter, is used as an air sheath to surround the sample air stream. This device is useful to maintain the laminar flow and to protect the sample air against the eddy deviation out of the light scattering part. A halogen lamp is used for the light source because of its stability and efficiency. The intensity of source light is calibrated by periodically feeding through a light tube to the same photomultiplier.

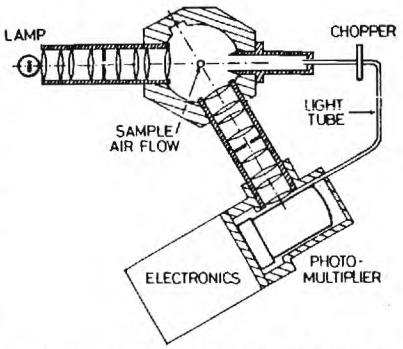

Fig. 1 Design of optical system of balloon-use light-scattering aerosol counter.

1) This paper was presented at the Japan-U.S. Seminar on "Review of work related to sensing of stratospheric aerosol and gas components", Fukuoka, 12-14 June 1984.

There are a few problems peculiar to this kind of light scattering type aerosol counter. One is the effect of the shape and the refractive property of aerosols to be measured. It has to be considered that the scattered light intensity, even though from the same size particle, is different according to the particle being spherical or of irregular shape or of different refractive index. The main composition of stratospheric aerosols is considered as 75% sulphuric acid droplet (Rosen, 1971; Hamill *et al.*, 1977) except for the period just after the serious volcanic eruptions, so it is reasonable to regard the measured aerosols being spherical and of refractive index $m=1.4$. The actual procedure for calibrating the apparatus is made by using standard particles of polystylen latex ($m=1.6$), and then we convert the scattering intensities to those of $m=1.4$. Fig. 2 shows the result of Mie scattering computation for the scattered intensities of particles of $m=1.4$ and 1.6, respectively, for the design applied to our optical system. For the diameter of 0.3 μm the output intensity for the particle of $m=1.4$ is only half of that of $m=1.6$. Hence to count the stratospheric aerosols of 0.3 μm in diameter, the increase of signal to noise ratio was required. It was realized by improving the structure of scattering chamber so as to minimize stray light and by raising the source light intensity.

The other problem is the coincidence loss, which is a count miss occurring when the aerosol density exceeds an expected value. For example, if two or more particles come in the scattering part at the same instant, the apparatus will count one scattered pulse whose intensity corresponds to somewhat larger size particle. The aerosol density at which this count miss occurs relates to the size of scattering part and the flow rate. The design here is confirmed empirically to well meet the density up to several tens particles per cubic centimeter. The stratospheric aerosols larger than 0.3 μm in diameter usually have the density less than 10 cm^{-3} except for the period under a strong aftereffect of large scale volcanic eruptions such as Agung and El Chichon.

For the performance of sucking pump, it is desirable to keep the efficiency uniform over a wide external pressure and temperature range from the earth's surface to the stratospheric height. We have adopted a lobe pump which was newly designed so to

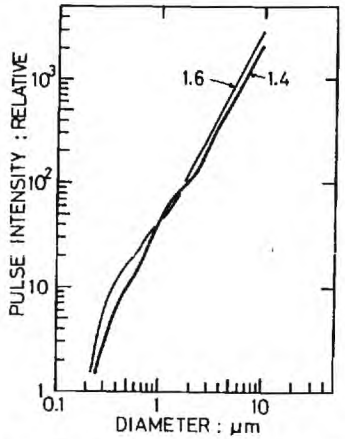

Fig. 2 Size dependence of scattered light pulse intensity calculated for the particle refractive index of 1.4 and 1.6 in the case of the optical system design shown in Fig. 1.

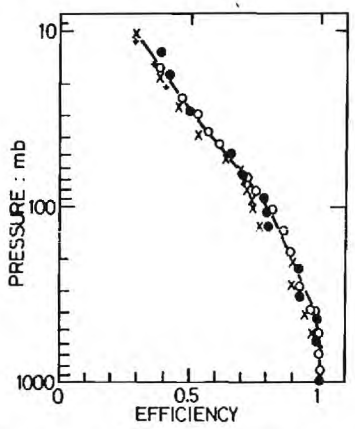

Fig. 3. Pressure dependence of volume flow rate efficiency for sucking pump rotation. Respective symbols correspond to different series of laboratory experiments.

partly meet the above demand. Fig. 3 is the result of laboratory experiment on the efficiency of volume flow rate. It is shown that the sucking efficiency for one rotation of pump falls gradually with descending pressure and reaches at 30 mb about half of that on the ground. The rotation rate of pump at a constant voltage power supply, on the other hand, increases with descending pressure up to 30% at 100 mb and then holds an almost constant value. This increase of rotation rate works to partly compensate the efficiency decrease in higher altitudes. In the actual balloon observations we measure the rotation per minute to estimate the flow rate as accurate as possible.

Fig. 4 shows as an illustration of the performance of apparatus the result of comparative measurement made at Laramie, Wyoming. Two aerosol counters, ours and that developed at University of Wyoming (Hofmann *et al.*, 1975), were launched on board the respective balloons with about 4 hours time interval in the early morning of May 30, 1975. The profile of aerosol density obtained by our counter after revising for the flow rate and refractive index was in a good agreement with that of University of Wyoming. For the details of apparatus and the results of observations refer to Morita and Takagi (1983). The total weight including batteries of the capacity of 8 hours operation is 30 kg.

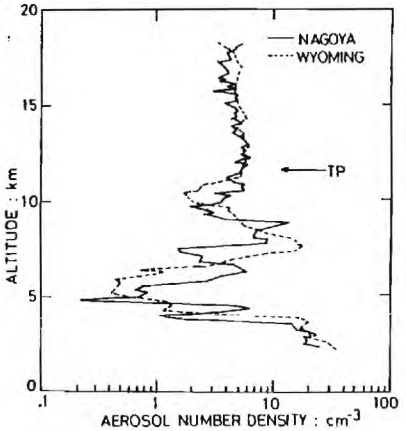

Fig. 4 Vertical profiles of aerosol number density larger than 0.3 μm in diameter in the comparative balloon measurements at Laramie, Wyoming on May 30, 1975. Two profiles were obtained with the respective aerosol counters developed at Nagoya University (full line) and at University of Wyoming (broken line).

For the aerosols in Aitken size range an apparatus equipped with a special type of cloud chamber is being prepared. The electric conductivity meter of balloon use gives also an indirect indication of extraordinary increase of stratospheric Aitken particles (Kondo *et al.*, 1982).

3. Satellite global observation

It is important in the stratosphere to know the variations over very wide area, and the global monitoring by satellite is expected to be effective in this point. The satellite aerosol experiments have been conducted by U.S. scientists with SAM II and SAGE I, and SAGE II is just in operation. We also are making observations of stratospheric aerosols with ALA (Aerosol Limb Absorption) experiment on board the satellite "Ohzora" which was launched in February 1984. The principle of those satellite observations is the measurement of sunlight extinction caused in the earth's limb atmosphere. The sunlight intensity I_0 in the case of small solar zenith angle, where no attenuation of light may be considered, and the intensity $I(h)$, when the sun is seen at the tangent height h above the earth's horizon, are compared. The optical depth $\tau(h)$ of the light path is obtained from the ratio of I_0 and $I(h)$. If we assume a uniform layer structures of aerosols and neutral molecules in the same altitude within the extinction area, we can convert $\tau(h)$ to the vertical profile of extinction coefficient with an inversion procedure. The method of analysis was reported in detail by Takagi and Kondo (1983).

The measurement of aerosols is made at the wavelength of 1 μm, where the extinction is actually composed of Mie scattering of aerosols and Rayleigh scattering of neutral molecules. For subtracting the effect of

neutral molecules, the calculation is made by applying the standard atmosphere within the expected accuracy of 10%.

A weakness of this method is the low spatial resolution in horizontal direction, which comes from the length of ray path where the sunlight suffers attenuation. If the satellite altitude is 1000 km planned to be the apogee, the horizontal resolution is about 200 km corresponding to the vertical resolution of 1 km. In addition to this the satellite moves more than 1000 km on the globe for a few minutes when the sun sets or rises between the earth's surface and 50 km tangent height. It means that the profile thus obtained for each sunrise or sunset is an average over the horizontal scale of the order of 1000 km on the globe.

There are a few points to be considered in the design of sensing unit. Fig. 5 shows the size and shape of solar disk at several altitudes in the vertical cross-section above the tangential point. When the solar disk is close to the earth's horizon, the image becomes flat because of atmospheric refraction. Although the size of disk image depends on the satellite altitude, it somehow has to be divided into small segments to obtain the vertical resolution of 1 km. In our satellite device a CCD image sensor of 380×488 elements is used. Overall sensing area is 8.8×11.4 mm. We use a lens of focal length of 76 mm, and

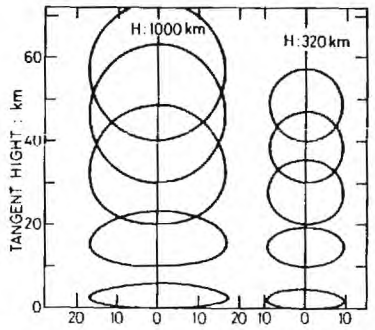

Fig. 5 Image of solar disk in the vertical cross-section above the tangential point for two satellite altitudes corresponding to the planned apogee and perigee (H=1000 and 320 km).

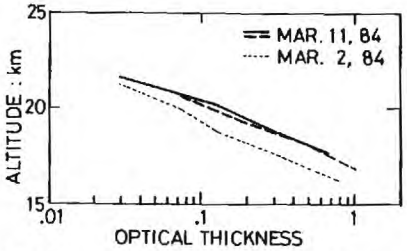

Fig. 6 An example of the measurement of optical thickness against the tangent height preliminarily estimated. The data were obtained at the latitude of 60-70°S. The effect of Rayleigh scattering is not yet subtracted.

the whole field of view covers 6°, within which the satellite may point at the sun. The solar disk of 32′ in diameter is divided into about 30×30 elements and the intensity of each element is measured.

Another problem comes from the disagreement between the directions of the horizon and the scan in CCD sensor. The satellite "Ohzora" is controlled in two axes but not regarding to the phase angle around the axis pointing at the sun. Some special means are taken for data acquisition, to suppress the data quantity to a limited data transfer and moreover to secure a necessary accuracy. The details will appear elsewhere.

The observation data are being accumulated. Here we can only present an example of preliminary reduction. Fig. 6 shows the profile of optical thickness against tangent height obtained on March 2 and 11, 1984 at the latitude 60-70°S. The estimation of tangent height still involves an uncertainty of a few kilometer, which is improved through further detailed analysis of satellite orbit and attitude.

4. Lidar observation

The merit of lidar is that the frequent observation can be made easily. It enables us to follow the stratospheric aerosol content variations in various time scales. Our lidar system (Iwata *et al.*, 1983) at Toyokawa (34.8°N, 137.4°E) has entered in a routine base observation since December 1982. It was

eight months behind the eruption of El Chichon, but it could run after the decaying behaviors of aerosol cloud over Toyokawa (Iwata and Takagi, 1984).

The system parameters are given in Table 1. The system is composed of Nd:YAG laser, whose fundamental, the second and the third harmonic wavelengths are usable, and dye laser which is pumped by the second harmonic of the former. This combination was adopted to observe the aerosols with three wavelengths of YAG laser and the minor gas constituents such as ozone with tunable dye laser output.

For the routine observation of aerosols the wavelength of 532 nm, the second harmonic of YAG laser, has been mainly used because of its high emitting power and efficiency of detecting photomultiplier. The system is usually operated in photon counting mode with a height resolution of 300 m in the altitude range from 6 to 44 km. Accumulation of received signals for 10 to 20 min (6000 to 12000 laser pulse shots) gives an accurate aerosol profile up to 30 km within 10% measurement error. The analogue output mode treated with a transient memory is used to obtain more detailed aerosol structure in the lower altitudes with a height resolution of 15 m.

All the data collecting system are controlled with a minicomputor. Quick-look display of the collected data on the screen can be made anytime after the data have been stored on the magnetic disc. At the end of a series of measurement the data from the magnetic disc are copied in the magnetic tape and processed with a main computer.

Fig. 7 is an example showing the result of lidar observation. In winter at Toyokawa we are favored by relatively good weather and can carry out the observations without long

Table 1 System parameters of lidar at Toyokawa.

YAG laser	fundamental	2nd harmonic	3rd harmonic
wavelength (nm)	1064	532	355
energy/pulse (mJ)	1200	500	180
repetition rate (pps)		10	
pulse width (ns)		15	
dye laser	fundamental	2nd harmonic	
wavelength (nm)	550-730	280-360	
energy/pulse (mJ)	130	30	
receiving telescope	500 mm Newtonian		
transient memory	10 ns-500 ms	2048 words	8 bit
photon counter	2 μs-10 μs	128 memories	12 bit

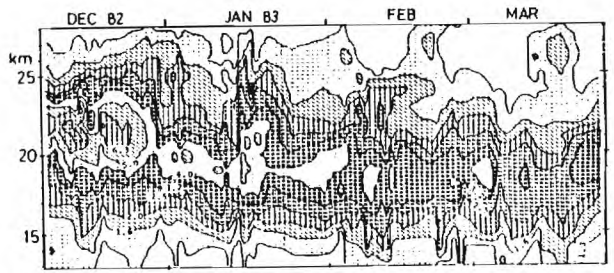

Fig. 7 Variation of lidar backscattering ratio during the period from December 9, 1982 to March 25, 1983. The observations were made at evening hours of 55 days. The interruption of data, which is interpolated in the figure, was 6 days at longest during this period.

interruption. Fig. 7 shows the contours of backscattering ratio during about 100 days from December 9, 1982 to March 25, 1983. In this period the aerosol cloud originated in El Chichon eruption was in the phase of gradual decaying accompanied with occasional abrupt changes. These patterns will be useful to understand the general behavior of stratospheric aerosols.

5. Concluding remarks

Three different techniques for the observations of Mie size aerosols in the stratosphere have been described. The techniques have the respective merits and demerits according to the spatial or temporal scales to be observed. It is useful to correlate the results obtained with one technique to the others for the comprehensive understanding of aerosol circumstances and at the same time for the mutual valuation of the respective measurements.

References

Hamill, P., C. S. Kiang and R. D. Cadle, 1977: The nucleation of H_2SO_4-H_2O solution aerosol particles in the stratosphere. *J. Atmos. Sci.*, **34**, 150-162.

Hofmann, D. J., J. M. Rosen, T. J. Pepin and R. G. Pinnick, 1975: Stratospheric aerosol measurements I: Time variation at northern midlatitudes. *J. Atmos. Sci.*, **32**, 1446-1456.

Iwata, A., Y. Kondo and M. Takagi, 1983: A laser radar system for the observation of minor atmospheric constituents in the stratosphere. *Proc. Res. Inst. Atmos., Nagoya Univ.*, **30**, 25-35.

——— and M. Takagi, 1984: Lidar observation of decaying El Chichon eruption cloud over Toyokawa, Japan (35°N). *Res. Lett. Atmos. Elec.*, **4**, 11-16.

Kondo, Y., R. Reiter, H. Jäger and M. Takagi, 1982: The effect of the Mt. St. Helens eruption on tropospheric and stratospheric ions. *Pure Appl. Geophys.*, **120**, 11-17.

Morita, Y. and M. Takagi, 1983: Balloon measurements of stratospheric aerosol by light-scattering aerosol particles counters. *Bull. Inst. Space Astron. Sci.*, **8**, 87-99.

Rosen, J. M., 1971: The boiling point of stratospheric aerosols. *J. Appl. Metor.*, **10**, 1044-1046.

Takagi, M. and Y. Kondo, 1983: A method of analysis in the solar occultation measurements. *Proc. Res. Inst. Atmos., Nagoya Univ.*, **30**, 1-14.

成層圏エーロゾルの観測手法について

高木増美・森田恭弘・岩田 晃・近藤 豊

名古屋大学空電研究所

NOTES AND CORRESPONDENCE

Lidar Measurement of the Stratospheric Aerosol Layer at Syowa Station (69.00°S, 39.35°E), Antarctica[1)]

By Yasunobu Iwasaka

Water Research Institute, Nagoya University, Chikusa-ku, Nagoya 464

(Manuscript received 10 December 1984 in revised form 22 February 1985)

Abstract

The measurements on polar stratospheric aerosol particles using lidar and meteorological sonde at Syowa Station (69.00°S, 39.35°E), Antarctica revealed that the content of stratospheric aerosols noticeably increased in winter when atmospheric temperature frequently fell down to about −80°C in the lower atmosphere.

Introduction

The observations of stratospheric aerosols on high latitudes have not been sufficient because of technical difficulties. Most of previous measurements such as balloon-borne particle counter and sampling of particles using aircraft have been made from late spring to early fall, and not in winter. Recently the satellite measurements by McCormick and his co-workers (McCormick *et al.*, 1982) showed that extremely highly concentrated particle layer was formed in the winter polar stratosphere (They called it "Polar Stratospheric Clouds"). Behavior of polar stratospheric aerosols in winter, even though its nature is not fully known, seems to be very important phenomenon which possibly influences on global budget of water vapor and/or sulfur.

Lidar measurements on stratospheric aerosol has been made at Syowa Station (69.00°S, 39.35°E), Antarctica, since March 1983 as a part of the international project Antarctic Middle Atmosphere (MAP/AMA). Noticeable enhancement of the stratospheric aerosol layer which correlated with very cold atmospheric temperature was frequently observed in winter. Informations presented here should be useful for studies on particle formation processes of "Polar Stratospheric Cloud", the effect of the winter enhancement of polar stratospheric aerosol layer on global budget of aerosol particles, water vapor, and sulfur compounds in the stratosphere.

In this paper we should like to present the results on the polar stratospheric aerosol layer which were gained at Syowa Station (69.00°S, 39.39°E), Antarctica in 1983. As far as we know, they are first lidar measurements on polar stratospheric aerosols and thus should be very interest even if they are preliminary.

Measurement

The main characteristics of lidar used here are listed in Table 1. During the observational period, we performed lidar observation under the system condition that the height resolution was 0.5 km, laser pulse power in the range from 0.1 J/pulse to 0.5 J/pulse, and pulse repetition rate 0.5 Hz.

The scattering ratio is defined by follow-

1) This paper was presented at the Japan-U.S. Seminar on "Review of work related to sensing of stratospheric aerosol and gas components", Fukuoka, 12-14 June 1984.

Table 1 Main characteristics of lidar system used at Syowa Station (69.00°S, 39.35°E), Antarctica.

Laser		
Wavelength	:	694 nm
Polarization	:	Vertical
Max. Rep. Rate	:	60 ppm
Pulse Energy	:	1.5 J Max.
Pulse Length	:	Approx. 36 nS & 1.5 J, 60 ppm
Wavelength	:	374 nm
Polarization	:	Horizontal
Pulse Energy	:	Approx. 325-375 mJ & 1.5 J of 694 nm
Beam Divergence	:	Approx. 78% of energy in 3 mr & 60 ppm, 1.5 J
Beam Diameter	:	Approx. 8.5 mm after output coupler
Stability of Fundamental	:	Approx. ±7.5% & 60 ppm, 1.5 J
Transmitter Telescope	:	10 cm ϕ
Receiver Telescope	:	50 cm ϕ
Data Processing	:	Melcom 70/10 minicomputer system

ing relation,

$$\text{Scattering ratio}=[B_1+B_2]/B_1 \qquad (1)$$

where B_1 and B_2 are backscattering coefficient of atmospheric molecules (Rayleigh scattering) and of aerosol particles (Mie scattering) respectively. In order to estimate the value of scattering ratio, we used so-called "matching method" (e.g., Russell *et al.*, 1976). Air density was estimated on the basis of radio sonde data.

The vertically integrated value of B_2 in the stratosphere given by,

$$\int_{z_2}^{z_1} B_2(z)dz,$$

where z_1: upper boundary of integration,
z_2: lower boundary of integration,

is recognized as the parameter showing the column density of particulate matter in the stratosphere.

Fig. 1 indicates the temporal change of the value of the vertically integrated backscattering coefficient of aerosols (Here we call the integrated value IBC). Various time scale changes of IBC are found in figure. Here we should like to give attention to the variation with the time scale of about several months. Noticeable maximum of IBC is easily found in winter season form curve in Fig. 1. Maximum value of IBC measured at Syowa Station is larger than the peak value of IBC which was measured immediately after the

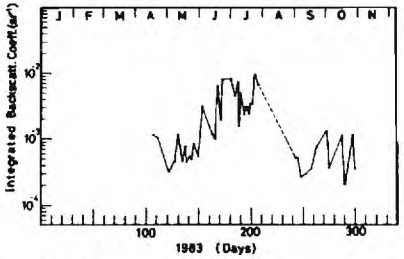

Fig. 1 The temporal change of the vertically integrated backscattering coefficient in the stratosphere, measured at Syowa Station (69.00°S, 39.35°E), Antarctica, 1983.

volcanic eruption of Mt. El Chichon (Spring, 1982: Mexico) at Japan. This result certainly confirmed the sudden increasing of extinction in winter polar stratosphere which was measured by satellite, SAM II (McCormick *et al.*, 1982).

Usually it has been considered that sudden increase of backscattered light and/or IBC certainly is due to severe eruption of volcanos (for example St. Helens and El Chichon). However the winter maximum of IBC measured at Syowa Station is not due to the direct effect of volcanism since there was no information on the volcanic eruptions which strongly affected on the winter Antactic stratosphere. Additionally increase of extinction in the polar stratosphere has been measured in every winter since 1979 by

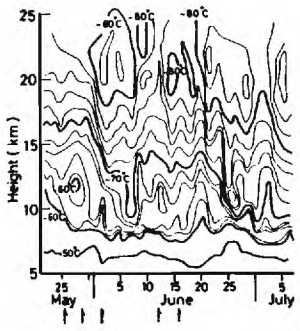

Fig. 2 The variation of temperature measured at Syowa Station (69.00°S, 39.35°E), Antarctica. The rapid decrease of stratospheric temperature was measured on the end of May 1983. Since then the cold region with temperature lower than −80°C was frequently measured. The arrow ↑ shows the day when lidar measurement was done.

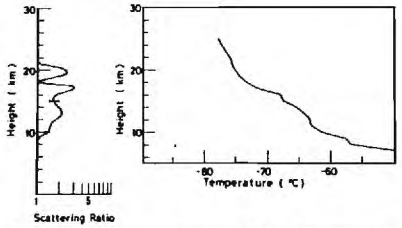

Fig. 3a Temperature profile at 1430 LT 25th May and the scattering ratio measured on the night of 25th May (1900 LT-2300 LT). The bar is the range of error.

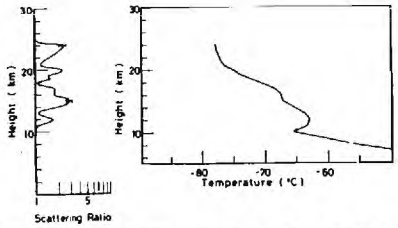

Fig. 3b Temperature profile at 1430 LT 29th May and scattering ratio measured on the night of 29th May (1900 LT-2300 LT).

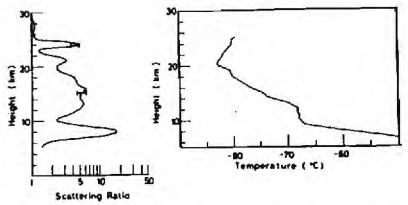

Fig. 3c Temperature profile at 1430 LT 2nd June and the scattering ratio on the night of 2nd June (1900 LT-2300 LT). Very cold atmosphere with $T<-80$°C appeared above 20 km altitude and the noticeable enhancement of aerosol layer was first measured. The peak centered at 8 km was certainly thin cirrus cloud.

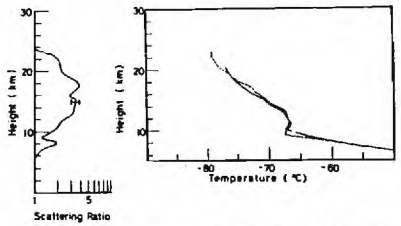

Fig. 3d Temperature profile at 1430 LT 12th June (solid line) and at 0230 LT 13rd June (dotted line), and the scattering ratio measured on the night of 13rd June (1900 LT-2300 LT).

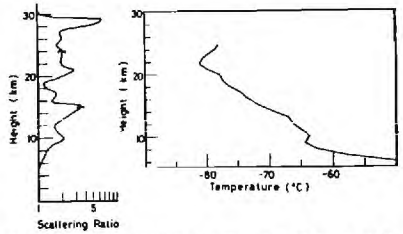

Fig. 3e Temperature profiles at 0230 LT 16th June, and the scattering ratio measured on the night of 16th June (1900 LT 15th June-0300 LT 16th June). The temperature profile measured at 0230 LT 16th June suggested that the temperature possibly fell down to the value lower than −80°C above about 20 km altitude on the night of 15th June.

satellite (McCormick *et al.*, 1982).

Winter enhancement of the stratospheric aerosol layer became to be noticeable on early June, 1983. The results on the early phase of the enhancement are shown in Fig. 2 and 3. The general tendency of temperature change of the stratosphere in early winter is shown in Fig. 2 on the basis of radio sonde measurements which were made routinely (0230 LT and 1430 LT, the difference between local time of Syowa Station and Greenwich mean time was 3 hours). The arrow ↑ in figure means the date when lidar measurement was made.

The scattering ratios measured from the end of May to the middle of June are shown in Fig. 3. The profiles of scattering ratios in Fig. 3 were made by integration of about 700 laser pulse firings. The statistical error due to photon-counting method was at most 7%. The measurement on 2nd June, 1983 was the first one which showed noticeably enhanced feature. As shown in Fig. 2, the very cold air with temperature (T) lower than -80°C was found at about 20 km altitude on 30th May. Since then the region with $T<-70$°C rapidly spreaded to near the bottom of the stratosphere.

All of scattering ratio profile measured after the appearance of cold air showed enhanced shape (increase of scattering ratio, expansion of aerosol layer), and apparently there was large difference between results gained in May and those in June concerning the shape of scattering ratio profile.

Summary and discussion

We presented the lidar measurements on polar stratospheric aerosols in 1983. McCormick *et al.* (1982) reported that the large increase of extinction was found in the polar winter stratosphere and concluded that this event was certainly due to the particulate matter increase which was caused by the decrease of stratospheric temperature (They call this thick aerosol layer "Polar Stratospheric Cloud").

The results presented here also suggested that the decrease of atmospheric temperature in winter was an important factor which caused noticeable increase of stratospheric particulate matter.

In Table 2 we summarized the occurrence ratio of the enhanced stratospheric aerosol layer on the basis of the lidar measurements in 1983. It can be easily found that the enhanced aerosol layer with the value of IBC larger than 2×10^{-3}sr^{-1} was measured only in very cold stratosphere with $T<-80$°C. However converses are not always true. Even when the cold air with $T<-80$°C was found in the lower stratosphere, a few cases did not indicate the enhanced stratospheric aerosol layer. But such cases are minor ones. Here we chose the threshold value of IBC to be 2×10^{-3}sr^{-1} considering that the minimum value of IBC measured during the enhanced period of the aerosol layer was about 2×10^{-4}sr^{-1}.

Steele *et al.* (1983) presented the idea that the active growth of ice crystal was main processes which caused the drastic increase of polar stratospheric particulate matter. According to them the ice crystal growth becomes to be very active in the cold atmosphere with $T<-80$°C. It is difficult to conclude that the factor which caused the stratospheric aerosol layer enhancement is only decrease of the stratospheric temperature to -80°C. However the decrease of stratospheric temperature (possibly lower than -80°C) is at least one of the important factors which control the enhanced stratospheric aerosol layer.

Table 2 Appearance of the enhanced aerosol layer (Syowa Station, Antarctica, 1983).

	The vertically integrated B_2 was larger than 2×10^{-3}sr^{-1}	The vertically integrated B_2 was smaller than 2×10^{-3}sr^{-1}
Cold air temperature (<-80°C) was measured in the lower stratosphere	36.0%	4.5%
Cold air temperature (<-80°C) was not found in the lower stratosphere	0.0%	59.5%

Particle concentration is, of course, controlled not only by temperature field but also by other various factors such as density distributions of gases (water vapor, sulfuric acid vapor, and so on) related to aerosol formation, transport of particles due to dynamical air motions and gravity, and others. Therefore it is difficult to show the typical observations which are indicating enhancement due to only the decrease of stratospheric temperature, and reasonable to consider that there is a usually a little difference between the height of cold region and the peak height of aerosol concentration. So it might be meaningless to discuss only complete coincidence of the height of aerosol density peak with that of cold atmosphere region in profiles shown in Fig. 3.

Concerning the effect of wind, we should like to point out that the north-south wind component alternated very often in the lower stratosphere from the end of May to the middle of June, 1983 and that the relation between wind component and enhancement of the stratospheric aerosol layer could not be made clear within the limits of the present experiments.

Summarizing the present observations, the Antarctic stratospheric aerosol layer noticeably enhanced in winter, and the decrease of stratospheric temperature to the level lower than -80°C is possibly an important factor which causes the enhancement of aerosol layer. The winter enhancement of the Antarctic aerosol layer described here is certainly same phenomenon with "Polar Stratospheric Cloud" shown by McCormick *et al.* (1982). In order to take reasonable understanding about the vertical profile of aerosol content and its temporal change during the enhancement period, it should be necessary, in addition to lidar data, to take information on distribution of H_2O, H_2SO_4, wind system, aerosol size, chemical composition and so on.

Acknowledgement

We wish to acknowledge technical supports by wintering members of Japan Antarctic Research Expedition 24th Team (Leader Prof. S. Mae, National Institute of Polar Research). We thank also staff members of upper atmospheric physics, National Institute of Polar Research, Prof. T. Hirasawa, Drs. H. Fukunishi, R. Fujii, and H. Miyaoka for their encouragement.

References

McCormick, M.P., H.M. Steele, P. Hamill, W.P. Chu and T.J. Swissler, 1982: Polar stratospheric cloud sightings by SAM II. *J. Atmos. Sci.*, **39**, 1387-1397.

Russell, P.B., W. Viezee, R.D., Jr. Hake and R.T.H. Collins, 1976: Lidar observation of the stratospheric aerosol: California, October 1972 to March 1974. *Quart. J. Roy. Met. Soc.*, **107**, 675-695.

Steele, H.M., P. Hamill, M.P. McCormick and T.J. Swissler, 1983: The formation of polar stratospheric cloud. *J. Atmos. Sci.*, **40**, 2055-2067.

南極昭和基地 (69.00°S, 39.35°E) における成層圏エアロゾル層のライダー観測

岩坂泰信

名古屋大学水圏科学研究所 千種区, 名古屋 464

NOTES AND CORRESPONDENCE

On Dispersion Processes of the El Chichon Dust Particles in the Lower Stratosphere[1)]

By Osamu Uchino

Meteorological Research Institute, Tsukuba, Ibaraki 305, Japan

(Manuscript received 7 November 1984, in revised form 22 February 1985)

1. Introduction

After the violent volcanic eruptions of Agung (Bali, 8.4°S, 115.5°E) on 17 March 1963, observations of the stratospheric aerosols by a ruby lidar were carried out for the first time by Fiocco and Grams (1964). Since then lidar technique has been used to monitor the stratospheric aerosol layer. Especially unusual increase of the stratospheric aerosols injected by the eruptions of El Chichon (Mexico, 17.3°N, 93.2°W) on 28 March, 3 and 4 April 1982 was detected at many lidar stations. At Tsukuba (36.1°N, 140.1°E), Japan, a new aerosol layer was observed at an altitude of 15 km on 25 April 1982. On 5 May, a main aerosol layer at 23 km was detected with a scattering ratio R (=total backscattering coeff./molecular backscattering coeff.) of about 12 accompanying a sub layer around 15 km. Until September 1982 this double structure of the aerosol layers was observed (Uchino *et al.*, 1984). Based on the observations at many lidar stations, dispersion processes of the volcanic dust particles in the lower stratosphere will be estimated.

2. Dispersion processes of dust particles observed by lidars

Between the eruptions of Agung and El Chichon, several volcanic eruptions occured in low latitudes such as Fuego (Guatemala, 14.5°N, 90.9°W, 10-23 October 1974), Soufrière (St. Vincent, 13.3°N, 61.2°W, 13-17 April 1979), Sierra Negra (Galapagos Island, 0.8°S, 91.2°W, 13 and 17 November 1979) and etc.. Among these, the eruptions of Fuego and El Chichon violently disturbed the burden of the stratospheric aerosols (Swissler *et al.*, 1982).

Fig. 1 shows the characteristics of dispersion processes of the dust particles in the northern stratosphere after the eruptions of Fuego and El Chichon, respectively. The date of initial increase of R and that when the largest value of scattering ratio R_{max}* was observed are shown for each lidar station. In the case of El Chichon, those dates are plotted for the upper- and the lower-layer of stratospheric aerosols. References related to El Chichon are omitted since they were already shown in Fig. 6 in our previous paper (Uchino *et al.*, 1984). The dates of initial increase of stratospheric aerosols detected from changes of twilight are also shown in Fig. 1 for the eruptions of Fuego. From this figure the mean meridional speed of the leading edge v_l was about 1.29 m/s (=1 deg/day) for the El Chichon dust particles in the lower layer (≈100 mb). This value is comparable to that of Soufrière ($v_l \approx 1.16$ m/s) (Hirono *et al.*, 1981), and it is about two times larger than that of Fuego ($v_l \approx 0.66$ m/s) (Fujiwara *et al.*, 1975), and it is to some extent smaller than that of Sierra Negra ($v_l \approx 1.53$ m/s) (Fujiwara *et al.*, 1982).

The mean meridional speed of dispersion of the air parcels including the highest concentration of aerosols v_h was roughly 0.8 v_l

1) This paper was presented at the Japan-U.S. Seminar on "Review of work related to sensing of stratospheric aerosol and gas components", Fukuoka, 12-14 June 1984.

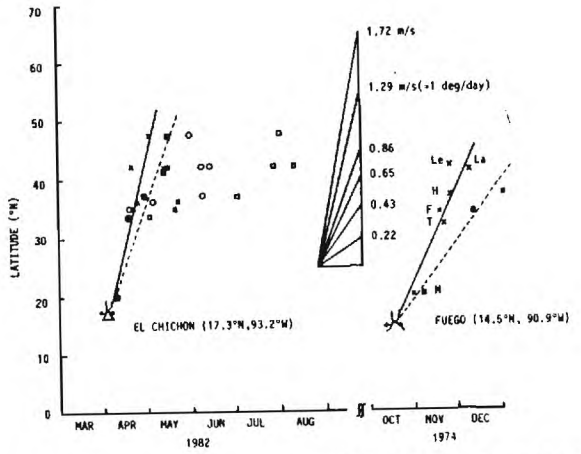

Fig. 1 Dispersion of the particles injected by the eruptions of El Chichon in 1982 and Fuego in 1974. ×, ○: the date when the first increase of the volcanic particles was observed below and above 20 km, respectively. ■, □: the date when the largest value of scattering ratio R_{max}* was observed by lidar below and above 20 km, respectively. The data of the Fuego particles are Le (Voltz, 1975), La (Hofmann and Rosen, 1977), H (McCormick *et al.*, 1978), F (Fujiwara *et al.*, 1975), T (Meinel and Meinel, 1975) and M (Fegley and Ellis, 1975).

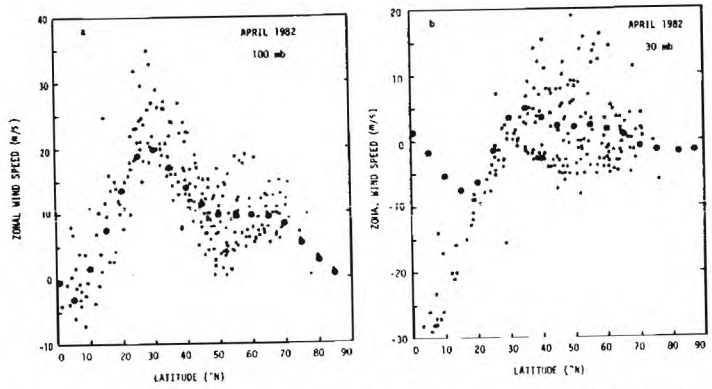

Fig. 2 Zonal wind speed; (a) the 100-mb surface and (b) the 30-mb surface. The large black circles represent the monthly-mean zonal wind of the OAM of JMA. The small circles denote the mean zonal wind at each station quoted from Monthly Climatic Data for the world.

on an average in the lower layer below 20 km. Compared with the lower layer, the mean meridional speed of the dust particles v_A in the upper layer was very slow in the northern part of 37°N as shown in Fig. 1.

It must be noted that there are some uncertainties to calculate v_L and v_A since volcanic eruptions occurred during several days and ground-based lidar observations of the stratospheric aerosols can be done only on clear nights. It is interesting to compare these results by lidars with a result of trajectory analysis of the El Chichon particles. As it is very difficult to obtain vertical wind, the trajectories of the dust particles were calculated on an isobaric surface without taking account of microphysical processes such as sedimentation.

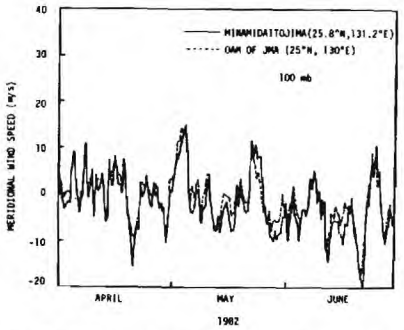

Fig. 3 A comparison between meridional wind speed at a grid point of the OAM and that at Minamidaitojima in Japan.

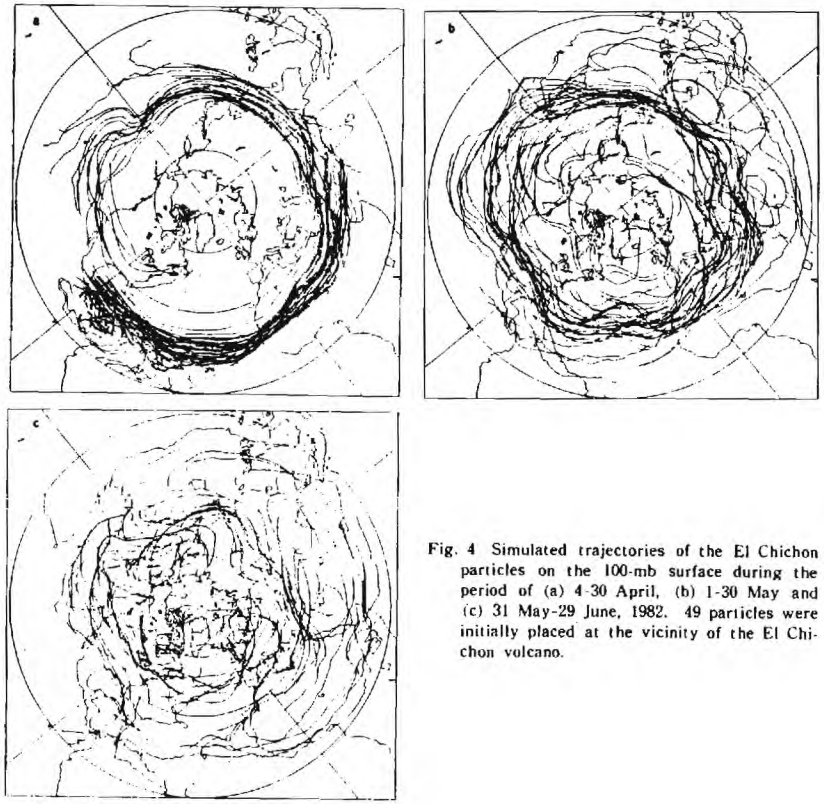

Fig. 4 Simulated trajectories of the El Chichon particles on the 100-mb surface during the period of (a) 4-30 April, (b) 1-30 May and (c) 31 May-29 June, 1982. 49 particles were initially placed at the vicinity of the El Chichon volcano.

3. Trajectory analysis of the El Chichon dust particles

The Objective Analysis Model (OAM) of Japan Meteorological Agency (JMA) is available to get the wind data on the isobaric surfaces (Report of E.C.C. 1983). Fig. 2 shows comparisons between monthly-averaged mean zonal wind of the OAM and mean zonal wind at each meteorological station from the Monthly Climatic Data for the World in April 1982. There is a clear difference between them in latitudes below 20°N for the 30-mb surface. This might be because of shortcoming of the OAM. The meridional wind component at a grid point of the OAM is compared with that obtained at Minamidaitojima near to the grid point as shown in Fig. 3. These data approximately agree with each other within 5 m/s. From these comparisons, for the present, wind data of the OAM of JMA will be usable for the trajectory analysis of the El Chichon particles except at low latitudes on the 30-mb surface.

To calculate trajectories of the El Chichon particles every one hour on an isobaric surface, wind data were interpolated from data of 5×5 degrees and 12 hours. On 4 April 1982, 49 particles were initially placed in the range of a radius of about 850 km around El Chichon, which are based on the observations of Nimbus 7 satellite (Kruger, 1983). Fig. 4(a) shows the trajectories of these particles on the 100-mb surface until 30 April. Most of the particles moved eastward. The particles initially placed at the extreme northern border of El Chichon circled around the globe for this period, and moved northward to some extent. The first increase of R in the lower layer on 18 April at Fukuoka (33.5°N, 130.4°E) is simulated in this trajectory analysis, but latitudinal dispersion of these particles is necessary to explain the initial increase of R on 21 April at Frascati (41.8°N, 12.7°E). There is a possibility that the dust particles injected on 28 March were detected at this observatory.

Continuous trajectories of the particles from May to June are shown in Fig. 4(b) and (c). The particles were dispersed into higher latitudes with northern and southern meander. Fig. 5 shows instantaneous positions of the dust particles at the end of time in Fig. 4(a), (b) and (c). It is clear that the leading edge of the particles was moved to high latitudes within about three months on the 100-mb surface. This rate of dispersion of the particles (≈1 deg/day) is similar to the observational results of the El Chichon dust cloud by lidars.

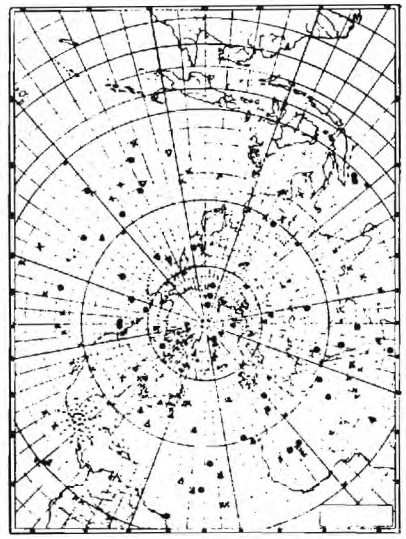

Fig. 5 Instantaneous positions of the El Chichon particles on 4 April (•), 30 April (×), 30 May (●), and 29 June (△) 1982.

A simulation of the El Chichon particles on the 30-mb surface was also carried out with the same initial conditions on the particles as those on the 100-mb surface. These particles moved westward and about ten percent of them traveled around a semicircle of the globe. This result is not consistent with the observational result by satellites (Robock and Matson, 1983). The satellite data show that the El Chichon cloud traveled completely around the globe in three weeks and distributed over a latitude band of 20°N ± 10° approximately on 25 April. The difference

may be due to unrealistic wind data of the OAM in latitudes below 20°N. To travel around the globe on a latitude range of 10–20°N in three weeks, the mean zonal wind speed is estimated to be 21.7–20.7 m/s, which is comparable to the wind speed as shown in Fig. 2(b).

Based on the above-mentioned satellite data, a uniform distribution of 45 particles was assumed around a latitude circle of 20°N on 26 April. Their trajectories were calculated for three months. In this analysis, the leading edge of the particles did not reach Japan by the end of the first month (Fig. 6(a)), although R_{max}* was observed over Japan in May, as shown in Fig. 1. However, if they were assumed to be initially positioned on a latitudinal circle of 30°N, a part of the particles reached Japan within the first month.

In June, the trajectories of the particles deviated a little in the range of latitude 30–60°N (Fig. 6(b)) and in July particles moved almost zonally in the southern part of 60°N (Fig. 6(c)). During the first four months after the El Chichon eruption, the particles on the 30-mb surface were dispersed as far as 60°N in this trajectory analysis. The simulated dispersion rate on the 30-mb surface was also slower than that on the 100-mb surface. This is consistent with the observation.

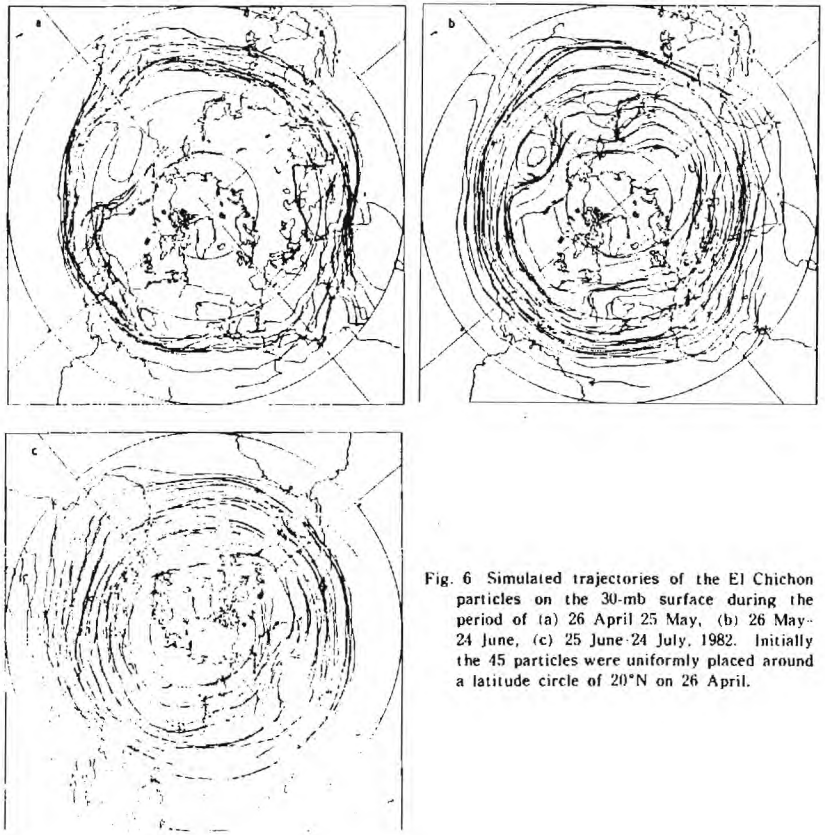

Fig. 6 Simulated trajectories of the El Chichon particles on the 30-mb surface during the period of (a) 26 April–25 May, (b) 26 May–24 June, (c) 25 June–24 July, 1982. Initially the 45 particles were uniformly placed around a latitude circle of 20°N on 26 April.

4. Remarks

In this note, the movement of the leading edge of the El Chichon particles was mainly discussed. Initial increase of the El Chichon particles was observed at two levels of about 16 km and 25 km almost the same time over Japan (Hirono and Shibata, 1983; Hayashida and Iwasaka, 1983). The particles in the lower level were transported by westerly wind. The mean meridional speed of the leading edge of the particles was about one degree per day (=1.29 m/s) in a latitude range of 17.5–47.5°N based on the observations by lidars. The particles in the upper level were transported by easterly wind and traveled completely around the globe in three weeks as shown by the satellite data.

A preliminary trajectory analysis was done using wind data of the OAM of JAM. Initial increase of the El Chichon particles in the lower level over Japan was approximately identified. During the first three months after the eruption, the particles were dispersed into higher latitudes in the calculation. This rate of dispersion of the particles is similar to the observational results by lidars.

Acknowledgements

The author gratefully acknowledges Drs. Hideji Kida and Masaru Chiba of the Meteorological Research Institute for their valuable comments on trajectory analysis. Many thanks are due to staffs of JMA who kindly supplied necessary data. The numerical calculation was performed using HITAC M-200H at MRI.

References

Fegley, R.W. and H.T. Ellis, 1975: Optical effects of the 1974 stratospheric dust cloud. *Appl. Opt.*, **14**, 1751–1752.

Fiocco, G. and G. Grams, 1964: Observations of the aerosol layer at 20 km by optical radar. *J. Atmos. Sci.*, **21**, 323–324.

Fujiwara, M., T. Itabe and M. Hirono, 1975: Sudden increase of stratospheric aerosol content after the eruption of Fuego volcano; lidar observation in Fukuoka. *Rep. Ion. Space Res. Japan*, **29**, 74–78.

———, T. Shibata and M. Hirono, 1982: Lidar observation of sudden increase of aerosols in the stratosphere caused by volcanic injections II. Sierra Negra event. *J. Atmos. Terr. Phys.*, **44**, 811–818.

Hayashida, S. and Y. Iwasaka, 1983: Lidar observation of stratospheric aerosol increase after the El Chichon eruption: Nagoya, April to December 1982. *Mem. Nat. Inst. Polar Res., Spec. Issue*, **29**, 191–200.

Hirono, M., M. Fujiwara and T. Shibata, 1981: Lidar observation of sudden increase of aerosols in the stratosphere caused by volcanic injections I. Soufrière 1979 event. *J. Atmos. Terr. Phys.*, **43**, 1127–1131.

——— and T. Shibata, 1983: Enormous increase of stratospheric aerosols over Fukuoka due to volcanic eruption of El Chichon in 1982. *Geophys. Res. Lett.*, **10**, 152–154.

Hofmann, D.J. and J.M. Rosen, 1977: Balloon observations of the time development of the stratospheric aerosol event of 1974–1975. *J. Geophys. Res.*, **82**, 1435–1440.

Kruger, A.J., 1983: Sighting of El Chichon sulfur dioxide clouds with the Nimbus 7 total ozone mapping spectrometer. *Science*, **220**, 1377–1379.

McCormick, M.P., T.J. Swissler, W.P. Chu and W.H. Fuller, Jr., 1978: Post-volcanic stratospheric aerosol decay as measured by lidar. *J. Atmos. Sci.*, **35**, 1296–1303.

Meinel, A.B. and M.P. Meinel, 1975: Stratospheric dust-aerosol event of November 1974. *Science*, **188**, 477–478.

Monthly Climatic Data for the World, 1982: **35**, No. 5, April.

Robock, A. and M. Matson, 1983: Circumglobal transport of the El Chichon dust cloud. *Science*, **221**, 195–197.

Staff Members, 1983: Outline of operational numerical weather prediction at Japan Meteorological Agency. Periodic Report on Numerical Weather Prediction, E.C.C., J.M.A. Available form, E.C.C. at J.M.A. (Japanese)

Swissler, T.J., P. Hamill, M. Osborn, P.B. Russell and M.P. McCormick, 1982: A comparison of lidar and balloon-borne particle counter measurements of stratospheric aerosol 1974–1980. *J. Atmos. Sci.*, **39**, 909–916.

Uchino, O., K. Takahashi, I. Tabata, I. Akita, Y. Okada and K. Naito, 1984: Ruby lidar observations of the El Chichon dust clouds at Tsukuba (36.1°N) and comparisons with UV lidar measurements at Fukuoka (33.6°N). *J. Meteor. Soc. Japan*, **62**, 679–687.

Voltz, F.E., 1975: Volcanic twilights from the Fuego eruption. *Science*, **189**, 48–50.

エルチチョンダスト粒子の下部成層圏における拡散過程

内野 修

気象研究所 筑波, 茨城 305

NOTES AND CORRESPONDENCE

Comparative Study of the Aerosol Properties Measured by Two-wavelength Lidar and Detector on Balloon[1]

By Motokazu Hirono*, Noboru Fujiwara**, Motowo Fujiwara* and Takashi Shibata***

* Department of Physics, *** Department of Electrical Engineering, Kyushu University Fukuoka 812, ** Fujitsu Inc. Kawasaki 213 Japan

(Manuscript received 7 November, 1984, in revised form 12 February 1985)

1. Introduction

Two wavelengths F=1.06 μm and S=0.53 μm of Yag lidar system were used to obtain profiles of atmospheric aerosols at Fukuoka (Hirono *et al.*, this issue). The normalization of the profiles are made by using the same parameters calculated from the observed aerosol size distributions near the tropopause by University Wyoming group at south Texas and Wyoming in May, August, October 1982 and January 1983 (Hofmann *et al.* 1983). The results are shown to have good quality to estimate the order of magnitude of aerosol concentrations between the height range from 9 to 30 km i.e. including several kilometers of the upper troposphere. But the two-wavelengths are insufficient to give detailed information of aerosol size distributions which are shown to be bimodal for the Chichon clouds. The normalization procedure used to the profiles is very sensitive to various parameters. If we use conventional procedure, that the minimum scattering ratios $R_{min}(\lambda)=1$ ($\lambda=F, S$), between the altitude range from 9 to 32 km—often near 30 km—then obtained profiles of the ratios of the backscattering coefficients $I'=\beta_A(S)/\beta_A(F)$ take unreasonable values which cannot readily reconcile with theoretical anticipation.

[1] This paper was presented at the Japan-U.S. Seminar on "Review of work related to sensing of stratospheric aerosol and gas components", 12-14 June 1984.

However, the following method gave good results from the view point of sound aerosol formation theory.

According to recent study results (Hirono *et al.* 1984, Shibata *et al.* 1984) the diffusivity takes extremely small values in the easterly wind region higher than about 20 km at middle and lower latitudes for spring and summer. In the westerly wind region lower than about 20 km at the above mentioned latitudes, the diffusivity takes much higher values which are of the same order of magnitude as shown by Luther (1973) or Cadle *et al.* (1976) in a more sophisticated fashion. The numerical results of the latters using two dimensional analysis suggest that the aerosols near tropopause would be fairly uniform for latitudes from 33°N (Fukuoka) to 28°N (S. Texas) several months after the volcanic injection, if there were no significant settling of large particles from upper diffusion-free region to those altitudes. The upper region contained densest aerosols for about three seasons, therefore the problem of settling should be seen with special care at least for one season, but at first we ignored the effects.

We used spline fit of balloon data for 3 km above tropopause to calculate parameters of aerosols based on the Mie theory for the above mentioned period. These parameters are used to renormalize lidar profiles at the same altitudes over Fukuoka, though the distance of the two stations is about 13.5×10^3 km apart.

The optical properties represented by spectral extinction of the obtained data agree well with those of the other global data (Spinhirne *et al.* 1983, DeLuisi *et al.* 1983), but those of May '82 should be seen with special care as explained later in the next section.

The integrated aerosol backscattering $B_d=\int\beta_A(F)dz$ obtained after renormalization is about 1.8 times conventional value B_c for $R_{min}=1$, since August 1982. The column mass M_d obtained by renormalization is therefore about 1.8 times conventional value M_c, but the optical depth $\tau(550)$ at 550 nm is obtained from B_d multiplied by about 69.7 ± 24 sr being about one 1.8th of the conversion factor of Pinnick *et al.* (1980).

In Fig. 1 we compared the values of M_d with those obtained by balloon sonde and zonal mean column mass deduced by Solar Mesosphere Explorer (Thomas *et al.* 1983). The details will be given in the next section by using Table 2.

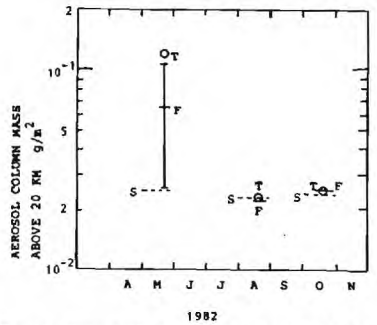

Fig. 1 Aerosol column mass above altitude 20 km. SME monthly zonal mean values are denoted by dashed lines S. The values at Fukuoka (33°N) and south Texas (27°N) are denoted by F and T, respectively. These values are shown by M_{dw} and M_u(H. & R.) in Table 2. In May, $\phi=1/2$ is taken for M_{du}(Fukuoka).

2. Calculated results and discussion

The details of the procedure to obtain normalized backscattering profiles mentioned in the previous section are given in this section.

The aerosol backscattering and extinction coefficients can be expressed by the following equation

$$\beta_A(\lambda, z)=(4\pi)^{-1}\int_{r_1}^{r_2}\pi r^2 Q_{bs}(r, \lambda)n(r, z)dr,$$
$$E_A(\lambda, z)=\int_{r_1}^{r_2}\pi r^2 Q_{ext}(r, \lambda)n(r, z)dr. \quad (1)$$

where $\lambda=F, S$; r=radius of the aerosol: $r_1=0.05$ μm, $r_2=3$ μm, z=altitude, $n(r, z)$=aerosol differential size distribution; Q_{bs}, Q_{ext}=backscattering and extinction efficiency, respectively, which are calculated for the refractive indices $1.443-0.005i$ at $\lambda=F$ and $1.455-0.005i$ at $\lambda=S$ according to Mie theory.

Equations (1) can be calculated against altitude if $n(r, z)$ is estimated by a reasonable method.

The relation between scattering ratio and backscattering may be written as

$$\beta_A(\lambda, z)/\beta_M(\lambda, z)=R(\lambda, z)-1,$$

where β_M denotes molecular backscattering coefficient.

The renormalized scattering ratio $R(\lambda, z)$ near the tropopause can be expressed by

$$R(\lambda, z)-1=\{R_c(\lambda, z)-1\}C_t(\lambda) \quad (2)$$

where R_c stands for the scattering ratio when its minimum value is assumed to be unity at some altitude from 9 to 32 km.

As shown in the previous section, by using the same as averaged values of aerosol parameters for three km height range over tropopause of south Texas and Wyoming we determine values of $C_t(F)$ and $C_t(S)$.

The values of (2) at a first guess are those for $E_A=0$ meaning zero extinction in the height range of lidar observation. The first approximate value $\beta_1(\lambda)$ of $\beta_A(\lambda)$ is obtained by using equation (2). The ratio $I'_1(z)=\beta_1(S, z)/\beta_1(F, z)$ is used to infer the first approximate size distribution $n_1(r, z)$ according to a rule explained later.

The first approximate value $E_1(\lambda, z)$ of $E_A(\lambda, z)$ is obtained by using $n_1(r, z)$ with equation (1).

The principle to determine aerosol size distribution is based on the experience obtained after exhaustive study based on Mie theory of the spline fit of six channel balloon data mentioned above at every three km in-

terval of altitude. It is found that although multimode size distribution prevails during the whole period May '82—January '83, the main target of the F and S wavelengths is almost a single mode which has largest radius, and other modes have negligible contribution to the receiving signals.

If every mode of bimodal size distribution makes equal contribution to the receiving signals, at least six wavelengths would be necessary to determine the distributions. In other words, we cannot obtain detailed information on the optically minor modes, by using the two-wavelength lidar system. The essential part of our procedure is the use of an empirical mode (b) as explained below.

The determination of size distribution at every step of approximation is made as follows:

(a) If $2<\Gamma(z)<3$, we used the form of function,

$$n(r, z)=n_z = \frac{N}{(2\pi)^{1/2}\ln\sigma}\exp\left\{\frac{-(\ln r-\ln r_M)^2}{2\ln^2\sigma}\right\} \quad (3)$$

which is a Zold distribution with $\sigma=1.8$(const.), $N=a$ const. to be determined by (1) and r_M is a variable being used to fit the value of Γ.

(b) If $\Gamma(z)<2$, we used the form of function

$$n(r, z)=n_{\log} = \frac{N_1}{(2\pi)^{1/2}(\ln\sigma_1)r}\exp\left\{\frac{-(\ln r-\ln r_m)^2}{2\ln^2\sigma_1}\right\} \quad (4)$$

which is a lognormal distribution with $N_1=a$ const. to be determined by (1), $\sigma_1=1.2$ (const.) and $r_m=a$ variable being used to fit the value of Γ.

If we use β_1 and E_1, the second approximate value β_{II} is obtained from

$$\beta_{II}(\lambda, z)=\beta_I(\lambda, z)T^{-2}(z_0, z; \lambda) \quad (5)$$

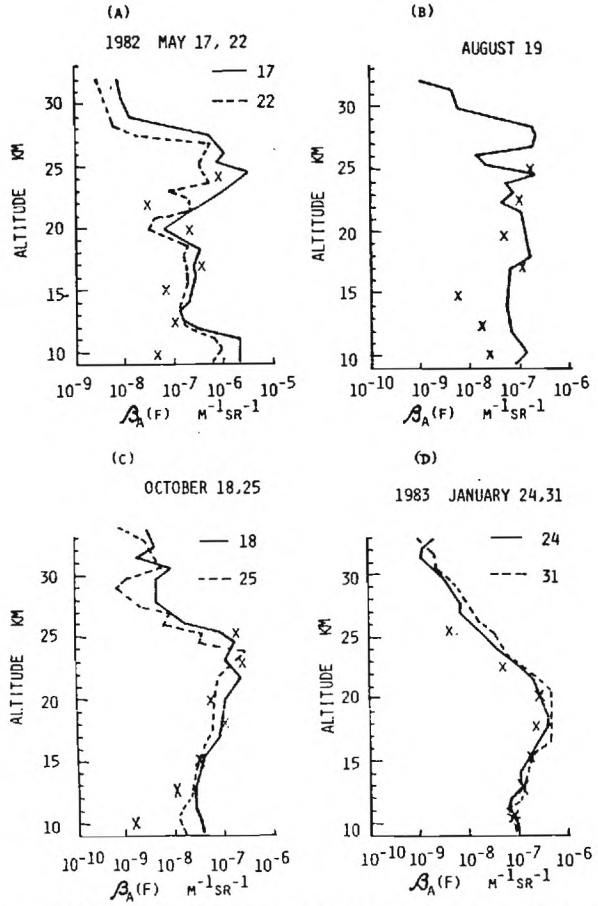

Fig. 2 Renormalized profiles of $\beta_A(F)$. The mark x shows calculated values on Mie theory by using balloon data at south Texas (May—Oct.) and Wyoming (January 1983). $F=1.06\,\mu$m.

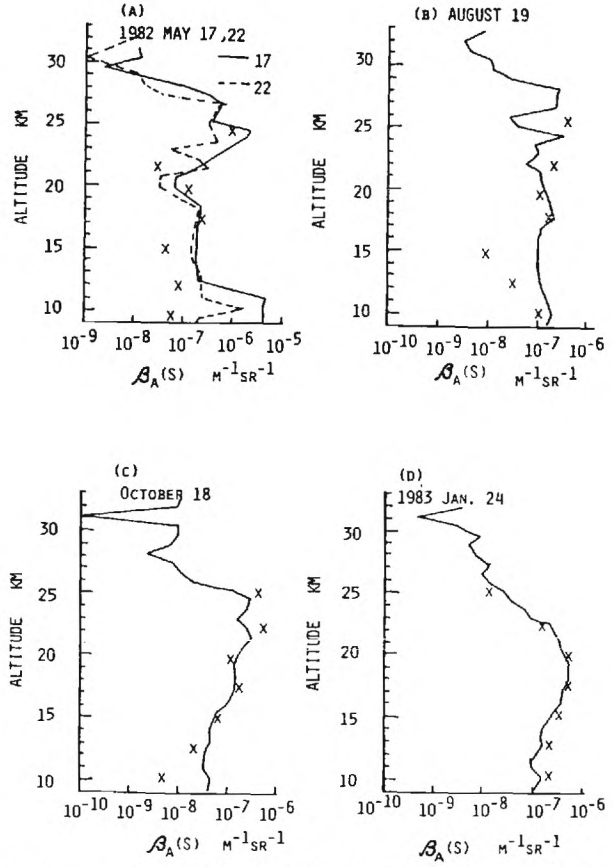

Fig. 3 Renormalized profiles of $\beta_A(S)$. The same mark x is used as in Fig. 2. $S=0.53\,\mu$m.

$$T=\exp\left\{-\int_{z_0}^{z} E_{\mathrm{I}}(\lambda, z')dz'\right\}$$

where z_0 stands for the lowest height of observation. By using $\Gamma'_{\mathrm{II}}(z)=\beta_{\mathrm{II}}(S, z)/\beta_{\mathrm{II}}(F, z)$ we obtain $n_{\mathrm{II}}(r, z)$. This procedure is repeated ten times until $n=n_{\mathrm{XI}}$, $\beta_A(F)=\beta_{\mathrm{XI}}(F)$, $\beta_A(S)=\beta_{\mathrm{XI}}(S)$, $\Gamma'(z)=\Gamma_{\mathrm{XI}}(z)$ are obtained as shown in Fig. 2, 3 and 4. The convergence of the repeated procedure was, in fact, sufficiently good after half repeated times.

If $n(r, z)$ is used, the effective mean radius for the lidar observation at wavelength λ can be calculated as follows:

$$\bar{r}_{\mathrm{eff}}(\lambda)=\int_{r_1}^{r_2} r\pi r^2 Q_{bs}(r, \lambda)n(r)dr \Big/ \int_{r_1}^{r_2} \pi r^2 Q_{bs}(r, \lambda)n(r)dr \qquad (6)$$

which is different from mean radius because of the presence of weighting factor $Q_{bs}(r, \lambda)$. The values of $\bar{r}_{\mathrm{eff}}(F)$ vs. altitude are shown in Fig. 5 for the period May '82 to January '83.

In May $\bar{r}_{\mathrm{eff}}(F)\sim 1.4\ \mu$m but after August this value is less than or about equal to 1 μm. For the period May and June '82 we made frequent observations and the data are well

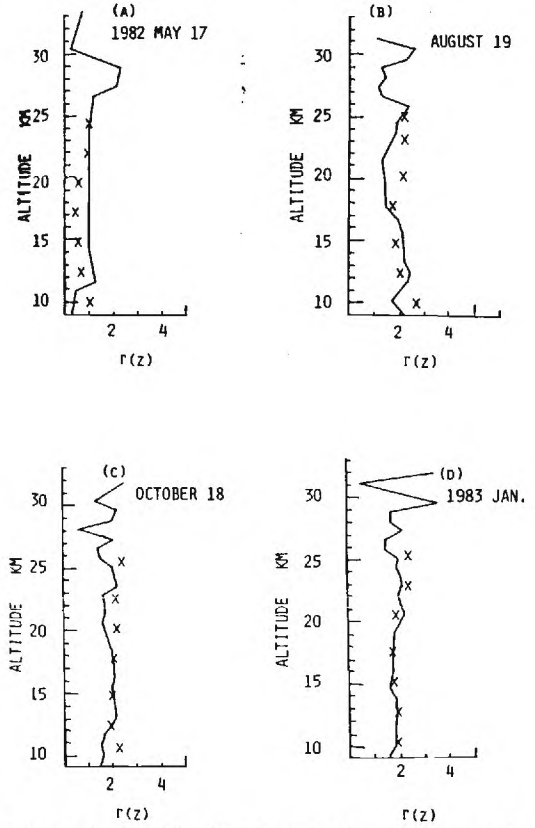

Fig. 4 Renormalized profiles $\Gamma'(z)=\beta_A(S)/\beta_A(F)$. The same mark x is used as in Fig. 2.

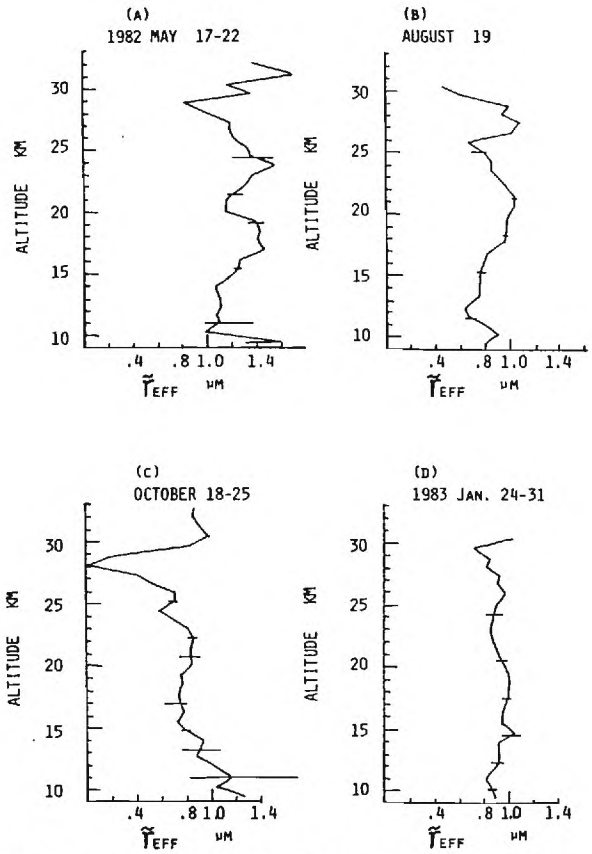

Fig. 5 Effective mean radius of aerosol particles at the lidar wavelength $F=1.06\ \mu$m: denoted by $\bar{r}_{\mathrm{eff}}$. This shows the most probable target radius of the lidar.

documented, which should be given special attention.

(1) The numerical results of Cadle *et al.* (1976) suggest that near the tropopause the aerosol concentrations at 28°N (south Texas) and 33°N (Fukuoka) are approximately equal after two months since volcanic injection on the model without including sedimentation of giant particles. During one season after the eruption of El Chichon (April 1982) the falling of ash and giant particles ($r>1\ \mu$m) was thought to be significant. Then the densest part of aerosols above 20 km altitude was located at latitudes from about 15°N to 25°N (Thomas *et al.* 1983). Meridional gradient of aerosols in the region near tropopause would not be quite negligible in May, if the existence of falling giant particles are taken into account.

On May 22, the renormalization gives $C_t(F)\sim 4f$ and $C_t(S)\sim f$, including uncertain factor f which is equal to unity at the present

Table 1 Mean values of $\beta_A(F)$ at every height range in units $10^{-6}\,m^{-1}\,sr^{-1}$

Height range (km)	May	June (1982)	July	
13—16	4.06± 1.83	2.86±0.63	1	
11—13	6.78±13.75	2.6 ±1.1	0.996±0.71	
9—11	8.32±13.6	3.17±1.18	1.6	±0.27

renormalization. The values of f, however, may be less than unity in reality, as mentioned above. If we have $f\sim0.5$ which would be most probable, the values of $\Gamma(=0.7-1$ for $f=1)$ would become about 1.5 times these values and hence roughly equal to those in August. Thus it is impossible to discuss the difference of the effective radii $\bar{r}_{ef}$ between May and August.

(2) The profiles below 15 km are examined, on the next stage, to examine the influence of settling of giant particles. For this height range, the influence of extinction on the way of laser pulse propagation is negligible. The Yag laser does not emit fluorescence and hence the obtained profile is reliable if the normalization is reasonable. We have eleven, seven and two profiles in May, June and July, respectively. The values of $\beta_A(F)$ calculated on the assumption $R(F)_{min}=1$ are shown in Table 1. From values shown in the table, gradual decreasing until July is noted.

Among available data on eleven days in May, which are shown in Table 1, for the selected days 17th, 19th, 21st and 22nd, the renormalization was performed to give $\beta_A(F)=2\times10^{-6}$, 2×10^{-7}, 10^{-7} and $7\times10^{-7}\,m^{-1}\,sr^{-1}$ and hence including again uncertain factor f mentioned above

$$\beta_A(F)=f(7.5\pm7.5)\times10^{-7}\,m^{-1}\,sr^{-1}$$

at the height range 9-11 km. Here $f=1$, and the values at $f=0.25$ agree with those obtained by conventional method $R_{min}=1$. The significant dispersion of the values would be due to appreciable meandering of the zonal wind in addition to the situation mentioned in the previous section.

The integrated aerosol backscattering $B_c=\int\beta_A(F)dz$ (from 13 to 29 km) obtained for the conventional normalization procedure $R_{min}(F)=1$ is multiplied by a factor 33 sr this being a factor by Pinnick *et al.* (1980), to obtain column aerosol mass M_c in g/m^2. The column aerosol mass M_d obtained by the present normalization procedure are also calculated, and additional suffix u denotes those calculated for the range higher than 20 km, which are shown in Table 2 together with observed data by other kind of measurements for comparison.

The meandering of the Chichon zonal cloud and significant settling of giant particles in May would produce a little meridional gradient of aerosols at the level of renormalization. Suppose that the corrected value of M_d against this cause is represented by ϕM_d, then $\phi=0.18$ is obtained by equating the product with M_c. The value $0.18<\phi<1$ and especially $\phi\sim0.5$ seem to be appropriate.

In Fig. 1, We compared the values M_{du} ($\phi=0.5$ in May) with M_u (H. & R.) and M_u (SME) calculated from Hofmann *et al.* (1983) and Thomas *et al.* (1983), respectively in May, Aug. Oct. 1982. It may be seen that $\phi=0.5$ in May could be tentatively adopted to be the best value, but it is not conclusive. After August these values are in satisfactory agreement.

Optical depth $\tau(S)=E_A(S,z)$ obtained by the same renormalization at the wavelength S and $\tau(425)$ at Mauna Loa, $\tau(500)$ and $\tau(694)$ at 33°N obtained by airborne detectors are also shown in Table 2.

The difference of the optical depth depending on the wavelengths mentioned above seems to be very small amounting up to about 10% as compared with that at 550 nm during the season according to DeLuisi (1983) and results of Mie calculations by using the aerosol size distribution presented here.

It may be seen from the Table that the column mass M_d and $\tau(S)$ agree well with those by other methods and $\phi\sim0.5$ and also $f\sim0.5$ may be adequate.

In April '82 $\tau(425)=0.466\pm0.24$ at Mauna Loa, showing significant spatial inhomogeneity of the cloud (DeLuisi *et al.* 1983).

It may be estimated that for several weeks after El Chichon eruption, the aerosol column

Table 2 Column aerosol mass M_c, M_d and optical depth τ. Observed data by other methods are also shown.

	May '82 17, 19, 21, 22	Aug. '82 19	Oct. '82 18, 21, 22, 25	Jan. '83 24, 25, 28, 31
M_d (g/m^2)	$\phi(0.17\pm0.1)$ $(0.18<\phi<1)$	0.046	0.032 ± 0.001	0.074 ± 0.01
M_c	0.03 ± 0.0001	0.02	0.019 ± 0.004	0.042 ± 0.007
M_d/M_c	5.67ϕ	2.3	1.62	1.78
M(H. & R.) $h>$Trop.	0.2 (S. Texas)	0.03 (S. Texas)	0.036 (S. Texas)	0.05 (Wyo.)
M_{du}	$\phi(0.13\pm0.08)$	0.033	0.025 ± 0.008	0.027 ± 0.004
M_u(SME) Lat. 27°N	0.025	0.023	0.024	
M_u(H. & R.)	0.12	0.023	0.025	
$\tau(S)$	$\phi(0.179\pm0.054)$	0.065	0.09 ± 0.019	0.13 ± 0.027
$\tau(425)$ 20°N	(a) 0.325 ± 0.083			
$\tau(500)$ 33°N				(b) 0.1
$\tau(694)$ 33°N			(c) 0.05 (d) 0.055—0.12	

(a) optical depth at $\lambda=425$ nm measured by DeLuisi *et al.* (1983) at Mauna Loa.
(b) optical depth at 33°N by sun photometer airborne (Dutton *et al.* 1983 $\lambda=500$ nm).
(c) the same as (b) except (Spinhirne 1983 $\lambda=694$ nm).
(d) airborne lidar at 33°N (Swissler *et al.* 1983, $\lambda=694$ nm).

mass near Mexico within longitudinal distance 30° from El Chichon would be about ten times or more as compared with zonal mean value judging from these figures and El Chichon cloud distribution shown by Robock *et al.* (1983).

After August $\tau(S)/B_c=125\pm24$ sr which is essentially equal to the conversion factor 130 sr of Pinnick *et al.* (1980) as a result of the cancelling of multiplying factors to B_c.

In conclusion, after four months of the eruption of El Chichon, the concentrations and optical parameters of aerosols at S. Texas (28°N) and Fukuoka (33°N) near the tropopause in the stratosphere are shown to be almost equal. But for several months after eruption, the concentration at the lower latitude (28°N) might be about twice or more than that at (33°N). The two dimensional model including densest aerosols in the higher altitude than 20 km should be completely revised.

Acknowledgments

We thank Profs. D. J. Hofmann and J. M. Rosen for their valuable discussions on our previous paper in 1983 and for sending us several manuscripts before publication.

References

Cadle, R. D., C. S. Kiang and J.-F. Louis, 1976: The global scale dispersion of eruption cloud from major volcanic eruptions., *J. Geophys. Res.*, **81**, 3125-32.

DeLuisi, J. J., E. G. Dutton and K. L. Coulson, 1983: On some radiative features of the El Chichon volcanic stratospheric dust cloud and cloud of unknown origin observed at Mauna Loa., *J. Geophys. Res.*, 88, 6769-72.

Dutton, E. G. and J. J. DeLuisi, 1983: Spectral extinction of direct solar radiation by the El Chi-

chon cloud during December 1981., *Geophys. Res. Lett.*, **10**, 1013-16.
Hirono, M., T. Shibata, M. Fujiwara and N. Fujiwara, 1984: Enormous increase of volcanic clouds in the stratosphere over Fukuoka after April 1982, *Geofisica Internacional*, **23**, 259-276.
Hofmann, D. J. and J. M. Rosen, 1983: Stratospheric sulfuric acid fraction and mass estimate for the 1982 volcanic eruption of El Chichon., *Geophys. Res. Lett.*, **10**, 313-6.
Luther, F. M., 1973: Monthly mean values of eddy diffusion coefficients in the lower stratosphere., AIAA Paper No. 73-498, 1-9.
Pinnick, R. G., S. G. Jennings and P. Chýlek, 1980: Relationships between extinction, absorption, backscatteriing, and mass content of sulfuric acid aerosols., *J. Geophys. Res.*, **85**, 4059-66.
Spinhirne, J. D., 1983: El Chichon eruption cloud. Latitudinal variations of the spectral optical thickness for October 1982., *Geophys. Res. Lett.*, **10**, 881-4.
Swissler, T. J., M. P. McCormick and J. D. Spinhirne, 1983: El Chichon eruption cloud: Comparison of lidar and optical thickness measurements for October 1982., *Geophys. Res. Lett.*, **10**, 885-8.
Shibata, T., M. Fujiwara and M. Hirono, 1984: The El Chichon volcanic cloud in the stratosphere: Lidar observation at Fukuoka and numerical simulation, *J. Atmosph. Terr. Phys.*, **46**, 1121-46.
Thomas, G. E., B. M. Jakosky, R. A. West and R. W. Sanders 1983: Satellite limb-scanning thermal infrared observations of the El Chichon stratospheric aerosol: First results., *Geophys. Res. Lett.*, **10**, 997-1000.

2波長ライダーと気球搭載測器により測定されたエアロゾルの特性の比較

広野求和・藤原　昇・藤原玄夫・柴田　隆
九州大学理学部物理学科

NOTES AND CORRESPONDENCE

A Possible Relationship of Volcanic Aerosol Variations with El Niño Southern Oscillations—Lidar Observations of Volcanic Aerosols in the Atmosphere[1]

By Motokazu Hirono*, Takashi Shibata** and Motowo Fujiwara*

* *Department of Physics,*
** *Department of Electrical Engineering Kyushu University, Fukuoka 812, Japan*
(*Manuscript received 7 November 1984, in revised form 22 February 1985*)

1. Introduction

Dunkerton (1983) showed that the temperature rise in the tropical (20°S−20°N) stratosphere after Agung volcanic eruption 1963 was consistent with those inferred from the thermal wind structure of the abnormal QBO (Quasi Bienniel Oscillations, calculated by his one-dimensional model. The situation would be similar to those after El Chichon eruption 1982 and the recent observed data seem to support this presumption (Labitzke and Naujokat 1984). A necessary condition of his theory is volcanic aerosols confined near the equator for about 5 years. He showed that aerosol atmospheric heating can modify QBO. Also he suggested a second possibility that the modification of QBO was due to the excitation by abnormal equatorial waves in the troposphere which might be related to the ENSO (El Niño Southern Oscillation). This event started almost at the same time as the eruption of El Chichon (Philander, 1983).

In his theoretical treatment the effect of the aerosol was limited within the altitude range from 17 to 30 km and judging from the observed results for the El Chichon event (Hirono *et al.* 1984), the assumed residence time of aerosols near the equator would be too long.

In this paper we shall make estimates of the atmospheric heating by the aerosols falling through the upper troposphere for one season after the eruption of El Chichon 1982 April. The results suggest that the heating is strong enough to modify the Hadley circulation to initiate the variation of the trade wind leading to the ENSO.

2. Variations of column concentration of aerosols and equatorial Pacific surface teperature

Yag lidar system was used at Fukuoka (33°N, 131°E), since 1979 at the wavelength $F=1.06\ \mu$m, and $S=0.53\ \mu$m. The integrated aerosol backscattering $B_c=\int\beta_A(F)dz$ is shown in Fig. 1 for the period from 1979 through Feb. 1983, (Hirono and Shibata, 1983; Hirono *et al.*, 1984).

El Chichon eruption in April 1982 is clearly a tropical one, located at 17.33°N, 93.20°W, according to the classification by Lamb (1970).

In May 1982, $B_c=(1.08\pm0.48)\times10^{-3}\ \mathrm{sr}^{-1}$ and the optical depth at the wavelength 550 nm $\tau(550)$ is about 0.108 ± 0.05 and attained a maximum value 0.2 in January 1983, decreasing to 0.02 in May 1984 about one tenth of the maximum value (not shown in Fig. 1).

Recently Handler (1984) showed that the ENSO took place after very large volcanic eruptions at low latitudes (<20° tropical);

[1] This paper was presented at the Japan-U.S. Seminar on "Review of work related to sensing of stratospheric aerosol and gas components", Fukuoka, 12-14 June 1984.

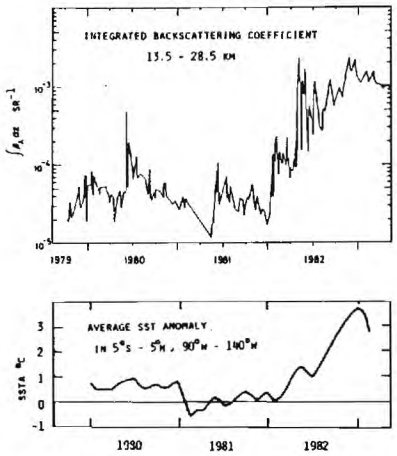

Fig. 1 Variation of integrated backscatterig $B_c(F)$ for the period 1980-1982 and sea surface temperature anomaly averaged over eastern tropical Pacific: 5°S-5°N, 90°W-140°W.

Krakatoa 1883, Santa Maria 1902, Agung 1963 and El Chichon 1982. Schatten *et al.* (1984) made numerical calculations by a zonally symmetric model and showed that low latitude volcanic eruptions might trigger ENSO. They suggested that the eruption of El Chichon may provide a trigger for inducing the 1982-83 anomalous ENSO. But the latter authors advocated urgent need for more sophisticated theories on the subject.

The averaged sea surface temperature anomaly (SSTA) over the eastern equatorial Pacific can be a good measure of the ENSO. In Fig. 1 SSTA values over 90°W-140°W, 5°S-5°N (Quiroz, 1983) are also shown. It should be noted that the SSTA started to increase dramatically at the same time as the eruption of El Chichon. This fact suggests a much shorter response time of SSTA to volcanic eruptions, than those of Robock (1985) and Hansen *et al.* (1978). It seems to emphasize the importance of the dynamical effect on the atmosphere and ocean, in addition to the radiative and thermodynamical equilibrium models of these authors.

3. Estimation of the volcanic aerosol concentration in the upper troposphere at northern low latitudes and its atmospheric heating

According to Hofmann and Rosen (1983), initial loading of stratospheric El Chichon cloud in April 1982 was about 20 Tg ($T=10^{12}$), probably one half of which settled through tropopause for early several months. The center of the zonal stream of El Chichon cloud was about 20°N (Thomas *et al.*, 1983) until August 1982. The active settling of giant particles at south Texas for early few months can be estimated from the value of accumulated aerosol concentration $N_{.95}$ with radii larger than .95 μm averaged from tropopause to 30 km being about 0.67 and 0.038 in May and August '82, respectively (Hofmann and Rosen, 1983). But only one observation in May is available at south Texas for three months after El Chichon eruption.

If aerosol unit mixing ratio $m_1=10^{-9}$ g/g air is used, in May near the altitude 10 km at south Texas the aerosol mixing ratio $m(a)$ is estimated at $m(a)\sim5.6m_1$. At Fukuoka there are many lidar observation data and the renormalization was made on May 17, 19, 21 and 22 (Hirono *et al.*, in this issue) giving $m(a)=f(70\pm70)m_1$ ($0.26<f<1$, probably $f\sim0.5$), for the altitude 9-11 km in this month and $m(a)\sim10m_1$ on August 19 at the same altitude. The Yag lidar does not emit fluorescence and hence a mechanical shutter is unnecessary. Therefore the profile near 10 km is reliable if the normalization is correct. The Mauna Loa lidar observation data suggest $m(a)\sim100m_1$ in April and May 1982 near altitude 10 km as shown in the next section. These values give some reliable bases to discuss concentrations of settling aerosols in the upper troposphere.

According to Czeplak and Junge (1974) and Kida (1983), at the tropics from latitudes 0° to 25° in the troposphere the horizontal eddy diffusion is smallest so that the dispersion of the pollutant is mainly due to mean atmospheric motion, i.e., Hadley circulation. In higher latitudes than 25° the horizontal eddy diffusion gradually increases with latitude and is the main cause of dispersion. This point

is an important basis of the present analysis. The meridional mean velocity $\langle v\rangle$ for Mar.-May at 10°-20°N is about 0.6 m/s and −0.3 m/s (northward positive) at altitudes 10 and 2 km, respectively (Newell *et al.* 1972).

The conventional treatment of settling aerosols through the troposphere is to neglect their radiative impact upon the atmosphere because of rapid dispersion in the troposphere. In the following, we shall show that if the concentration of the settling aerosols is sufficiently large, the atmospheric heating by them may be strong enough to modify the Hadley circulation and the residence time near the injected region would be much longer than the conventional estimates.

Suppose that the mean radius of the settling aerosols through altitude 15 km be 2 μm zonally distributed with peak at 20°N and meridional half width 10°, *i.e.*, from 15°N to 25°N and the vertical profile of the aerosol over 15 km is so disposed that total amount 10 Tg settles down through 15 km in 3 months (Fig. 2). It can be calculated from these figures that at 15 km, 20°N, the aerosol concentration μ_1 is 20 μg/m^3 and the number concentration is 0.3/cm^3. This may be compared with the observed value at south Texas (28°N) $N_{0.95}\sim0.2$/cm^3 in May 1982, which would give less μ_1 than the above value.

Then the mixing ratio $m(a)$ at 15 km in the center of the zonal belt is estimated at 10^{-7} g/g air $\sim100m_1$. When the settling continues downward, at the lower altitude 10 km the mixing ratio will be reduced to $60m_1$ due to the increase of air density, although the settling velocity decreases as shown in section 4. The latter value may be several times

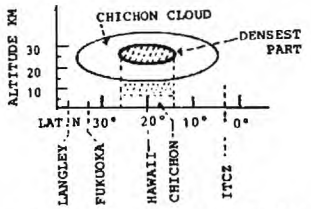

Fig. 2 Schematic illustration of zonal El Chichon volcanic cloud. Densest part is shown by shading and dotted region is discussed on radiative and thermodynamical theory in the text.

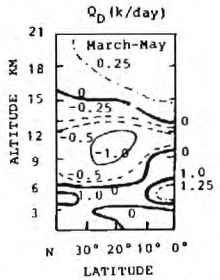

Fig. 3 Atmospheric diabatic heating rate Q_D for March May, which includes condensational, radiative, and boundary layer heating (Newell *et al.* 1974).

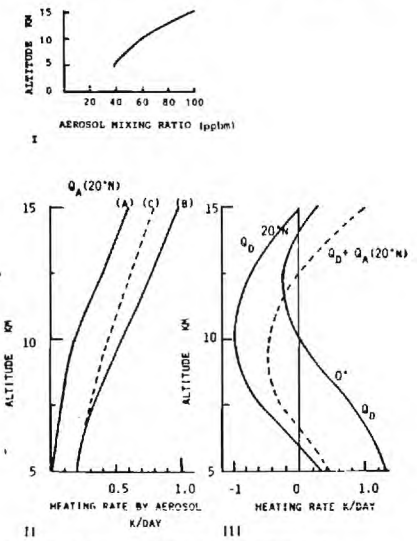

Fig. 4 Aerosol profiles and heating rate:
I Profile of aerosol mixing ratio in units $m_1=10^{-9}$ g/g air, which is estimated to be present for one season after eruption of El Chichon April 1982.
II Profiles of heating rate by aerosols Q_A induced by absorption of radiation at 20°N (in units K/day): Curves (A), (B), and (C) denote different aerosol refractive indices (see text).
III Profiles of Q_D at 20°N and 0°N (Newell *et al.* 1974) and Q_D+Q_A at 20°N.

those estimated by lidar at Fukuoka (33°N) $f(70\pm70)m_I$ ($f\sim0.5$). In May the meandering of El Chichon zonal flow was appreciable, and hence at times they might be of the same order of magnitude. At the present stage the influence of the mean Hadley circulation to the distribution of aerosols is neglected, as is that of horizontal diffusion.

We assumed the distribution of settling aerosols vs. altitude as shown in Fig. 4 I for the latitude 20°N, which would be expected for 3 months after the injection. The initial injection of some volcanic aerosols in the same altitude range might be present. The distribution is also assumed to have Lorentzian distribution with half width 10°, *i.e.*, the aerosol mixing ratio at the latitude ϕ is given by $m(\phi)=m(\phi_0)\Delta^2/[(\phi-\phi_0)^2+\Delta^2]$, where $\phi_0=$ 20°N and $\Delta=5°$.

We calculated atmospheric heating rate Q_A due to aerosols induced by the absorption of solar short wave and terrestrial long wave radiations, according to the theoretical study by Mugnai *et al.* (1978) as shown in Fig. 4 II. The heating rate is compared with diabatic atmospheric heating rate (radiative, condensational and boundary layer heatings all included) for Mar.-May by Newell *et al.* (1974) which is thought to be the motive power of the atmospheric general circulation (Fig. 3). The curves (A), (B) and (C) in Fig. 4 II are obtained by using aerosol models with refractive index $m=n-i\kappa$:

(A) $\kappa(vis.)=0$: sulphuric acid aerosol with no impurities. *vis.* denoting the value for the visible wave length range.

(B) $\kappa(vis.)=0.005$: impure sulphuric acid,

(C) volcanic ash particles.

The case (B) would be most probable for the present event. In Fig. 4 III, diabatic heating rate Q_D at the equator, 20°N and combined heating rate Q_A+Q_D at 20°N are shown. In the calculation of Mugnai *et al.* (1978) the heating of the atmosphere does not contain atmospheric absorption of the aerosol infrared emission and hence it may be underestimated to some extent. In Fig. 5 the diabatic heating rate Q_D at the altitudes 12, 10, 8, and 6 km are shown in I, II, III and IV, respectively by dashed curves. The combined heating rate

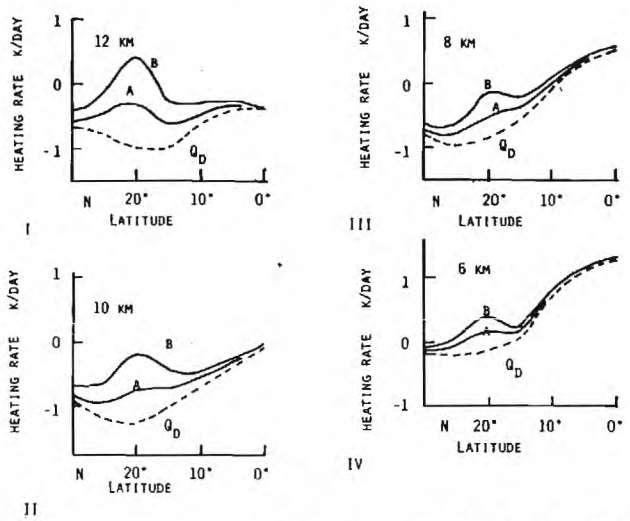

Fig. 5 Diabatic heating rate Q_D at altitudes I : 12 km, II : 10 km, III : 8 km, IV : 6 km. denoted by dashed lines (Newell *et al.* 1974) and A : Q_D+Q_A, B : Q_D+2Q_A at every altitudes.

Q_D+Q_A, and Q_D+2Q_A are shown by the solid curves A and B, respectively in the same figures at every altitude. It may be seen that Q_A or $2Q_A$ are of the same order of magnitude as Q_D near 20°N and have opposite sign at some altitude range.

Holton (1972*a*) shows by diagnostic equation that tropical Hadley circulation is generated by meridional gradient of heating rate in the upper troposphere. The heating Q_A over 15°-25°N may greatly reduce the meridional gradient due to Q_D alone and hence may slow down the Hadley circulation in northern tropical region or even reverse the sense of the mean motion, if the value of $m(a)$ is more than the present estimates for the early period of one season of concern.

According to Quiroz (1983) the westerly wind at the altitude 200 mb (11.5 km) over tropical Pacific (165°W-115°W) and easterly wind at the altitude 850 mb (1.5 km; over 135°E-170°W) began to change to opposite directions, respectively in April 1982. The triggering of El Niño Southern Oscillation represented by the variation of SST might be accomplished by the mechanism mentioned above, followed by coupled oscillations of atmosphere and ocean as shown by a preliminary model by Philander *et al.* (1984).

The neglection of mean atmospheric motion to determine the distribution of settling aerosols is reasonable under the considerations, but the horizontal diffusion in higher latitudes than 25°N may have some effect. The northern boundary of the zonal flow may be more obscure than that explained here.

4. Discussion of the results

Stratospheric warming following El Chichon eruption was discussed by Labitzke *et al.* (1983), Angell and Korshover (1983) and Fujita (1984). According to the first law of thermodynamics, the heating rate Q is related to the variation of the atmospheric temperature as follows:

$$\frac{d}{dt}C_pT=\alpha\frac{dp}{dt}+Q \qquad (8)$$

where conventional notation as in Holton (1982*a*) is used.

The relation between the variations of Q and T is not straightforward and can have opposite sign. In order to discuss the dynamical effect, the heating rate Q should be estimated as in the present note.

It follows from equation (8) that

$$\left(\frac{\partial}{\partial t}+V\cdot\nabla\right)\ln\theta+w\frac{\partial\ln\theta}{\partial z}=\frac{Q}{C_pT} \qquad (9)$$

where w is vertical velocity and θ is potential temperature.

In the absence of the first term of the left hand side of (9), the value of w is given by

$$w=(H/\kappa)(Q/C_pT) \qquad (10)$$

where $\kappa=(\partial\ln\theta/\partial z)H$ is proportional to the static stability. Essentially similar equation is a basic process of QBO modification theory by Dunkerton (1983). The aerosol heating would produce upward advection, but in reality the value of Q should include other kind of radiative cooling superposed on the aerosol heating as shown in Fig. 5. Therefore unless the net value of Q becomes positive, cancellation of the falling velocity of aerosols would be small. Moreover the first term of the left hand side of (9) will be important.

As shown in the previous section, the aerosol heating would reduce the meridional gradient of the diabatic heating rate, and hence the meridional velocity of the Hadley cell. If atmospheric heating by the infrared aerosol radiation is taken into account, the values of Q_A may be increased by a factor being probably not greater than 2.

Thus the dispersion in the upper troposphere would be much reduced at subtropical latitudes 15°-25°N, and hence the residence time of settling aerosols near the original injection point would become much longer than those suggested by conventional theory.

For simplicity, we may use the following equations to show the total amount of falling aerosols:

$$v_s\cdot\mu_s\cdot ST=M_{st} \qquad (11)$$

$$m(a)=\mu_s/\rho_{air} \qquad (12)$$

where v_s=falling velocity of aerosols, μ_s=aerosol mass concentration per unit volume at the center of the zonal flow, ρ_{air}=air density.

S=bottom area of zonal flow of El Chichon cloud from 15° to 25°N, $T\sim7.8\times10^6$ s (3 mo.) and $M_{st}\sim10Tg$. According to U.S. Standard Atmosphere Supplements 1966 at 15°N the air density ρ_{air} increases downward more slowly in the upper troposphere than it does at 30°N. The value of $v_s=(2/9)(\rho_p r^2 g/\eta)(1+A\lambda/r)$ decreases downward, where η=dynamic viscosity coefficient, λ=mean free path, ρ_p=density of material of particles, $A=a$ constant =0.864, g=acceleration by gravity. And hence the value of μ_s increases downward from the equation of continuity. Thus we obtained the vertical distribution of $m(a)$ shown in Fig. 4 I as the intermediate values between 15°N and 30°N. We have $v_s(\sim0.15$ cm/s) at 15 km and it can be readily seen that μ_s is inversly proportional to $(v_s T)$ for a given value of M_{st}.

We utilized the calculated results by Mugnai *et al.* (1978) which are made based on the U.S. Standard Atmosphere Supplements 1966 at 15°N, and the infrared flux due to the theoretical method of Rodgers and Walshaw (1966).

The latter showed that if the tropical troposphere is reasonably cloudless, an absorber near the tropopause can cause considerable heating due to absorption of radiation from ground at high temperature. Near 20°N it will fit the situation and now the absorber is the aerosols consisting mainly of sulfuric acid and of few impurities like silicate and carbon denoted by (B) in the previous section. The imaginary part of the refractive index for the visible wavelength $\kappa(vis.)$ is 0.005 for the aerosols and 0.05 for the silicate. The solar heating is about twice the above mentioned infrared heating at the altitude near 10 km and the net heating is shown in Fig. 4 II. The solar heating will increase with possible increase of impurities in the aerosols.

The amount of heating rate 1 K/day for the altitude range 9-11 km is due to the absorption of radiative flux 9 W/m². This value is larger than 2 W/m²: the mean rate of dissipation of atmospheric kinetic energy by the friction at the surface of the globe. The absorption 6 W/m² of the above 9 W/m² is about 2% of the solar radiative flux 350 W/m² and remaining 3 W/m² is about 1% of the infrared upward flux from the globe. Therefore the perturbation of the radiation field by the presence of the above mentioned aerosols will be very small.

The calculation of heating rate by Mugnai *et al.* (1798) are made on the assumption: the amount of aerosols is so small that the variations of the radiation and the temperature distributions due to the aerosol heating in the atmosphere are negligible.

In the present work, it is further assumed that the variation of atmospheric temperature due to significant aerosol heating is very small due to the dissipation of increased internal energy by the mechanical work done to decrease or modify the Hadley cell mean motions and that the surface temperature is held almost constant for one season due to the large thermal inertia of the ocean. If there are significant temperature rise in the altitude range mentioned above, the infrared cooling would increase and hence the present calculations would show overestimated heating rate than the real value. Recent analysis of Angell and Korshover (1984) seems to support our treatment.

In the early period of one season after the Chichon injection, the height range 12-15 km near 20°N will be heated by aerosols. The equatorward gradient of heating would transport a small amount of aerosols towards ITCZ where very low temperatures (<−83°C) exist at limited places (Newell and Gould-Stewort, 1981). The settling aerosols over ITCZ will form cirrus-like cloud, in such a very low temperature, according the theory of Steele *et al.* (1983). The cirrus like cloud will act as a semi-transparent resonator with earth surface due to the size of its particles being not much less than the half wavelengths of the infrared earth radiation. The infrared earth radiation inside the resonator will be intensified and hence the absorption of the radiation by the atmosphere or aerosols will be increased. This zonally very inhomogeneous heating at the height range might modify the Walker circulation.

Thus far zonal homogeneity of the Chichon cloud was assumed. But according to Robock and Matson (1983) appreciable zonal inhomogeneity and meandering of the cloud was present. It would be possible that the settling cloud concentration at the altitudes 8-12 km near Mexico within the longitudinal distance about 30° from El Chichon was ten times the zonal mean value assumed in Fig. 4 for several weeks. Then atmospheric heating by these aerosols will be about 5 K/day or more for about several weeks at the altitudes. If significant inclusion of impurity like carbon in addition to sulfuric acid is taken into account, heating would be appreciable. Meandering or broadening of the zonal wind would transport the cloud to lower latitudes temporarily for significant fraction of the period. According to the study of Holton (1972*b*) the heating of the atmosphere of this order of magnitude is possible to excite the mixed Rossby-gravity waves and Kelvin waves in the tropical region, of which the latter can significantly modulate the trade wind at the surface. In reality the weakening of the trade wind began in April 1983 (Philander, 1983; Quiroz, 1983).

The supposed modification of the circulation should be subject to numerical model simulations to test the validity. Much more work is still needed to confirm the situations.

When this note is written, Dr. J. J. DeLuisi kindly sent us all lidar data at Mauna Loa (19°N) for one season after April 1982. A renormalization of the data in a similar way as in a companion paper (Hirono *et al.*, this issue) gave results supporting our model shown in Fig. 4 I. The details will be reported in a later paper.

5. Concluding remarks

In the tropical upper troposphere, the horizontal diffusion coefficient is thought to be lowest on the globe. The Chichon volcanic zonal cloud had its center at about 20°N for the first one season and the densest part was located at latitudes from 15°N to 25°N. The profiles of settling aerosols during this season is supposed to be within this subtropical region, where the amount of precipitation is also small, especially above altitude 5 km. The residence time of settling would be much longer than about 10 days estimated by conventional analysis in the middle and higher latitudes. It is shown that the atmospheric heating rate around 15°-25°N is sufficiently strong to modify Hadley circulation. For the season, the Hadley circulation in the northern tropics would be weakened and also the trade wind at the same time. This may be effective for the triggering of El Niño Southern Oscillation, which would be followed by the coupled atmosphere-ocean oscillations.

For several weeks after eruption, the Chichon cloud was zonally very inhomogeneous. In the region near Mexico, the concentration of falling aerosols including ash near the altitudes 8-12 km might be ten times those zonal mean values presented here (Hirono *et al.*, in this issue). Therefore the atmospheric heating by them might be strong enough to excite equatorial waves, of which Kelvin waves may modify the trade wind at the surface.

These mechanisms are qualitative at present. Much more work is essential to confirm the situation.

Acknowledgements

We thank Prof. P. Handler of University of Illinois at Urbana-Champaign for sending us a manuscript before publication in Geophysical Research Letters. Many thanks are also due to Dr. M.P. McCormick and other members of NASA SAGE II Science Team for their valuable discussions during meeting in Fukuoka for June 1984.

References

Angell, J.K. and J. Korshover, 1983: Comparison of stratospheric warming following Agung and Chichon., *Month. Weather Rev.*, **111**, 2129-2135.

——, ——, 1984: Comparison of tropospheric temperatures following Agung and El Chichon volcanic eruptions, *Mon. Weath. Rev.*, **112**, 1457-1463.

Czeplak, G. and C. Junge, 1974: Studies of interhemispheric exchange in the troposphere by a diffusion model. *Adv. Geophys.*, **18B**, 57-72.

Dunkerton, T.J., 1983: Modification of stratospheric circulation by trace constituent changes?. *J. Geophys. Res.*, 88, 10831-10836.

Fujita, T., 1984: Preprint at the Spring meeting, *Met. Soc. Japan*, 1984 (in Japanese)

Handler, P., 1984: Possible association of strato-

spheric aerosols and El Niño Type events. *Geophysical Res. Lett.*, **11**, 1121-1124.

Hansen, J. E., W.-C. Wang and A. A. Lacis, 1978: Mount Agung eruption provides test of a global climatic perturbation. *Science*, **199**, 1065-1068.

Hirono, M. and T. Shibata, 1983: Enormous increase of stratospheric aerosols over Fukuoka due to volcanic eruption of El Chichon in 1982, *Geophys. Res. Lett.*, **10**, 152-154.

———, ———, M. Fujiwara and N. Fujiwara, 1984: Enormous increase of volcanic clouds in the stratosphere over Fukuoka after April 1982., *Geofisica Internacional*, **23**, 259-276.

Hofmann, D. J. and Rosen J. M., 1983: Stratospheric sulfuric acid fraction and mass estimate for the 1982 volcanic eruption of El Chichon., *Geophys. Res. Lett.*, **10**, 313-316.

Holton, J. R., 1972a: An introduction to dynamic meteorology. *Acad. Press.*

———, 1972b: Waves in the equatorial stratosphere generated by tropospheric heat sources. *J. Atmos. Sci.*, **29**, 368-375.

Kida, H., 1983: General circulation of air parcels and transport characteristics derived from a hemispheric GCM. Part I. Determination of advective mass flow in the lower stratosphere., *J. Meteor. Soc. Japan*, **61**, 171-187.

Labitzke, K., B. Naujokat and M. P. McCormick, 1983: Temperature effects on the stratosphere of the April 4, 1982 eruption of El Chichon Mexico. *Geophys. Res. Lett.*, **10**, 24-26.

——— and ———, 1984: On the effect of the volcanic eruption of Mount Agung and El Chichon on the temperature of the stratosphere., *Geofisica Internacional*, **23**, 223-232.

Lamb, H. H., 1970: Volcanic dust in the atmosphere with a chronology and assessment of its meteorological significance., *Phil. Trans. Roy. Soc. Lon.*, **266**, 441-533.

Mugnai, A., G. Fiocco and G. Grams, 1978: Effects of aerosol optical properties and size distributions on heating rates induced by stratospheric aerosols. *Quart. J. R. Met. Soc.*, **104**, 783-796.

Newell, R. E. and S. Gould-Stewart, 1981: A stratospheric fountain?, *J. Atmos. Sci.*, **38**, 2989-2996.

Newell, R. E., J. W. Kidson, D. G. Vincent and G. J. Boer, 1972: The general circulation of the tropical atmosphere and interactions with extropical latitudes, Vol. I, M. I. T.

———, ———, ———, ———, 1974: Vol. II, M. I. T.

Philander, S. G. H., 1983: El Niño southern oscillation Phenomena., *Nature*, **302**, 295-301.

———, T, Yamagata and R. C. Pacanowski, 1984: Unstable air sea interactions, *J. Atmos. Sci.*, **41**, 604-614.

Quiroz, R. S., 1983: The climate of the El Niño winter of 1982-1983—A season of extraordinary climate anomalies. *Mon. Wea. Rev.*, 111, 1685-1706.

Robock, A. and M. Matson, 1983: Circumglobal transport of the El Chichon volcanic dust clouds., *Science.*, **221**, 195-197.

———, 1985: Climate model simulations of the effects of the El Chichon Eruption, *Geofisica Internacional* (in press.)

Rodgers, C. D. and C. D. Walshaw, 1966: The computations of infrared cooling rate in planetary atmospheres, *Quart. J. Roy. Mete. Soc.*, **92**, 67-92.

Schatten, K. H., H. G. Mayer, I. Harris, H. A. Tayler Jr., 1984: A zonally symmetric model for volcanic influence upon atmospheric circulation, *Geophys. Res. Lett.*, **11**, 303-306.

Steele, H. M., P. Hamill, M. P. McCormick and T. J. Swissler, 1983: The formation of polar stratospheric clouds, *J. Atmos. Sci.*, **40**, 2055-2067.

Thomas, G. E., B. M. Jakosky, R. A. West and R. W. Sanders 1983: Satellite limb-scanning thermal infrared observations of the El Chichon stratospheric aerosol: First results. *Geophys. Res. Lett.*, **10**, 997-1000.

火山変動とエル・ニーニョ南方振動の関連の可能性
—大気中の火山性エアロゾルのライダー観測

広野求和・柴田　隆・藤原玄夫
九州大学理学部物理学科

NOTES AND CORRESPONDENCE

A Comparison of SAGE I Data During the Stratospheric Warming of February-March, 1979

By Ronald M. Nagatani

Climate Analysis Center NOAA, Camp Springs, MD 20233 USA

M. P. McCormick and L. R. McMaster

NASA Langley Research Center Hampton, VA 23665 USA

(Manuscript received 7 November 1984, in revised form 30 January 1985)

Abstract

The fine scale vertical structure of SAGE I ozone and aerosol data during a stratospheric warming is investigated using meteorological and SBUV ozone data. By stratifying the ozone and aerosol data for a limited time period, we are able to compare the structure of profiles under different meteorological conditions. For example, the cold air region shows more laminated structures than the other regions. In addition, vertical motions calculated at the same locations as the SAGE profiles show that they are consistent with variances found in the ozone and aerosol data.

I. Introduction

The purpose of this paper is to characterize some of the fine scale structure in profiles of ozone and aerosols during a stratospheric warming using data from the Stratospheric Aerosol and Gas Experiment (SAGE I). In order to do that, the large-scale synoptic conditions are assessed with maps produced by the U. S. National Meteorological Center (NMC). The main stratospheric products of the U. S. National Meteorological Center are globally analyzed and numerically gridded meteorological fields of heights and temperatures. These stratospheric gridded fields, at levels from 70 to 0.4 mb, have been analyzed and archived on a daily basis at NMC since September 1978. Stratospheric heights and temperatures up to 10 mb have been available since 1964. The maps have been analyzed by an iterative correction scheme discussed by Cressman (1959) with some modifications discussed by Yanai (1964). Gelman *et al.* (1983) summarize some of the data and analysis procedures that went into the maps. They also discuss the limitations of the products. Also available as a product from NMC are hemispherically analyzed maps of ozone mixing ratios from the Nimbus 7 Solar Backscatter Ultraviolet (SBUV) instrument at the same stratospheric levels as the height and temperature data from 30 to 0.4 mb. The SBUV ozone data are also analyzed by the same scheme discussed above for the meteorological maps. These maps will be used as a guide to stratify the SAGE data.

The SAGE I program is described by McCormick *et al.* (1979) and the SBUV instrument is described by Heath *et al.* (1975). The SAGE I instrument is a four-channel photometer that measures the intensity of sunlight at sunrise and sunset events with a vertical resolution of 1 km. The stated accuracies are 5% at 25-40 km for ozone and

[1] This paper was presented at the Japan-U. S. Seminar on "Review of work related to sensing of stratospheric aerosol and gas components", Fukuoka, 12-14 June 1984.

10% for aerosols between the tropopause and 25 km and 30% at 25-35 km (Russel, 1979). SBUV senses the solar backscatter ultraviolet radiation at the nadir point, yielding more than 1000 data points over the globe each day with a vertical resolution between 5 to 8 km. Comparisons with ground truth indicate a bias of about 5% lower for SBUV below the mixing ratio peak and a 5% agreement with optical ozonesonde rockets at higher levels (Fleig *et al.*, 1982). With a clear difference in horizontal and vertical resolution for the ozone data, we see that both instruments can complement each other to enhance their capabilities. In this context, given the fine scale vertical resolution of data from SAGE I, we will compare SAGE ozone and aerosol data together with NMC analyses of heights and temperatures and ozone analyses from the SBUV instrument on Nimbus 7.

McCormick *et al.* (1983) have looked at data from the Stratospheric Aerosol Measurement (SAM II) satellite system and found aerosol profiles with lower optical depths to lie within the lower pressure region of the polar vortex at 50 mb for a single day. Following up on their investigation, for this paper we will focus our attention on the 2 mb level near the ozone volume mixing ratio peak during a dynamically active period at this level. The

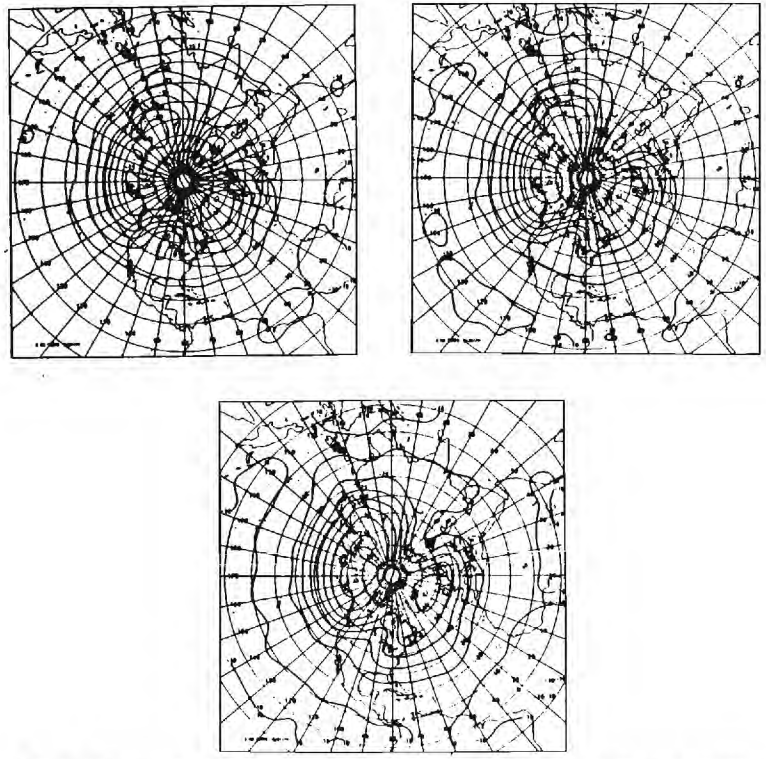

Fig. 1 2-mb temperatures (Centigrade). Letters C(cold) and W(warm) determine locations of SAGE data points plotted in Fig. 4c and 4b, respectively. a) February 27, 1979. b) February 28, 1979. c) March 1, 1979.

period investigated is during a time when a stratospheric warming was in progress in late February to early March 1979. The profiles we look at will extend to the lower stratosphere; thus we will also utilize some meteorological data at other levels.

II. Stratospheric Warming of February-March 1979

In late February 1979, by February 21, a strong warming occurred in the stratosphere between 50 to 0.4 mb culminating in a circulation reversal at 2 mb on February 27, 1979 near the polar regions. The warming is documented by Quiroz (1979). Others have investigated various phases of the winter period that included the major warming. Wang *et al.* (1983) used SAGE I data to investigate ozone transports during the period of the warming. Nagatani and Miller (1984) used SBUV data to investigate, on a monthly basis, transports and ozone-meteorological relationships during the course of the first year of SBUV operation. We will focus our attention to the three days when the warming was already in progress from February 27 through March 1, 1979. These three days were chosen because SAGE I data were obtained at desirable latitudes and the meteorological data collected during this period were optimal also.

Figures 1a-1c show the 2 mb temperatures on February 27, 28, and March 1, 1979 while

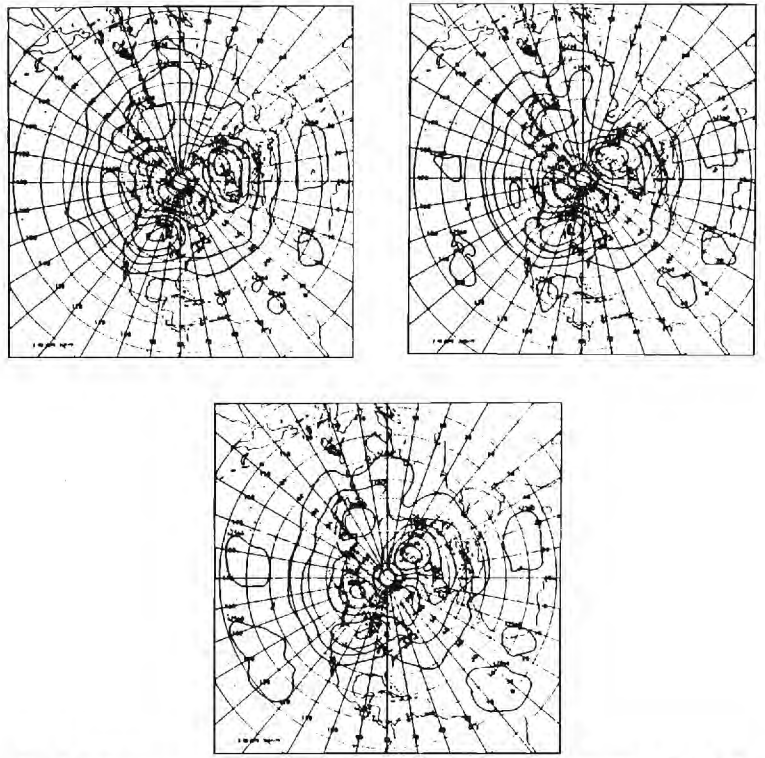

Fig. 2 2-mb geopotential meters. Letter L(low pressure) determines locations of SAGE data points plotted in Fig. 4d. a) February 27, 1979. b) February 28, 1979. c) March 1, 1979.

Figs. 2a-2c show the geopotential heights for the same days. On February 27, the warming had already reached its peak, with the warmest air over the Barents Sea region near the polar regions as shown in Fig. 1a. Figure 2a for the same day shows a circulation reversal near the polar regions, with the anticyclone splitting the polar vortex into two main lows and a third weaker low over the Siberian region. On the succeeding two days in Figs. 1b-1c for the temperatures and Figs. 2b-2c for the heights, the warm air weakens and recedes and the anticyclone begins to retrogress to its more normal position over the Aleutian region.

The ozone distributions at 2 mb obtained from an analysis of SBUV data for the same three days are shown in Figs. 3a-3c. We see that the warm air (Fig. 1) is accompanied by an ozone minimum over the Barents Sea region. This good negative correlation in the general patterns between temperature and ozone is expected on the basis of ozone photochemical theory in the upper stratosphere. As the warming weakens, the strength of the ozone minimum also decreases on February 28 and March 1. Note that the highest ozone amounts remain fairly static near the Kamtchatka Peninsula.

Having noted how the circulation, temperature, and ozone behaved during the stratospheric warming, we now group the SAGE I data according to similar meteorological conditions. We first use the SBUV analyzed maps to determine the horizontal extent of highest and lowest ozone amounts and the regions affected during the three days. The location of the SAGE I profiles selected for these high and low ozone regions are represented by the letters H and L, respectively, in Figs. 3a-3c. The profiles for the high ozone regions on these three days are then plotted in Fig. 4a. The location of the points move from day to day because of the characteristics of the satellite and we therefore do a composite of the points. As in any composite, one must be careful in interpreting any differences or similarities in the data. In the case of the

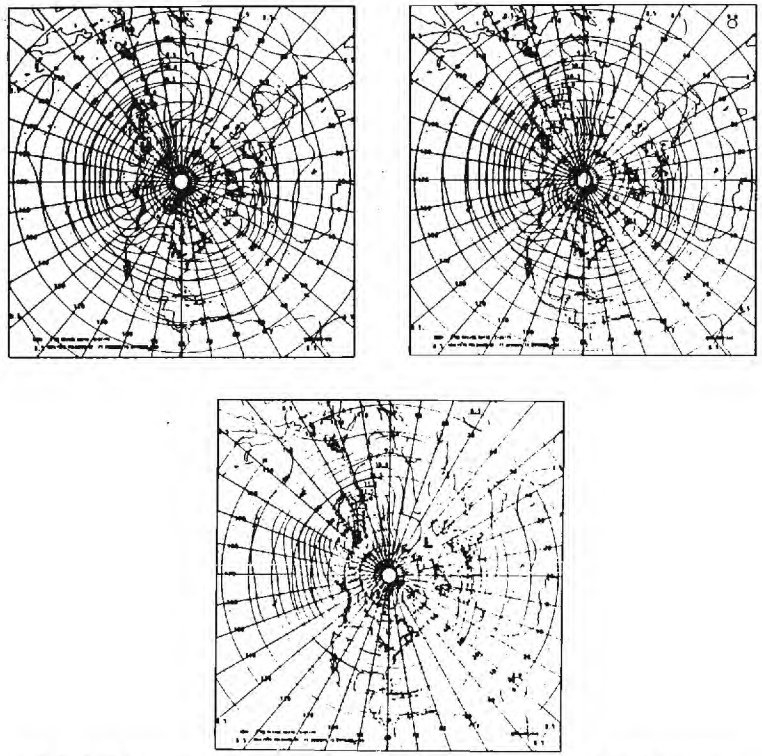

Fig. 3 2-mb ozone mass mixing ratios (μgm/gm). Letters H(high ozone) and L(low ozone) determine locations of SAGE data points plotted in Fig. 4a and 4b, respectively. a) February 27, 1979. b) February 28, 1979. c) March 1, 1979.

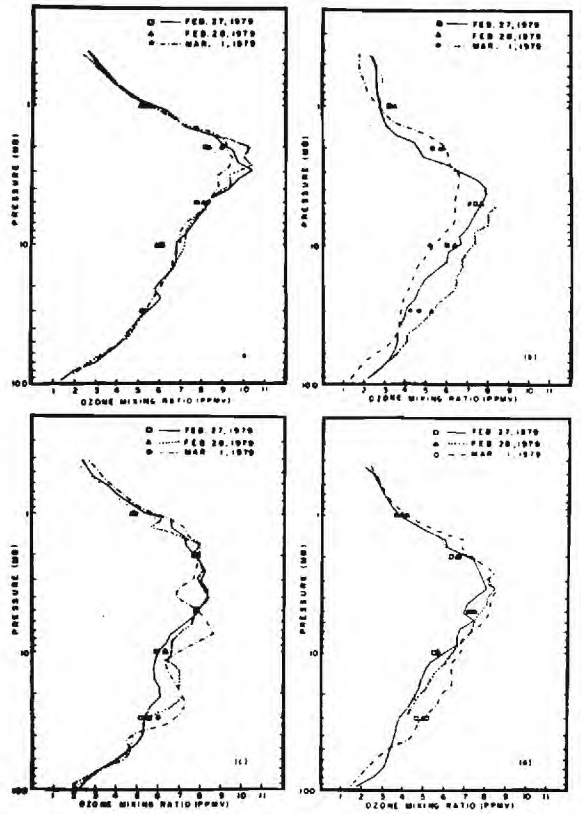

Fig. 4 Vertical profiles of ozone volume mixing ratios (ppmv) from SAGE I. Squares, triangles, and circles represent SBUV data interpolated from maps to SAGE measurement locations. a) Profiles from high SBUV ozone regions (indicated by letter H in Fig. 3). b) Profiles from warm temperature region (indicated by letter W in Fig. 1) and from low SBUV ozone region (indicated by letter L in Fig. 3). c) Profiles from low temperature region (indicated by letter C in Fig. 1). d) Profiles from low pressure region (indicated by letter L in Fig. 2).

study here, we are more interested in profiles under various conditions, so the changing conditions at a specific location is not crucial here. The squares, triangles, and circles in Figs. 4a-d represent SBUV data from analyzed maps interpolated to SAGE measurement locations. A comparison between SBUV and SAGE shows that aside from any biases between the two systems, both systems indicate similar profile shapes and changes of ozone with time.

A striking feature of the vertical profiles in Fig. 4a is the relative stability or low variability among the profiles. This should become more evident as we compare plots of other profiles under different conditions, with the level of the ozone maximum between 2 and 3 mb. Note also the sharp peak in the ozone maximum. Figure 4b shows the vertical profiles of ozone in the region of low SBUV ozone (high temperature) at 2 mb. The profiles show greater variability, especially below the ozone peak, indicating a more dynamically active region than shown in Fig. 4a for the high ozone region. A comparison between the two figures show the dramatic differences between the two regions including a lower peak between 6 and 3 mb for the low ozone (high temperature) region. The high ozone region represents a somewhat static region, where the winds are not as strong as in the other regions. The warm air or low ozone region, on the other hand, is in a highly dynamic region where the stratospheric warming is in progress and where large-scale overturning of the atmosphere is occurring. As a result, the profiles also reflect this difference. Details of the warming are found in Quiroz (1979), where he shows a circulation reversal at the mid-stratospheric level at 10 mb and he also shows time-height sections of the warming having significant amplitudes down to the lower stratospheric levels between 50 and 100 mb.

The region of low ozone amount also correspond to the region of high temperatures. We can therefore compare Fig. 4b with the next group of SAGE I profiles plotted in Fig. 4c, which correspond to the low temperature regions. The SAGE measurement locations are represented by the letter C in Fig. 1. The vertical profiles show an interesting laminated structure, much more than the other regions, possibly being caused by advection of different layers of air into the region. Also there is no sharp distinct maximum as in the previous two figures. Note the region between 20 and 30 mb shows a secondary maximum, faintly visible on February 27 and strongly evident on February 28 and March 1. Also note that the broad upper layer shown in the February 27 and 28 profiles from 1 to 10 mb appears in the SAGE data to break up into two separate layers in the March 1 profile. We will focus our attention on this same region when we look at the aerosol plots.

A final plot of SAGE I ozone profiles, corresponding to regions in the polar vortex centered over Canada and indicated by the letter L in Fig. 2, is shown in Fig. 4d. There was a tongue of warm air coming into Canada at the time, though not as strong as the one over the Barents Sea region, associated with low ozone amounts evident in both the SBUV and SAGE data. The profiles are similar to those in Fig. 4b near the warm air region, with similar variances and structures. A slightly higher peak is evident compared to that of Fig. 4b, reflecting a situation somewhere in between that of Fig. 4a and Fig. 4b, compatible with the meteorological conditions.

Profiles of the SAGE 1 μm aerosol extinction were also plotted for the same locations as for ozone and they also show very interesting features. Figure 5a is a plot of the aerosol extinction for the high ozone region. Expected errors for February 27 are plotted as horizontal lines. While the expected errors are large at upper levels, we can still gain some insight into the differences, especially since the expected error drop off quite rapidly at the lower levels. As in the case with ozone, the variability in Fig. 5a is much less than the variability in the other plots to follow. This implies that the exchange of air with the outside is minimal throughout the column of air compared to the other regions. Figure 5b is a plot of the local vertical motions computed by the adiabatic method:

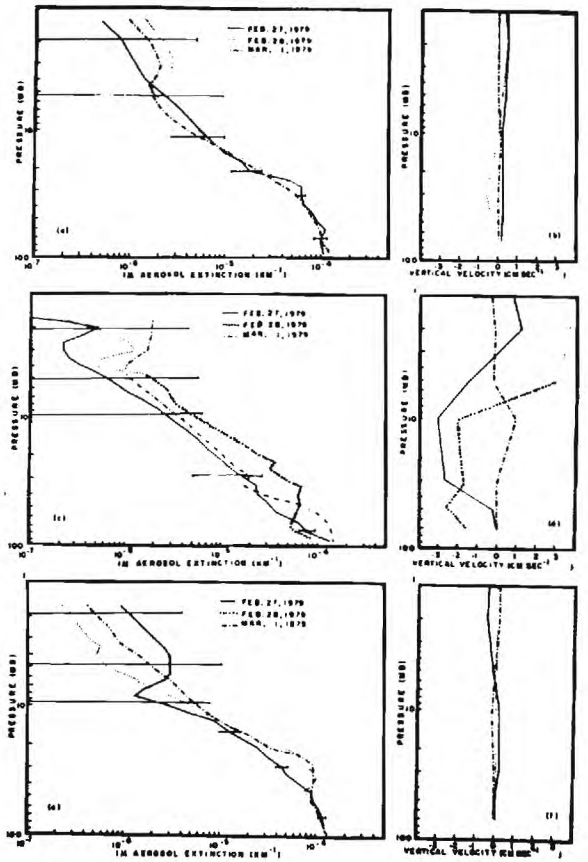

Fig. 5 Vertical profiles of 1 μm aerosol extinction from SAGE I with corresponding vertical velocities for the same points in the adjacent figure. Horizontal lines are expected errors for February 27. a-b) Same SAGE points in the high ozone region as in Fig. 4a. c-d) Same SAGE points in the low ozone (high temperature) region as in Fig. 4b. e-f) Same SAGE points in the low temperature region as in Fig. 4c.

$$w = \frac{\left(\frac{\partial T}{\partial t}\right)_p + (V_g \cdot \nabla T)_p}{\frac{pg}{RT}\left(\frac{\partial T}{\partial p}\right) - \frac{g}{c_p}}$$

where the subscript p means that the variable is evaluated at a constant pressure surface, V_g is the geostrophic wind, T is the Kelvin temperature, c_p is the specific heat capacity at constant pressure, g is the acceleration of gravity, R is the gas constant, and $(\partial T/\partial t)_p$ is evaluated in a 48-hour period. Gridded fields of heights and temperatures are used to compute the vertical velocities and interpolated to the SAGE data points. As seen in the figure, very weak upward and downward motions are evident throughout the

column, partially accounting for the low variability.

Figure 5c shows a plot of the aerosol extinction profiles in the high temperature (low ozone) region. For February 27 and March 1, the aerosol extinction is low throughout the whole column compared to many of the other profiles. As in the case with ozone, the variability between all three profiles is largest in this dynamically active region and the vertical motions plotted in Fig. 5d confirm this activity. Compared to the plot in Fig. 5b, we see larger upward and downward motions throughout the column of air.

Finally, Fig. 5e shows the aerosol extinction profiles for the low temperature region. Note the region between 20 and 30 mb for February 28 and March 1, where a layer of air with very different properties seems to have been advected into the region as in the case with ozone. The vertical motions in Fig. 5f show weak upward and downward motions, suggesting that the layer of air mentioned previously is probably a result of horizontal advection. Papers by Danielsen and Mohnen (1977) and Evans *et al.* (1979) have found similar types of structures at lower stratospheric levels, attributed to tropopause folding events. The features seen in the SAGE data, however, are at higher levels than those investigated with ozonesondes. Evans *et al.* (1979) also suggest photochemical sinks for their "notches". However, during a stratospheric warming, the most probable explanation would be vertical or quasi-horizontal advection, especially since the vertical mesoscale features are seen in both the ozone and aerosol data.

III. Summary and conclusions

The fine vertical resolution of SAGE I provides a unique dataset capable of being used for investigating synoptic and smaller scale features consistent with meteorological data and for comparison with other ozone data such as SBUV. We have used the data here in a complementary fashion and anticipate more studies in a similar vein. With SBUV 2 having been launched in December, 1984 on NOAA-F and SAGE II having been launched from the space shuttle also in October, 1984, the next generation of similar type instruments can also complement each other in further studies.

Summarizing some of the results of our limited study, if we focus our attention on the 2-mb level in stratifying the data for a limited time period during a stratospheric warming, we find that the cold air region shows more laminated structures than the other regions in addition to having a peak that is not well defined. The high ozone region shows a sharp peak, with the whole profile showing less variability than the other regions. Vertical motions calculated at the same locations as the SAGE profiles show that they are consistent with the variances found in the ozone and aerosol data.

Acknowledgements

This study has been supported by NASA. We wish to thank M. E. Gelman, R. S. Quiroz, and P. Wang for constructive comments on the manuscript, A. J. Miller for his helpful discussions, and D. F. Heath and A. J. Fleig for consultations on the original SBUV data.

References

Cressman, G. W., 1959L: An Operational Objective Analysis System, *Mon. Wea. Rev*, 87, 367-374.

Danielsen, E. F. and V. A. Mohnen, 1977: Project Dustsorm Report: Ozone Transport, in Situ Measurements, and Meteorological Analyses of Tropopause Folding, *J. Geophys. Res.*, 82, 5867-5877.

Evans, W. F. J., I. A. Asbridge and C. L. Mateer, 1979: Observations of a 'Notch' in the Stratospheric Ozone Layer, *J. Geophys. Res.* 84, 2159-2524.

Fleig, A. J., K. F. Klenk, P. K. Bhartia, D. Gordon and W. H. Schneider, 1982: User's Guide for the Solar Backscattered Ultraviolet (SBUV) Instrument First-Year Ozone-S Data Set. NASA Reference Publication 1095, 66 pp.

Gelman, M. E., A. J. Miller, R. M. Nagatani and H. D. Bowman II, 1983: Mean Zonal Wind and Temperature Structure During the PMP-1 Winter Periods, *Adv Space Res.*, 2, 159-162.

Heath, D. F., A. J. Krueger, H. A. Roeder and B. D. Henderson, 1975: The Solar Backscatter Ultraviolet and Total Ozone Mapping Spectrometer (SBUV/TOMS) for Nimbus-G, *Opt. Eng.*, 14, 323-331.

McCormick, M. P., C. R. Trepte and G. S. Kent, 1983: Spatial Changes in the Stratospheric Aerosol Associated with the North Polar Vortex, *Geophys. Res. Letters*, 1, 941-944.

McCormick, M. P., T. J. Pepin, W. P. Chu, T. J. Swissler, and L. R. McMaster, 1979: Satellite Studies of the Stratospheric Aerosol, *Bull. Amer. Meteor. Soc.*, 60, 1038-1046.

Nagatani, R. M. and A. J. Miller, 1984: Stratospheric Ozone Changes During the First Year of SBUV Observations, *J. Geophys. Res.*, 89, 5191-5198.

Quiroz, R. S., 1979: Tropospheric-Stratospheric Interaction in the Major Warming Event of January-February 1979, *Geophys. Res. Letters*, 6, 645-648.

Russel, P. B., editor, 1979: SAGE Ground Truth Plan—Correlative Measurements for the Stratospheric Aerosol and Gas Experiment (SAGE) on the AEM-B Satellite, NASA Technical Memorandum 80076, March 1979, 157 pp.

Wang, P., M. P. McCormick and W. P. Chu, 1983: A Study of the Planetary Wave Transport of Ozone During the Late February 1979 Stratospheric Warming Using SAGE Ozone Observation and Meteorological Information, *J. Atmos. Sci.*, 40, 2419-2413.

Yanai, M., 1964: An Operational Objective Analysis in the Tropics, Technical Paper No. 62, Dept. of Atmospheric Sciences, *Colorado State Univ.*, 21 pp.

1979年2～3月における成層圏突然昇温期間中の SAGE I データの比較

Ronald M. Nagatani

Climate Analysis Center/NOAA, Camp. Springs, MD 20233

M. P. McCormick and L. R. McMaster

NASA Langley Research Center, Hampton, VA 23665

NOTES AND CORRESPONDENCE

Measurements of Atmospheric Emission at High Spectral Resolution[1]

By David G. Murcray, Frank H. Murcray and Frank J. Murcray

University of Denver, Dept. of Physics, Denver CO 80208 USA

and

George Vanasse

Air Force Geophysics Laboratory, Bedford MA 01730, USA

(Manuscript received 7 November 1984, in revised form 28 January 1985)

Abstract

A liquid N_2 cooled infrared interferometer system was flown on a balloon and used to obtain atmospheric emission spectra at high spectral resolution at various altitudes. The instrument was also used to view the earth from 28 km. Samples of the spectra obtained during this balloon flight are presented.

1. Introduction

The role of the interaction between the earth's atmosphere and electromagnetic radiation in driving various meteorological processes has long been recognized. The complexity of the interaction particularly in the mid infrared precluded detailed theoretical studies until Elsasser (1942) introduced the so-called "Band Model" approximation which replaced the detailed line structure present in the absorption spectrum with an approximate function which smoothed out the spectral detail. The Elsasser model which was based on uniformly spaced lines was followed by a model by Goody (1952) based on randomly spaced lines. Incorporation of the band models into studies of the flow of radiation in the atmosphere resulted in a much better understanding of the flow and our ability to model meteorological processes. Elsasser pointed out that modeling the infrared molecular absorption spectra in detail was unnecessary for meteorological studies at that time since it was not possible to incorporate such detail into the models due to computational limitations. With the development of the large computers, this constraint has become less severe and many meteorological problems are being modeled using line-by-line calculations which retain the full spectral detail present in molecular absorption spectra. While the calculations can be carried out in great spectral detail, the absolute accuracy of such calculations depends on many factors not all of which are known with sufficient accuracy to allow such calculations to be performed accurately enough for some studies. Experimental investigations still play a major role in determining where the problems are and in furnishing the data needed to improve the calculations. The heart of such calculations lies in the accurate listing of the molecular absortion parameters for the various species present in the atmosphere. The data for a listing such as the AFGL tape come from laboratory investigations of the various compounds. Other factors which enter the calculations are the shape of the absorption lines, the widths of the lines, the temperature dependence of the absorption, etc. The test of the accuracy with which these calculations can be performed has to be based on spectra obtained within the atmosphere. As higher spectral resolution has become possible in the theoretical analysis, it has resulted in the requirement for increased resolution in the atmospheric experimental studies used to check the calculations. The majority of the experimental investigations have involved absorption studies. These have generally been made by using the sun as an infrared source and the atmospheric spectra obtained by operating the spectrometer from various platforms in the atmosphere (balloon, aircraft, ground). While in theory if one can calculate the transmission accurately it is also possible to calculate the atmospheric emisson accurately, in practice there are several aspects of the problem that require atmospheric emission spectra as a test of the theoretical calculations. In this paper we present high resolution atmospheric emission spectra obtained at various altitudes in the atmosphere using a balloon-borne spectrometer system.

[1] This paper was presented at the Japan-U.S. Seminar on "Review of work related to sensing of stratospheric aerosol and gas components", Fukuoka, 12-14 June 1984.

2. Instrumentation

The earth's atmosphere is a very weak source of infrared radiation and as a result instruments designed to measure the emission under high resolution at high altitude must be very sensitive. The sensitivity of the detectors used in the mid infrared is limited by the background radiation reaching the detector. This background radiation can be reduced by using cold baffles limiting the detector field of view, however for optimum sensitivity, everything within the detector field of view including the optical elements of the spectrometer must also be cooled.

The interferometer system used to obtain the emission spectra presented in this report was designed to operate at liquid nitrogen temperatures. Since the instrument was to obtain data in the atmosphere, this required that the unit be placed in a suitable vacuum dewar which kept frost from forming on the interferometer optics. The infrared transmitting window on the dewar, which allows atmospheric radiation to reach the system, should also be cooled for maximum sensitivity. Since the window is low emissivity and at the higher altitudes runs fairly cold (−40°C) it was not cooled for the results presented here.

The interferometer is a cat's eye system designed to operate at liquid nitrogen temperatures. It was also designed to maintain optical alignment when cooled from room temperature to 77 K. This was accomplished by constructing the total mechanical system of the same low temperature expansion coefficient material. Although the interferometer is run at 77 K, it is equipped with a Ge : Cu detector which requires cooling to at least 10 K to operate. A second dewar designed to hold the liquid helium required for cooling the detector is also incorporated into the system. The position of the moving mirror of the interferometer is monitored by optical fringes formed by passing a He-Ne laser through the interferometer system. The laser for this system is located outside the interferometer dewar and transferred to the interferometer by means of fiber optics. Data from the interferometer system are telemetered to the ground using a PCM telemetry system. A complete description of the instrument is given in a separate article (Murcray, 1984).

3. Results

The spectra presented in this report were obtained during a balloon flight made 23 October 1983. The total weight of the instrument ready for flight is approximately 1300 kgs. A 140,000 m^3 balloon was used to carry the payload to an altitude of 30 km. The balloon was launched at 0610 MDT from Holloman AFB New Mexico and ascended at an average rate of 250 m/sec. The balloon developed a

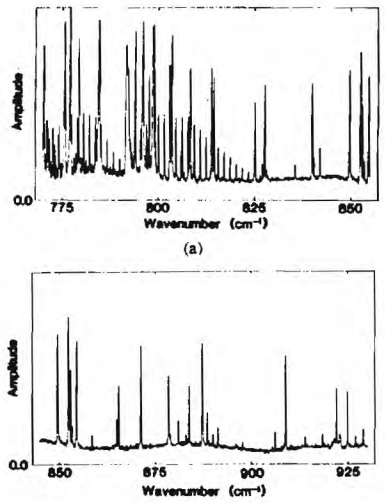

Fig. 1 Atmospheric emission spectrum obtained at an altitude of 4 km, viewing angle 7°. (a) 775 cm^{-1} to 850 cm^{-1}. The majority of the strong emission lines in this spectral region are due to H_2O, however the feature at 795 cm^{-1} is a CO_2 Q-branch and the lines due to the P & R branches are evident. (b) 850 cm^{-1} to 925 cm^{-1}. This region is dominated by H_2O lines.

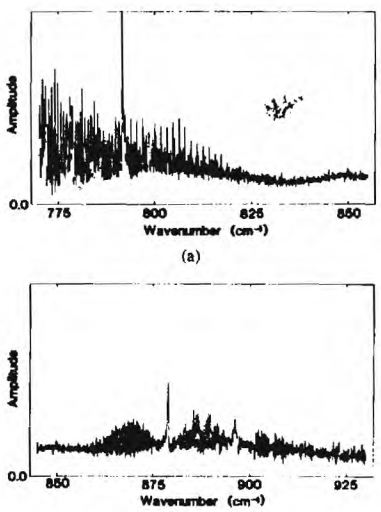

Fig. 2 Atmospheric emission spectrum obtained at an altitude of 15 km, viewing angle 7°. Vertical size expanded by ~2 from Fig. 1. (a) 775 cm^{-1} to 850 cm^{-1}. Emission is now dominated by lines due to CO_2 and O_3 with a continuum emission at 845-850 cm^{-1} due to $CFCl_3$. (b) 850 cm^{-1} to 925 cm^{-1}. HNO_3 emission features dominate this region with a small contribution from CF_2Cl_2 at 920-923 cm^{-1}.

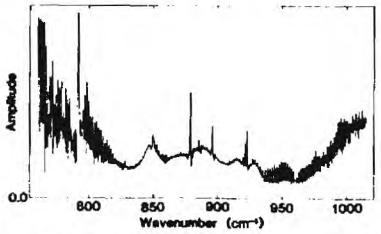

Fig. 3 Atmospheric emission spectrum obtained from an altitude of 30 km, viewing angle −3.2°. This spectrum shows emission in the 800 cm^{-1} to 1000 cm^{-1} window at a resolution of 0.12 cm^{-1}. The emission in the 845-850 cm^{-1} region is due to $CFCl_3$, 850-910 cm^{-1} by HNO_3, 910-935 cm^{-1} by CF_2Cl_2 and 950 cm^{-1} by CO_2.

leak shortly after reaching float altitude and gradually descended. During ascent the instrument was operated so that it looked at an elevation angle of 7°. Spectra obtained at intermediate altitudes are given in Figs. 1 and 2. Once the instrument reached float the instrument was rotated so that it received radiation from 3.2° below the horizontal. Figures 3 and 4 show a spectrum obtained when the instrument was viewing the limb emission. When it became evident that the balloon was descending a mirror was rotated into position so the instrument viewed the nadir. Spectra were obtained of the upwelling radiation until the flight was terminated. A spectrum obtained in the 600 cm^{-1} to 750 cm^{-1} region from float altitude is shown in Fig. 5.

4. Discussion

The data presented in Fig. 1 and 2 show the change in emission with altitude in the so-called "window" region. The compounds responsible for the various emission features

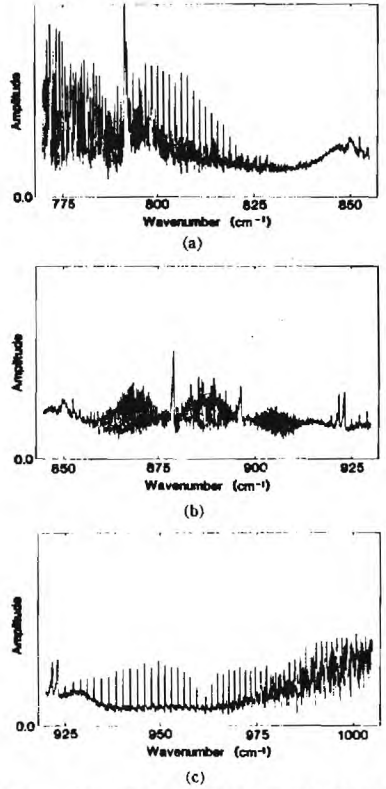

Fig. 4. Atmospheric emission spectrum obtained from an altitude of 30 km, viewing angle −3.2°. This spectrum was derived from the same interferogram as Fig. 3 but transformed at full resolution (0.06 cm^{-1}). (a) 775 cm^{-1} to 850 cm^{-1}. (b) 850 cm^{-1} to 925 cm^{-1}. (c) 925 cm^{-1} to 1000 cm^{-1}.

are identified in the figure captions. The main feature to note in these figures is the significant amount of spectral detail present in the data. These data form a unique set for comparison with theoretical calculations. It should be noted that in the upper troposphere and lower stratosphere the main emission in this region is due to HNO_3, $CFCl_3$ (F11), and CF_2Cl_2(F12). Generally these compounds are not considered in meteorological radiative transfer calculations, yet at these altitudes

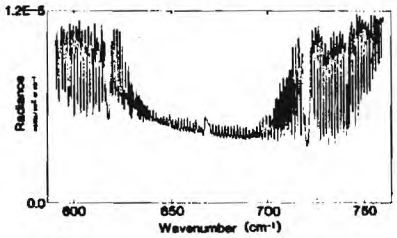

Fig. 5 Spectrum of the 600 cm^{-1} to 750 cm^{-1} region obtained with the instrument viewing the nadir from 27 km. Resolution 0.25 cm^{-1}.

they dominate the radiative transfer through this wavelength range.

The spectra in Fig. 3 and Fig. 4 are presented to show the dramatic change a slight difference in resolution can make in the appearance of the emission spectrum. The resolution obtained with an interferometer can be easily reduced by transforming a shorter portion of the interferogram. The spectra shown in these figures were obtained from the same interferogram, using different numbers of data points. (None of the spectra presented in the paper have additional apodization). The spectra show change in the HNO_3 spectra resulting from a change of a factor of 2 in spectral resolution. The spectra also point up a problem the theoretical calculations of such spectra must address. This is the calculation of spectra for compounds such as HNO_3 for which the fundamental spectroscopic parameters have not been determined but which exhibit a great deal of spectral structure. For HNO_3 this is handled on the AFGL listing of spectroscopic parameters by listing pseudo lines which reproduce the structure given here but are not the lines derived theoretically. Spectral resolution is also important in studies of the upwelling infrared radiation. Figure 5 shows an example of data obtained with this system when viewing the nadir. It should be noted that this figure presents the data in absolute radiance rather than relative units.

5. Summary

In this paper we have presented high

resolution infrared spectra obtained during a balloon flight with a cold interferometer system. The sample spectra presented here are indicative of the detail which must be ultimately achieved in theoretical studies of the flow of radiation in the atmosphere. The capability of the models to accurately predict radiative transfer in the atmosphere is important in many of the problems of current interest particularly the effect of man's activities on climate.

Acknowledgements

This work was supported by AFOSR under the atmospheric science project 2310 and performed as part of AFGL Task 2310G1. This paper has been approved for public release under ESD 84 882 dated 5 December 1984.

References

Elsasser, W.M., 1942: Heat transfer by infrared radiation in the atmosphere, *Harvard Meteorological Studies No.* 6, Harvard University Press.

Goody, R.M., 1952: A statistical model for water-vapor absorption, *Quart. J.R. Met. Soc.*, **78**, p. 165.

Murcray, F.H., F.J. Murcray, D.G. Murcray, J. Pritchared, G. Vanasse and H. Sakai, 1984: Liquid nitrogen cooled Fourier transform spectrometer system for measuring atmospheric emission at high altitudes, *J. Atmos. & Oceanic Tech.*, **1**, p. 351.

高分解大気放射測定

D. G. Murcray*, F. H. Murcray*, F. J. Murcray* and G. Vanasse**

* University of Denver, Dept. Phys., Denver CO 80208, USA

** Air Force Geophysics Laboratory, Bedford MA 01730, USA

NOTES AND CORRESPONDENCE

Balloon Measurements of Stratospheric NO_2[1]

By N. Iwagami, T. Ogawa and K. Shibasaki

Geophysics Research Laboratory, University of Tokyo, Bunkyo-ku, Tokyo 113

(Manuscript received 7 November 1984, in revised form 16 January 1985)

The stratospheric NO_2 has been measured extensively since its important role in the stratospheric ozone chemistry was pointed out (see *e.g.* WMO, 1982). We have measured the stratospheric NO_2 by using spectrophotometers on board balloons once at Sanriku, Japan, twice at Palestine, Texas and three time at Syowa, Antarctica. The results of the first balloon experiment at Sanriku in 1978 have already been published (Ogawa *et al.*, 1981; hereafter called Paper 1), and the data of the other experiments now being analysed will be reported in near future. In this short note we present some empirical estimations of errors of the measurement.

Since the instrumentation and the method of analysis have been described in detail in Paper 1, they are briefly outlined here. The spectrophotometer for the NO_2 measurement is composed of a sun-tracker, a monochromator and a photoelectric detector, and measures the solar spectrum in the wavelength region of 430-450 nm. The spectrophotometers used at Palestine and Syowa are different from the first version described in Paper 1 in the following points: (i) use of a Jobin-Yvon H20 monochromator equipped with a holographic grating in place of a Nikon P250 monochromator and (ii) faster data acquisition rate of 1 spectrum per minute in place of 0.25 spectrum per minute. The method of measurement is based upon a sort of absorption spectroscopy using the sun as a light source. This method is different from the usual method of differential absorption such as Dobson's method for the measurement of total ozone in the point that it utilizes all the information contained in the wavelength region. This is demonstrated in Fig. 1; the NO_2 column density is determined in such a way that the calculated spectrum may fit the measured one. The density profile can be retrieved from the apparent change in the column density during sunset or sunrise.

The errors in the present method may be classified into the following three categories: (i) random error in the column density, (ii)

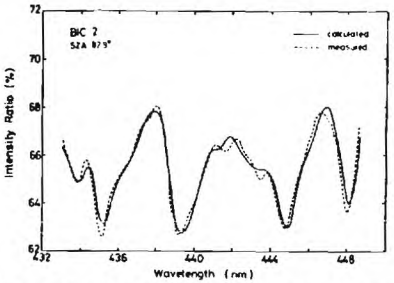

Fig. 1 Measured and calculated absorption spectra of NO_2. The measurement was made at 37.5 km when the solar zenith angle was 92.3°. The Fraunhofer lines in the measured solar spectrum have already been eliminated by calculating intensity ratios of the measured solar spectrum to the reference solar spectrum which is free from the NO_2 absorption. The NO_2 column density deduced is $(2.53 \pm 0.10) \times 10^{17}$ cm^{-2}.

[1] This paper was presented at the Japan-U.S. Seminar on "Review of work related to sensing of stratospheric aerosol and gas components", Fukuoka, 12-14 June 1984.

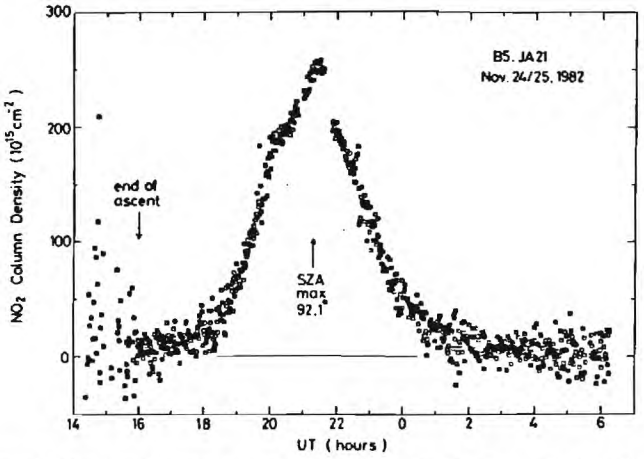

Fig. 2 NO_2 column densities measured on a balloon flown from Syowa (69°S, 40°E) on Nov. 24, 1982. At 2120 UT the solar zenith angle reached a maximum of 92.1°, and the height of the balloon was 25.4 km.

systematic error in the column density and (iii) error due to an ambiguity in retrieving the number density.

In the case of a balloon experiment, random errors in the column density are mainly due to spurious intensity variations caused by the error in the solar tracking against random motions of the balloon's gondola. The atmospheric flicker seems to be an important source of errors during sunset or sunrise. This sort of error may be found as a fitting error in Fig. 1 or as a dispersion of data points in Fig. 2. The lage dispersion of data points seen before 1600 UT in Fig. 2 is due to a bobing motion of the gondola during the ascent, and that seen after 0400 UT is due to the increase in telemetry noise. Summarizing our experiences in the past, one standard deviation of errors in the column density is 3×10^{15} cm^{-2} in daytime and 10×10^{15} cm^{-2} during sunset or sunrise as seen in Fig. 2. In the case of a ground-based observation, the atmospheric flicker including disturbances due to haze is always the dominant source of random errors. One standard deviation of errors in the column density is 2×10^{15} cm^{-2} in daytime and 10×10^{15} cm^{-2} during sunset or sunrise. Since the amplitude of diurnal variation in the vertical column density is (2 to 3) $\times10^{16}$ cm^{-2} at mid-latitudes (Noxon *et al.*, 1979), it is possible to detect the diurnal variation by averaging 10 to 20 data points measured with our spectrophotometer.

A systematic error in the column density is caused by an error in the absorption cross section and a neglection of temperature dependence in the absorption cross section. The absorption cross section used in the present method was measured at 300 K by Johnston (unpublished data, private communication), and the error estimated by the experimenter is 5%. The temperature dependence of the absorption cross section has been reported by Hicks *et al.* (1979). By comparing their results measured at 235 K and 298 K, the error due to this neglection is estimated to be less than 15%.

An error may occur due to an ambiguity in retrieving the number density from the measured column density. A simple inversion method called "onion peeling" is useful to derive the number densities at heights below the balloon (see *e.g.* Paper 1). The uncertainty in the number densities at heights

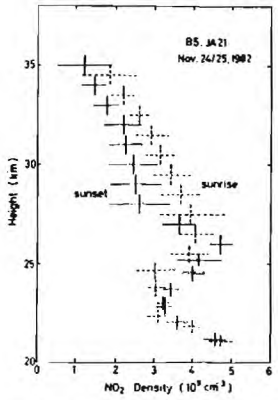

Fig. 3 NO_2 number density distributions derived from the column densities shown in Fig. 2. The uncertainty in the number density comes from the random error in the column densities and from the ambiguity of the retrieval procedure. The vertical bars indicate the thicknesses of the spherical shells which are assumed to be homogeneous in the retrieval procedure.

below 25.4 km in Fig. 3 depends mainly on the uncertainty in the column density, and is about 10%. On the other hand, there is no good method to derive the number densities at heights above the balloon. We used a method described in Paper 1. That is a sort of iteration method to find an approximate solution which minimizes the residual difference between the measured and calculated column densities. The uncertainty in the number densities above 25.4 km shown in Fig. 3 was estimated from the dispersion of solutions obtained for different values of initial guesses. It is found that the uncertainty due to this inversion procedure does not vary significantly with height, and is about 5×10^6 cm^{-3} in this case. This fact seems to be applicable to other cases; if a similar measurement is made at 20 km or at 30 km, the uncertainty in the number density at 35 km due to the retrieval procedure will not differ much from 5×10^6 cm^{-3}. In this inversion procedure, a steady state and a spherical symmetry are assumed implicitly for the NO_2 density distribution. These assumptions are reasonable approximations under the sunlit condition where dissociation of NO_2 is occurring, and cause an error less than 5% (Kerr *et al.* 1977).

Taking random and systematic errors into account, the uncertainty in the NO_2 density obtained by our balloon experiment during sunset or sunrise is estimated to be 20% at heights below the balloon, but it is a composite of a relative uncertainty of 20% and an absolute uncertainty of 5×10^6 cm^{-3} at heights above the balloon.

Acknowledgements

The balloon flight at Syowa was operated by the 23rd Japanese Antarctic Research Expedition of the National Institute of Polar Research. The authors are indebted the successful flight and the data acquisition to R. Fujii and M. Kikuchi. The BIC balloon observation is financially supported jointly by U.S. National Aeronautics and Space Administration and Chemical Manufacturers Association.

References

Hicks, E., B. Leroy, P. Rigaud, J.L. Jourdain and G.L. Bras, 1979: Spectres d'absorption dans le proche ultraviolet et le visible des composés minoritaires atmospheriques NO_2 et SO_2 entre 200 et 300 K. *J. Chimie Physique*, **76**, 693-698.

Kerr, J.B., W.F.J. Evans and J.C. McConnell, 1977: The effects of NO_2 changes at twilight on tangent ray NO_2 measurements. *Geophys. Res. Lett.*, **4**, 577-579.

Noxon, J.F., E.C. Whipple, Jr. and R.S. Hyde, 1979: Stratospheric NO_2, 1. Observational method and behavior at mid-latitude. *J. Geophys. Res.*, **84**, 5047-5065.

Ogawa, T., K. Shibasaki and K. Suzuki, 1981: Balloon observation of the stratospheric NO_2 profile by visible absorption spectroscopy. *J. Met. Soc. Japan*, **59**, 410-416.

WMO, 1982: The Stratosphere 1981: Theory and Measurement. World Meteorological Organization, WMO Global Research and Monitoring Project Report No. 11.

成層圏 NO_2 の気球観測

岩上直幹・小川利紘・柴崎和夫
東京大学理学部地球物理研究施設

NOTES AND CORRESPONDENCE

On Observation of Middle Atmosphere with LAS (Limb-atmospheric Infrared Spectrometer) on Board of Satellite "Ohzora" (EXOS-C)[1]

By A. Matsuzaki, T. Itoh and Y. Nakamura

The Institute of Space and Astronautical Science, Komaba 4-6-1, Meguro-ku, Tokyo 153, Japan

(Manuscript received 10 December 1984, in revised form 2 February 1985)

Abstract

For the global investigation on H_2O, CO_2, CH_4, O_3, N_2O, and aerosol in the middle atmosphere, the limb-atmospheric infrared spectrometer (LAS) on board the satellite "Ohzora" has been launched from Kagoshima Space Center, Japan, on Feburuary 14, 1984. This letter discusses the characteristics of the LAS observation.

1. Introduction

In view of the global investigation on atmospheric chemistry, there are many advantages to the optical remote sensing on board a spacecraft. The Institute of Space and Astronautical Science (ISAS) successfully launched the 9th scientific satellite "Ohzora" (EXOS-C) on Feburuary 14 in 1984 for studies on the atmospheric and electromagnetic circumstances of the earth. The limb-atmospheric infrared spectrometer (LAS) has been borne on this satellite to measure the distributions of atmospheric constituents, i.e. water vapor, carbon dioxide, methane, ozone, nitrous oxide, and aerosol. These constituents are recently of great interest with the relevance to atmospheric chemistry and environmental science. For example, ozone is a stratospheric molecule of great importance for our human life, because it absorbs the strong ultraviolet solar radiation that is harmful for life. The temperature structure in stratosphere is subject to ozone chemistry. Since ozone is very reactive, even the reactions with molecules of minor-constituents are believed to affect on the stratospheric ozone amount. On the other hand, the thermal radiation budget of the atmosphere is closely relevant to the concentrations of water vapor and carbon dioxide. Methane and nitrous oxide play the important roles in ozone chemistry, i.e. HO_x and NO_x cycles, as well as water vapor. LAS simultaneously measures the absorption spectra of these molecules. According to the author's knowledge, LAS firstly measures the limb-atmospheric absorption spectra from a satellite. As described previously (Matsuzaki *et al.*, 1983a, 1983b, 1984), the measurement of the whole spectrum generally gives new and more detailed informations compared with the measurement with a band-pass filter. Namely, in the present study, not only we can make fairly exact analysis of the absorption bands of these molecules, but also the analysis of the spectra observed confirmed to give the stratospheric aerosol extinction. As the first report from the LAS observation, this short communication describes the outlines of the objective and the instrumentation of the LAS observation and the preliminary evaluation of the data obtained.

[1] This paper was presented at the Japan-U.S. Seminar on "Review of work related to sensing of stratospheric aerosol and gas components", Fukuoka, 12-14 June 1984.

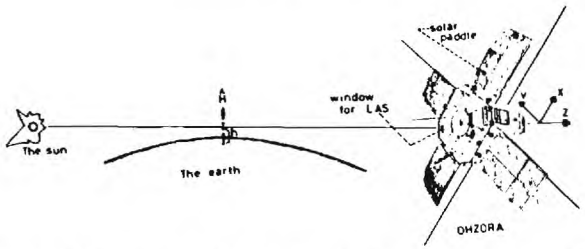

Fig. 1 LAS observation on the platform of satellite "Ohzora". Vector $\hat{H}$ is in the direction from the center to the surface of the earth, and perpendicular to the suface. The tangential height is indicated by h.

2. Limb atmospheric infrared spectrum measurement

The illustration in Fig. 1 shows the relationship of the locations among the sun, the earth, and the satellite for understanding the principle of the LAS observation. LAS mounted on the satellite going around the earth measures the infrared spectra of the solar radiation passing the limb-atmosphere of various tangential heights. Since these spectra of the solar radiation include the absorption bands of atmospheric constituents, the altitude profile of these constituents can be inferred by the analysis of these spectra.

The $-Z$-axis, which is defined as the axis perpendicular to the solar paddle plane of the satellite as shown in Fig. 1, was controlled in the direction to the sun. The spectrometer is installed on the inside of the solar-paddle plane. At the time of this installation, the optical axis of the spectrometer was precisely adjusted to be coincident with the $-Z$-axis. Yet, since attitude control of the satellite is not sufficiently precise for the spectrum measurement with LAS, LAS has the two-axes controlled solar tracking system.

Figure 2 gives the schematic diagram of the optical system of LAS. The solar light comming in this window is correctly introduced into the polychromator by using the two-axes

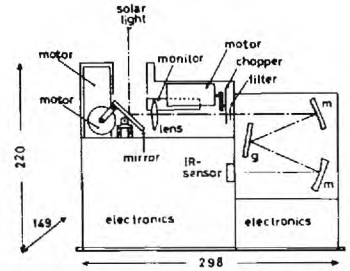

Fig. 2 Schematic diagram of the LAS optical system. The mirrors and grating of the polychromator are indicated by m and g, respectively. The dimensions, i.e. width, length, and height, are given in mm unit.

controlled mirror. The spectral image of the solar radiation dispersed with the polychromator is detected with the pyroelectric linear array sensor. Since the pyroelectric sensor detects only the temperature difference, the solar radiation is modulated at a frequency of 24 Hz with an optical chopper.

Since the intensity of the solar radiation decreases with the increase of the wavelength in the infrared range a wide dynamic range is required for the spectrum measurement over a wide wavelength range. Therefore, as shown in Table 1, LAS measures the spectra of the solar radiation in three wavelength ranges, i.e. 1.6-2.1 μm, 2.8-4.8 μm, and 8.8-10.2 μm for a better spectral resolution and a wider dynamic range. The 32-element and 64-element self-scanning pyroelectric arrays

Table 1 The wavelength ranges for the LAS observation

range	wavelength	sensor	constituents
I	1.6-2.4 μm	32-element $LiTaO_3$ linear array	H_2O, aerosol
II	2.8-4.8 μm	64-element $LiTaO_3$ linear array	CO_2, CH_4, N_2O, H_2O, aerosol
III	8.8-10.2 μm	16-element $PbTiO_3$ linear array	O_3

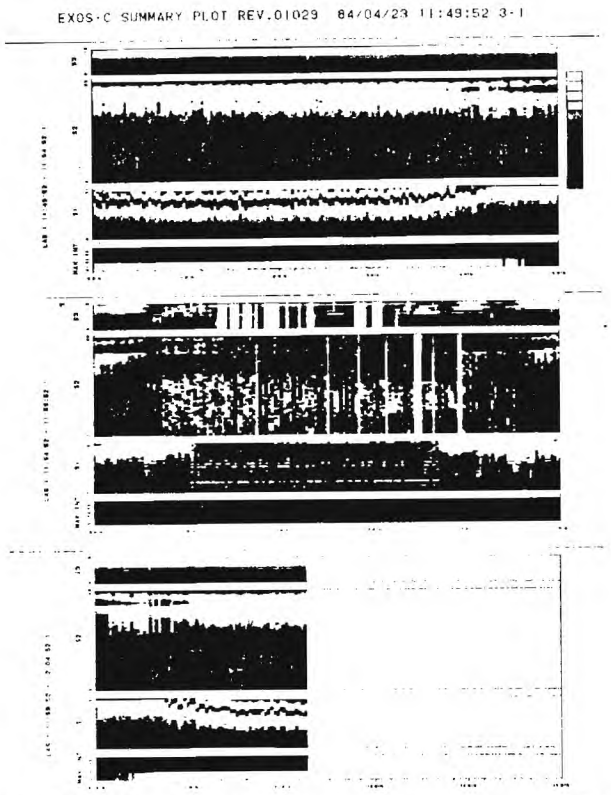

Fig. 3 The infrared spectra actually measured with LAS in orbital 1029. The horizontal axis represents time in minute from 114952 UT on April 23, 1984. In the vertical axis, MAX. INT. represents the maximum signal intensity of each spectra, and S1 (channel 0-31), S2 (channel 0-63), and S3 (channel 0-15) indicate the spectra in wavelength ranges I, II, III, respectively.

(Roundy 1981) are used for the spectral measurement in wavelength ranges I and II, respectively. Since the sensitivities of these self-scanning type detectors are insufficient for the measurement in wavelength range III, we measure the spectrum in this range by a lock-in amplifying technique with the 16-element pyroelectric array that has the preamplifier for each element.

The spectral data measured with LAS are processed with a microcomputer-based data processing unit and recorded with a recorder on the satellite and transmitted to the ground with telemetry systems at KSC (Kagoshima Space Center) in Japan and Esrange in Sweden. The real-time data also can be acquired at the Antarctic Syowa Base. The measurement is controlled by the organized command, which is a kind of the programing command, system.

The satellite was launched from KSC at 1700 JST on Feburuary 14 in 1984. After several technological operations for about two weeks, LAS was confirmed to measure the high quality limbatmospheric infrared spectra. Thereafter this spectrometer continues the observation to get the global data.

3. On informations obtained from LAS

Figure 3 shows the spectra actually measured around 114952 UT on April 23 in 1984 in orbital 1029. The signal intensity of each spectrum is displayed by twelve contrasts of lightness. The spectra were measured in the day-side. With the lapse of time, i.e. as the satellite was going on its orbital, the tangential height decreased; then the absorption intensity and the scattering extinction increased. The data show that two-axes controlled mirror correctly introduced the solar radiation into the spectrometer until the moment of the sunset. Thereafter, from around 115852 UT, the spectrometer successfully measured the spectra of the solar radiation from the moment of the sunrise for the satellite. By the analysis of these spectra we could confirm that LAS measured the absorption bands from water vapor in the first wavelength range, methane, carbon dioxide, and nitrous oxide in the second wavelength range, and

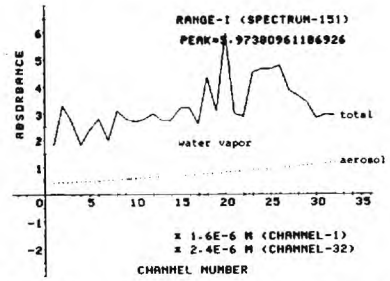

Fig. 4 As a function of serial pixel-number (channel), i.e. wavelength, the extinction intensity obtained for the spectra measured in wavelength range I during orbital 780. Solid line; total extinction, dotted line; scattering extinction from aerosol. The subtraction between them gives the absorption extinction from water vapor.

ozone in the third wavelength range. Furthermore, the total extinction, which was obtained by the integration of the extinction over the wavelength range, was confirmed to include the scattering extinction from the stratospheric aerosol. For example, Fig. 4 shows the extinction intensity of the spectrum, which was measured in range I during orbital 780. The total extinction intensity, the solid line in Fig. 4, includes both the absorption extinction from water vapor and the scattering extinction from aerosol. The molecular scattering extinction calculated with the aid of the standard atmospheric model (Valley 1965) turns out to be much smaller than the absorption extinction from water vapor and the aerosol scattering extinction in this wavelength range. Factly, we cannot find out any steep dependence on wavelength, i.e. the evidence of the minus fourth power dependence on wavelength, for the scattering extinction in the present spectrum. The analysis of the profile of the spectrum of water vapor gives the best mixing ratio of the scattering extinction from aerosol, the dotted line in Fig. 4. The wavelength dependence of the scattering extinction from aerosol utilizes the polynominal function that best fits the typical aerosol model (Valley 1965). The data analysis made in this way confirmed that the mixing

ratio of the scattering extinction from aerosol varies with altitude. Thus we can seperate the absorption extinction from water vapor and the scattering extinction from aerosol for the spectra measured in range I. The result of data analysis will be reported elsewhere. We should pay attention to the fact that this data analysis was made without any serious assumption nor estimation. This is attributable to the measurement of the "whole" spectrum.

We here discuss on the characteristics of the LAS observation. First, LAS measures the "whole" spectra of the solar radiation. Therefore, we can make data analysis to get the atmospheric constituents distribution with the aid of the least-square curve-fitting technique and/or the integration of the absorption intensity over the wavelength range. These methods enable us to estimate correctly the scattering extinctions from the stratospheric aerosol and atmospheric molecules. Furthermore, we can effectively exclude the effect from the curve-growth of the absorption band. In addition to these, since the dispersions of data are statistically averaged in the process of data analysis, the signal-to-noise ratio can be greatly improved. On the other hand, these excellences cannot be given in the measurement with a band-pass filter. A photometer with a band-pass filter usually measures the signal intensity of the single narrow wavelength range without the scan of wavelength. Since this signal intensity measured with the photometer includes both the absorption and scattering extinctions from various atmospheric constituents, we must make our efforts to estimate all these extinctions from only one of the data. Yet, this estimation is impossible in view of scientific logic. Namely, while we can estimate the molecular scattering extinction by using the standard atmospheric model, what can we do for the evaluation of the absorption and scattering extinc tions from the aerosol? Consequently, in this case, we cannot evaluate the molecular absorption extinction, either.

The second characteristic of the present observation is the limb-atmospheric measurement; this solar occultation method is best to get the altitude distribution of atmospheric constituents. Namely, since we can measure the spectra of the solar radiation passing various altitudes of the limb-atmosphere, the altitude profile can be easily obtained by solving the triangle matrix $\hat{L}$ of the simultaneous equations, i.e. $\hat{T}=\hat{A}\cdot\hat{L}$, where, $\hat{T}$, $\hat{A}$, and $\hat{L}$ are the matrices for the integrated extinctions actually observed, the extinction cross-section for each altitude, and the pass lengths, respectively (Matsuzaki *et al.*, 1983). By contrast, if the spectra of the solar radiation unquenched by atmospheric constituents are unavailable, the matrix $\hat{L}$ is not triangle and the magnitudes of the matrix elements are not much different each other. In that case, it is difficult to solve the simultaneous equations $\hat{T}=\hat{A}\cdot\hat{L}$, because the error for the numerical analysis becomes extremely large. Yet, since LAS can measure the spectra in which the absorption and scattering extinctions from the atmospheric constituents are negligibly small at higher altitudes, we can get triangle matrix $\hat{L}$ which can be solved without exception.

In order to make the best application of the solar occultation method, we also devise the vertical slit in LAS for better altitude resolution. The LAS optical system with two-axes controlled mirror makes the solar-disk image on the center of the entrance slit of the polychromator, then the vertical slit, which is put on the entrance slit, cut the solar radiation of other than the center of the solar disk. Since the orbital of the satellite has approx. 865 km of apogee, approx. 354 km of perigee, and approx. 74.6° of inclination, the whole solar disk, whose view angle is approx. 0.5°, includes the solar radiations that pass the atmosphere of 20-40 km altitude width. By using the vertical slit, LAS can measure the limb-atmopsheric spectra with better than 4 km altitude resolution.

In addition to these, another characteristic of the LAS observation is the simultaneous observation of H_2O, CO_2, CH_4, O_3, aerosol, and N_2O. It is of great interest to study on the distributions of these constituents by the measurement under the same condition, because their distributions vary with time. While the idea of the simultaneous observation of atmospheric constituents has already realized by a multicolor photometer with band-pass filters (Chu and McCormick, 1979), there is a difference between it and LAS, i.e., LAS measures the "whole spectrum" of each atmospheric constituent.

4. Conclusion

The limb-atmopsheric infrared spectrometer (LAS) mounted on the satellite "Ohzora" (EXOS-C) can successfully measure the whole spectra of the infrared solar radiation passing the limb-atmosphere. The present spectral measurement based on the solar occultation method would enable us to make data analysis to get the highly qualitative results. It is attributable to the facts that the quality of the data is high, and that we can use the mathematical techniques such as a least-square method in data analysis, etc.

Acknowledgement

The authors are indebted to the EXOS-C project team of ISAS.

References

Chu, W.P. and M.P. McCormick, 1979: Inversion of stratospheric aerosol and gaseous constituents from spacecraft extinction data in 0.38-1.0 μm wavelength region, *Appl. Opt.*, 18, 1404-1413.

Matsuzaki, A., Y. Nakamura and T. Itoh, 1983a: Spectrometers for rocket, balloon, and spacecraft experiments, multichannel image detectors. Vol. 2, ed. by Y. Talmi, pp 297-321, American Chemical Society.

———, 1983b: Measurement of stratospheric aerosol near Sanriku (39°N, 142°E) in Japan on May 31, 1979, *J. Geophys. Res.*, 88, 3783 3788.

———, 1984: Rocket observation of the rotational profile of the A-band absorption spectrum of atmospheric oxygen molecule, *Ann. Geophys.*, 2, 475-480.

Roundy, C.B., 1981: Supplementaly Data Sheet, pp 1-2, Spiricon Inc.

Valley, S.L., 1965: Ed., Handbook of geophysics and space environments, Air Force Cambridge Research Laboratories, Bedford, Massachusetts.

人工衛星おおぞら (EXOS-C) 搭載 LAS (Limb-atmospheric Infrared Spectrometer)

松崎章好・伊藤富造・中村良治

宇宙科学研究所 目黒区駒場, 東京 153